Republic of Iraq

Ministry of Higher Education and Scientific Research

University of Babylon / College of Science

Department of Physics

Study the Land Surface Temperature (LST) for Different Seasons in Babylon Government by Using GIS Technique

A Thesis

Submitted to the Physics Department, College of Science, University of Babylon in Partial Fulfillment of the Requirements for the Degree of Master of Science in Physics.

By

Maysaa Mezher Kadim Hussain

B.Sc. in physics 2018

Supervises By

Prof. Dr.

Ameerah Aboalsawd hammadi Al-Sadooni

2023 A.D. **1445 A.H.**

بسم الله الرحمن الرحيم

(يَرْفَعِ اللَّهُ الَّذِينَ آمَنُوا مِنكُمْ وَالَّذِينَ أُوتُوا الْعِلْمَ دَرَجَاتٍ)

صَدَقَ اللهُ العَلِيُّ العَظيم

سورة المجادلة الآية (11)

Dedication

To the soul of my dear martyr father .He left us physically, but his spirit still flutters in the sky of my life. To my venerable mother... May God prolong her life and provide her with health and wellness. To.....who spent her life And she is the one who .raising me and serving my mother gave her happiness and comfort... my virtuous mother

And do not forget my support and my back. My honorable family, my brothers (Tariq and Muhammad) and my sisters (Nour, Baraa and Sorour) may God prolong their lives so that they continue to help me through moral support in facing problems and avoiding psychological pressures, so I must not forget their generous bounty relatives and friends

I dedicate to you my humble scientific thesis

Mayssa Al-Janabi

Acknowledgments

First of all, I would like to thank(ALLAH) the Lord of Glory who has enabled me to reach this moment in my life .

I would cross from the depths of My heart to express my gratitude and appreciation to my supervisor, Dr. Ameerah Ab. Al-Sadooni , for suggesting the topic of the thesis and for her advice and continuous guidance during this work.

Many thanks to the Deanship of the College of Science at the University of Babylon and the Department of Physics for giving me the opportunity to complete my dissertation .

Finally, a big thank you, love and respect to everyone who helped me

Maysaa

Summary

Thesis examined the relationship between the Land Surface Temperature and environmental variables like air temperature and relative humidity. Using the following months (January, April, August, and October) to represent the four seasons of 2022 in the governorate of Babil (winter, spring, summer, and autumn).

This is done by relying on the data provided by the Landsat version 8 satellite, as it has the ability to image at a high range and has the ability to have high accuracy, as well as it contains different spectra that form images with an accuracy of (30-100) m. In the research, the following bands are adopted: red (B4), near infrared (B5), and thermal infrared (B10) through two sensors: Thermal Infrared Sensor (TIRS) and Operational Land Imager Sensor (OLI). Two images are used for each band to cover the governorate of Babil (5119 m^2).

Geometry and spatial modifications can only be accomplished when two portions have been merged into the Mosaic software, after which Arc GIS and sensing technologies must be used.

The RS is followed by deducting the search region (Babylon province). Our maps are obtained for the distribution of the land surface temperature of the study area, which represent the four seasons of the year under study. There are difference between the two main seasons in Iraq, summer and winter,as the maximum temperature of the land surface temperature during the summer reaches about (70) C^o.

While in winter, it decreases to (24) C^o, with a difference of (46) C^o. The minimum temperature of the land surface varies by only 14 C^o between seasons. As for the two short transitional seasons in Iraq, which are spring and autumn, there is a maximum temperature difference from (2) C^o to (1) C^o.

With the adoption of the meteorological station in Babylon governorate and the establishment of 10 virtual stations.

We are able to investigate factors such as air temperature. When comparing the air temperature with the surface temperature of the earth, we notice that the difference between them is from (2-3) C^{o}.As for the effect of moisture is inversely proportional to (LST). Urban islands (UHI), non-UHI (non-UHI), urban hot zones (UHS) and the Urban Thermal Field Change Index (UTFVI) were measured to quantity the extent of rising urban temperatures as a result of housing and urban development, where we note from the results that there is a large variation from season to season and from region to region.

In the season (spring and winter) there is a big difference in the spring season there are urban islands in the northern regions, but in the winter there are no urban islands in the northern section. As for the seasons (summer and autumn) are similar in distribution, and the northern and western regions do not contain thermal islands, and the eastern and southwestern regions contain thermal islands.

Contents

List of Tables

List of Figures

List of Symbols

LST	Land Surface Temperature
RS	Remote Sensing
TIR	Thermal Infrared
UHI	Urban Heat Island
LWIR	Long-Wave Infrared

MODIS	Moderate-Resolution Imaging Spector
AVHRR	Advanced Very High Resolution Radiometer
TM	Thematic Mapper
ETM	Enhanced Thematic Mapper
NDVI	Normalized Difference Vegetation Index
UHI	Urban Heat Island
BT	Brightness Temperature
PV	Proportion of Vegetation
E	Emissivity
Non-UHI	Non-Urban Heat Island
LULC	Land Use/Land Cover
CLHI	Canopy Layer Heat Island
BLHI	Boundary Layer Heat Island
SUHI	Surface Urban Heat Islands
OLI	Operational Imager thermal Infrared
UHS	Urban Hot Island
UTFVI	Urban Thermal Filed Variance Index
LSE	Land Surface Emissivity
TISI	Thermal Infrared Spectral Indices
AVHRR	Advanced Very High Resolution Radiometer
GOES	Geostationary Operational Environmental Satellites
GIS	Geographic Information System
CAD	Computer-Aided Design
GUI	Graphical User Interface
TES	Temperature Emissivity Separation method
IR	Infrared
USGS	United States Geological Survey
NASA	National Aeronautics and Space Administration
MSS	Multispectral Scanner
TIRS	Thermal Infrared Sensors

VIS	Visible
SWIR	Short Wavelength Infrared
DN	Digital Numbers
BT	Brightness Temperature
PV	Proportion of Vegetation
CFSR	Center for Climate Forecast System Reanalysis
EP/NCAR	European Environmental Prediction/National Center for Atmospheric Research
CFMRWF	Center For Medium-Range Weather Forecasts
GEOS	Goddard Earth Observing System
MERRA	Modern Era Retrospective-Analysis for Research and Applications
JCDAS	Japanese Meteorological Agency Climate Data Assimilation System
UTM	Universal Mercator
SSE	Surface Meteorology and Solar Energy
CFSR	Climate Forecast System Reanalysis
ER/NCAR	Environmental Prediction/National Center for Atmospheric Research (EP/NCAR)
MERRA	Modern Era Retrospective-Analysis for Research and Applications
JCDAS	Japanese Meteorological Agency Climate Data Assimilation System

CHAPTER ONE

INTRODUCTION

1.1 Introduction

The Land Surface Temperature (LST) is crucial for environmental and land cover research. The LST assesses the fluctuation in regional temperature distribution as a significant climatic variable linked to the surface energy balance. The LST is this low touch temperature. LST is a key climate variable that influences the global energy budget [1], climate prediction [2], climate variability [3], global marine circulation [4], and soil moisture [5]. The LST is the radiative temperature at the surface of the earth. Radiant temperature is also known as "skin temperature" since radiometry detects the heat emitted from the surface. Therefore, it is impossible to establish LST values over large areas from ground measurements. Thermal Infrared (TIR) remote sensing enables large-scale LST mapping. Aerial photography based on electromagnetic waves are used in the discipline of remote sensing (RS) to examine the land and ocean surfaces of the planet. Satellites digitise the RS spectrum. Digital data photos can be used to learn about culture, topography, land use, and biodiversity [6]. RS and Geographic Information System (GIS) work together to provide practical temporal-spatial layers. It can map floodplains and model urbanisation, surface energy flux, and hydrology. Pressure on the soil and plant expansion [7]. TIR data are used to determine the canopy layer and surface heat islands remotely. Accurate and widely available in-situ data, such that gathered by permanent meteorological stations, lacks location-specific information. Changing your perspective can help in some cases. The first attempt to determine thermal footprints in urban areas needs the only simultaneous and uninterrupted view of the city that can be obtained using remotely sensed TIR data, in order to provide an accurate assessment of the urban surface climate. Since then, LST and Urban Heat Island (UHI) have been studied using upgraded TIR sensor systems [8]. TIR sensors are now analysing the LST

and UHI. Early study mistook LST trends and UHIs. Low spatial resolution leads to heat islands that are "satellite-derived". More important are the "surface temperature patterns". LSTs gathered by satellites are used to model, simulate, and establish UHI parameters. Surface air temperature, vapour pressure gradients, and surface winds all affect the atmosphere's capacity to absorb the flux, which in turn affects how much energy is transported from the land surface to the atmosphere [9]. Such information is gathered by field and meteorological stations. Rarely do urban energy surface models employ TIR [10].

1.2 The Land Surface Temperature (LST)

At local to global scales, LST has considerable significance for several fields, including studies in hydrology, urban meteorology, and climate, and the study of plant growth [11]. Satellite remote sensing detects LST changes in space and time to estimate the influence of such geophysical factors on climate as evaporation, water stress in plants refers to the condition where plants experience a lack of water, soil moisture, and thermal inertia [12,13]**.** Techniques for LST calculation from satellite have been consistently created as its significance has been increasingly recognized [14]. Sensors like Moderate-Resolution Imaging Spector (MODIS) and Advanced Very High Resolution Radiometer (AVHRR) collect and release twice-daily global thermal data using a pair of Long –Wave Infrared (LWIR) bands. Thermal data with a single LWIR band is available from both Landsat-5 Thematic Mapper (TM) and Landsat-7 Enhanced Thematic Mapper (ETM) although these satellites' temporal resolution is just 16 days and their spatial resolution is only 1 meter. LST monitoring relies heavily on remote sensing through satellite due to the frequent synoptic views it offers of Earth's surface. Using (TIR) equipment in orbit, the LST can be located [15]. Theoretically, LST sensing relies on sunlight reflected off the planet's surface. According to Planck's

rule, it linearly increases with temperature. The LST, also known as the radiant temperature and the air temperature are two different things. Instead, the LST gives an exact and direct reading of the surface temperature of the Earth. According to Planck's rule, how much radiation there is emitted from Earth's surface area is directly related to its surface temperature. And this is the theoretical basis for LST sensing. The surface air temperature and the radiation temperature are not the same. LST accurately measures the Earth's surface temperature. The temperature of a dense plant canopy is different from that of bare soil. The LST focuses the light on the temperature recording region. High urbanization is the main factor affecting the surface temperature of the Earth [16].There is another factor that affects the LST, which is the vegetation factor Normalized Difference Vegetation Index (NDVI). NDVI and LST are related .These evaporation activities cause a fall in surface temperature of the Earth at a rate of (1-5) C^o because plants can use large thermal energy in their vital operations and can lower the surface temperature of the Earth by conjuring and consuming heat. The NDVI can also cause a rise in temperature by plants using carbon dioxide during the vital process of producing their food through photosynthesis and this vital process increase air temperatures by a few percentages. In general the effect of vegetation varies according to the type of vegetation that covers that area as trees and shrubs their impact can increase by 8.8%. When using a remote sensing approach to examine Urban Heat Island (UHI), the LST serves as both a starting point and a crucial metric. LST studies have focused on UHI. Despite working toward different ends [17].

1.2.1 Urban Heat Island (UHI) and non-Urban Heat Island (non -UHI)

The concepts of land surface temperature (LST) and urban heat island (UHI) are used to understand the changing land-use/land-cover (LULC) pattern in various

metropolitan areas [18]. Urbanization has accelerated globally since World War. According to the Population Reference Bureau, (3.4 billion) individuals, or 50% of the global population, reside in cities. The urban population is projected to reach 60% (5.0 billion) by 2030, with an additional two billion people residing in urban areas. There are 100 new cities with populations over 1 million between 2005 and 2015. The air and LST in UHI are higher than in rural regions. Low evaporation and absorption of solar energy explain why land masses retain heat near their surfaces. Temperatures are modeled and observed. To meet this exponentially high demand for homes, massive development projects are currently underway [20].

The rise of rapid and uncontrolled urbanization has had unintended collateral consequences across the world. Urbanization has led to the UHI in addition the UHI increases the concentration of pollutants over the metropolitan area. It also affects the local weather by changing wind patterns, forming clouds and fog, raising humidity, and influencing precipitation rate. The UHI refers to it as a "heat island" because of its rural location and cool surface temperatures. It proved to be high. The type of urban land cover affects the surface temperature we see there. Impermeable, heat-absorbing, non-evaporating materials are the reason why urban environment is much warmer than the neighboring rural areas.

Increasing industrial activity, vehicular traffic, and other human-related industrial activities, As well as the effect of land cover on UHI, contribute to the rise in ambient temperature in urban areas [21]. Canopy, boundary, and surface layer heat islands (Canopy Layer Heat Island (CLHI), Boundary Layer Heat Island (BLHI), and Surface Urban Heat Island (SUHI)) are the three categories under which UHI is classified. Urban atmospheric heat island often referred to as CLHI and BLHI [22]. They are described using temperatures one meter above the Earth's surface. Weather stations can is used to measure it. On the other hand, SUHI is defined as

urban land cover or urban surface temperature [23]. Due to the wind direction and air's ability to carry heat, planet's energy and heat surface can sometimes transfer to the air above it, leading to vertical expansion of SUHI. At night, it can tower over a few meters high. In a nutshell SUHI is a phenomenon known to city dwellers as UHI. On the other hand, infrared remote sensing is usually used to measure LST. The LST and SUHI are closely related because the different types of heat transfer allow the energy or heat radiated from a surface to infiltrate into or above the air around it. Studies at the local scale of UHI [24, 25] .The studies are conducted using data from the Landsat 8 Operational Land Imager (OLI) infrared temperature detector, with a spatial resolution of 100 m. Many algorithms have been used to extract LST from Landsat pictures, including the single window, single channel algorithm [26-27].Heat emissive separation [28] algorithms and split-window techniques [29].

1.2.2 Urban Hot Island (UHS)

These (UHS) are sometimes referred to as the hotter parts of a city. A significant area of bare terrain with exposed rock surfaces or sand deposits can naturally produce them. Intense industrial activity, heavy traffic, or a cluster of thermal power plants are often catalysts for the emergence of such distinctive urban characteristics, though. Identify how they are related to LULC. According to recent study, UHS is observed in urban regions where there is a higher density of UHI, which is correlated with higher LST areas. These studies warn that over the past ten years, there have been large increases in the heat rate in metropolitan areas, which are directly associated to an increase in the UHS [30]. Most existing research makes reference to LST determined from a single or multiple satellite photos chosen for their lack of cloud cover. The values on that day or those days are used to calculate the UHS index for the region under study. In order to propose

worldwide mitigation and resilience actions, these studies extrapolate their conclusions from the selected day(s) and time(s) of satellite passage to longer periods. Some research highlights considerable fluctuations in both LST and UHI both daily and historically, demonstrating that this assumption is incorrect [31]. It has become very difficult to understand how the rise temperature (LST) on Earth's surface is connected to changes in urban climate, such as Surface Urban Heat Islands (SUHI) or Urban Hotspots (UHS), and to the decline in the environmental quality of cities. In the face of climate change, societies around the world are looking for ways to take action that could buck these trends and enhance the standard of living in the area. The LST is used to pinpoint problem areas in the research region. The LST identifies hot spots, or regions of extreme heat that people tend to avoid, throughout the study area. They are regions of varying sizes, typical in warmer climates, and generally considered unfavorable to human operations.

1.2.3 Urban Thermal Filed Variance Index (UTFVI)

UHI impact frequently described using urban thermal field variance index (UTFVI) [32]. Due to human activity, UTFVI is more concentrated in metropolitan areas, which are also significantly warmer than the rural areas that surround them. The UTFVI has a considerable detrimental effect on the area weather patterns, humidity, air quality, indirect economic loss, comfort level, and mortality rate. The UTFVI's enormous heat generates a higher upward motion, which boosts shower and thunderstorm activity. The UHI is in charge of generating pollutants like ozone, which lowers the quality of the air and water**.** Future UTFVI predictions can be a useful tool for locating potential hotspots and for assisting city officials in formulating plans to reduce the impact of UHI and maintain a sustainable environment. Numerous elements, including heat waves, psychometric, alteration

of earth's surface, and illumination intensity, influence LST to cause as UTFVI phenomenon. The UHI effect is significantly mostly attributed to the LULC change. The most significant element altering LST is the changes in the proportion of LULC types. The rising tendency of UHI and UTFVI phenomena can be effectively avoided by forecasting future LULC changes and evaluating their interaction with LST. Future scenarios can be projected using LULC prediction studies, which also serve to ensure that environmental projection is based on socio-economic development. Researchers have run numerous simulations to establish the link between LULC and LST shifts, providing crucial information for communities as they craft long-term sustainable development strategies. UTFVI values below zero indicate no UHI, and define an area as having high environmental quality and suggest a high degree of thermal comfort. The intensity of SUHI increases in tandem with increasing UTFVI readings, reducing thermal comfort.

1.3 Normalized Difference Vegetation Index (NDVI)

The normalized difference vegetation index (NDVI) can be used to assess remote sensing readings taken space platform and to determine the trajectory of the observed target's green vegetation. Using the NDVI method, you may identify a wide range of features in three-color satellite image (green, red, and near-infrared). RS readings can be studied from a distance to detect if a target or object has living, green vegetation by using this indicator, which is a basic and meaningful digital signal [33]. The most accurate digital processing technique for presenting plant cover in satellite pictures where as it is founded on the fact that the vegetation exhibits low reflectivity in the wavelength range of red with strong reflectivity in near infrared. In recent decades, the NDVI has been widely employed for vegetation remote sensing. According to the reflectance or radiances that the red

channel (0.66 m) and the near-IR channel (0.86 m) are both recorded. By calculating the levels of chlorophyll found in the leaves, the state and health of the flora are determined. The near-IR band is able to record the vegetation's high reflectance plateau, while the red channel can track the region of intense chlorophyll absorption. Understanding the consequences for ecosystems and human health increasingly on the interaction between nature of land cover and the materials used in increasing temperatures and urbanization. Land anthropogenic heat discharges caused by energy use raise the surface temperature. Following this, there will be an increase in man-made materials covering the land surface, which have high heat conductivities and heat capacities. There are consequently less green spaces and porous surfaces that can absorb rainwater. Which absent them, would cause surface temperatures to drop through processes like evaporation and condensation [34].

Sensing from a distance can be a helpful tool for a variety of tasks, such as understanding the urban thermal environment, examination of urban vegetation Remote sensing can be an effective tool for the, including its use in the study of urban thermal ecology. Instruments used for remote sensing collect data on the temperature of the radiant surface and measurements of the energy reflected in the red and near infrared regions of the electromagnetic spectrum [35]. The Vegetation Index (NDVI) is used by remote sensors to create vegetation temperature maps. LST is a fundamental aspect of the physics of Earth's surface processes because it affects surface-atmosphere interactions and the energy flow between the atmosphere and the ground, both of which are affected by the presence of vegetation on a pixel-by-pixel basis. The highest NDVI values are associated with the lowest LST values.

Historically, NDVI levels have fluctuated between +1 and -1. Positive values indicate vegetation, while larger positive values indicate denser and healthier vegetation. Negative numbers represent a lack of greenery, in contras as shown in Figure (1-1) [36].

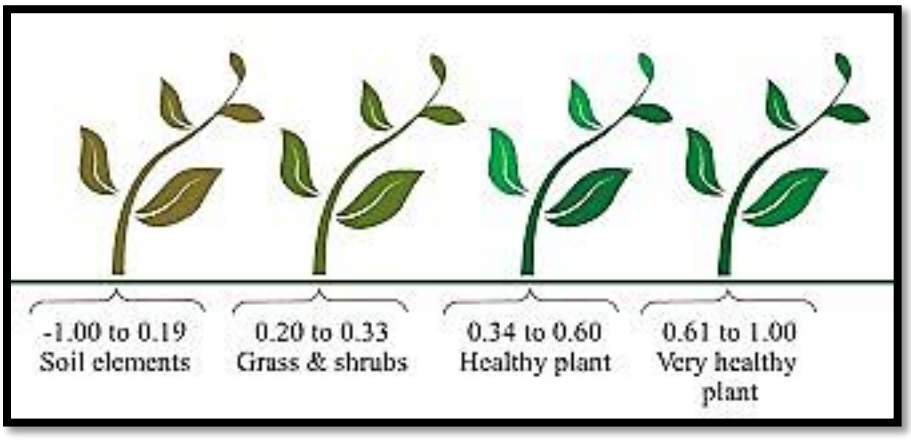

Figure (1-1): The NDVI values represent the health of the plant [37].

In order to determine the NDVI, the application of the formula shown below:
Utilizing the following formula, the NDVI is calculated [38].

$$\boldsymbol{NDVI = \frac{(NIR - R\,Visible)}{(NIR + R\,Visible)}} \qquad \boldsymbol{(1-1)}$$

Where

NDVI= The Distinction, Normalized plant cover index

NIR=The Near Infrared band.

Red= The Red band

$$\boldsymbol{In\ Landsat\ 8,} \qquad \boldsymbol{NDVI = \frac{(Band\ 5 - Band\ 4)}{(Band\ 5 + Band\ 4)}} \qquad \boldsymbol{(1-2)}$$

1.4 Black Body Radiation

The phrase "black body" has specific meaning here. Refers to an ideal physical body that is transparent, emits no electromagnetic radiation and absorbs all electromagnetic waves that come into contact with it .The development of statistical and quantum mechanics owed much to the failure of classical physics to account for the actions of black masses[39]. An improved black body description may result from more in-depth knowledge variations and generalizations of physical properties. Generalized statistical mechanics and a thermodynamic framework that applies to space plasmas and other stationary systems are used outside of thermal equilibrium. The black body performs exactly as the theoretical laws predicted.

In the natural world, though, some materials, such as pure water. between 8 and 12 meters deep, can come close to not having true black bodies. Therefore, no surface can radiate more energy than a black body at a given temperature and wavelength. Not all black bodies are flawless. Instead, they act like gray things. The ability of a heated body to absorb electromagnetic waves that occur at the same frequency with its ability to emit thermal electromagnetic radiation. If dark matter "absorbs all incident rays completely" as Kirchhoff proposed in 1860, then it would be ideal [40]. Planck theorists later agreed with this concept, and it is now generally accepted that no microscopic thing, regardless of shape, size, or temperature, can emit more thermal radiation than a perfect black object with the same parameters [41]. In fact, no microscopic thermal body can radiate more heat than a black body. In one widely used book, similar claims can be found. In their seminal work, Bohren and Hofmann state, for instance, that "the emissivity of a sufficiently large sphere is not greater than (1) [42]. Therefore, it is impossible to emit radiation

above the black body limit if the radius of the radiating sphere is much larger than the wavelength. An ideal physical body that is transparent, emits no electromagnetic radiation, and absorbs all electromagnetic waves that come into contact with it. Bυ(T) or Bλ(T) represents the appropriate spectral intensity or radiation.

This measures the strength of a black body, per solid angle, normal propagation area, and frequency or wavelength when it is in thermal equilibrium with the environment at a temperature T. The type of body material and its temperature affect this radiation's characteristics. Because infrared wavelengths cannot be seen with the human eye and are therefore mostly released at low temperatures, the body first appears dark when it is heating up. When a body's temperature reaches a particular point, it starts to glow in a color that tends to be red or orange and eventually turns white, which is to say that it starts to emit wavelengths in the visible spectrum. According to the study, the spectrum is a continuous spectrum that contains all of the various wavelengths. Some of which are in areas of infrared or ultraviolet radiation and are not visible the eye. According to Kirchhoff's law, a body with high absorption also has a high radiation, and the best illustration of an ideal black body is a small cavity formed of any material with a small hole, be it copper or iron total absorption when walls are heated. This cavity emits thermal radiation K onto the surrounding environment at a fixed temperature.

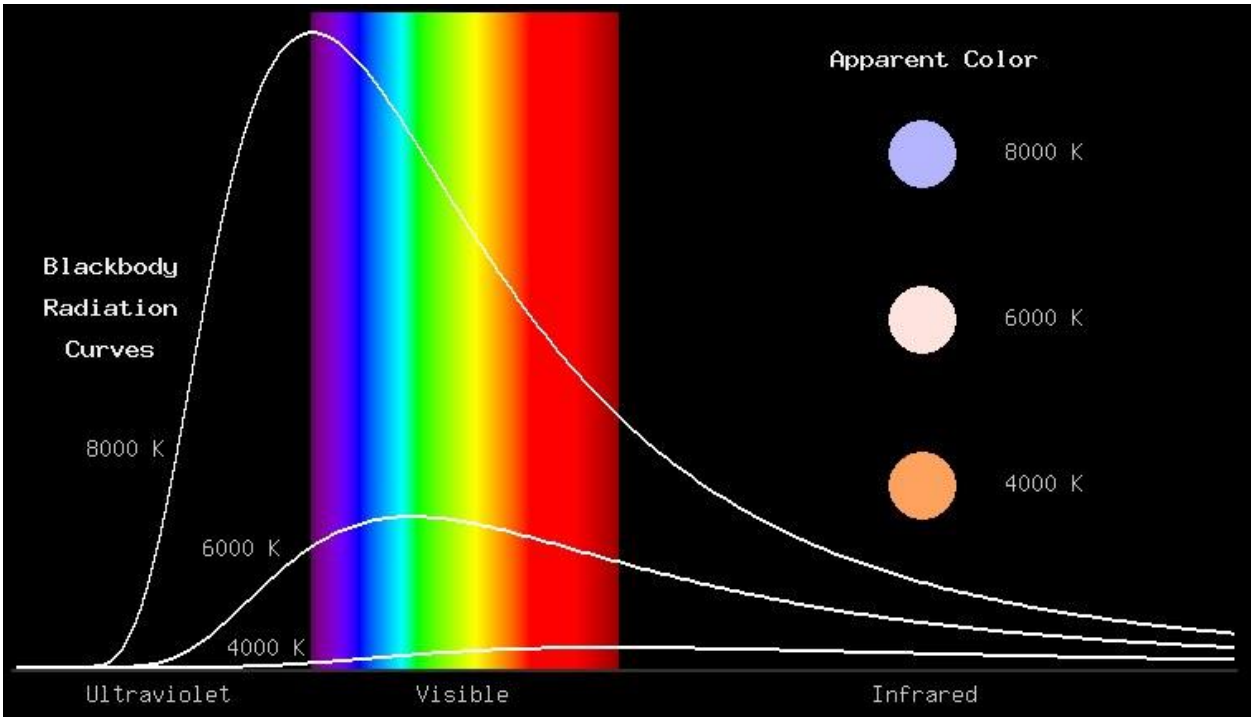

Figure (1-2): Blackbody radiation versus temperature curves [43].

Depending on the blackbody's temperature, we can describe the link between the total energy it emits Planck's radiation equation, Stefan-Boltzmann's law, and Wien's displacement can all be used to calculate the spectral distribution of that energy, or the radiation curve as shown in Figure (1-2).

1.5 The Law of Black-Body Radiation by Planck

The Planck equation describes blackbody radiation the intensity of a black body's emitted electromagnetic radiation varies directly with its temperature [44].During a specific wavelength (M_λ). Kirchhoff, Tyndall, Stephan, Boltzmann, Fenn, and Rayleigh are just a few of the prominent physicists of the nineteenth century who studied the relationship between an object's temperature and the quantity of radiation it gives off [44]. Since the Wien and Rayleigh-Jeans equations for the intensity of thermal radiation are not sufficient to explain the experimental measurement, Planck attempted to reconcile the experimental measurement with

black body radiation theory, which he developed after working on Statistical physics, thermodynamics, and the electromagnetic theory of radiation [45]. The random current source for thermal radiation is the charge agitation generated by temperature changes in any object. Propagating electromagnetic waves, which radiate from an emitter's surface into free space, and evanescent waves where one or both kinds of thermally driven electromagnetic waves degenerate (exponentially or otherwise) away from the ground level. Because of the dissipation of non-propagating waves at the surface of the emitter, they are unable to transmit energy in an impermeable medium unless something is placed nearby to permit the tunneling of non-propagating waves from the emitter. For black body radiation, Planck's classical theory as shown in Figure (1-3) only accounts for propagating modes when diffraction effects are small [46]. For thermal radioactive transmission to occur without significant diffraction or near-field effects from non-propagating modes, the characteristic linear dimensions and distance between objects must be larger than the nominal wavelength of heat radiation.

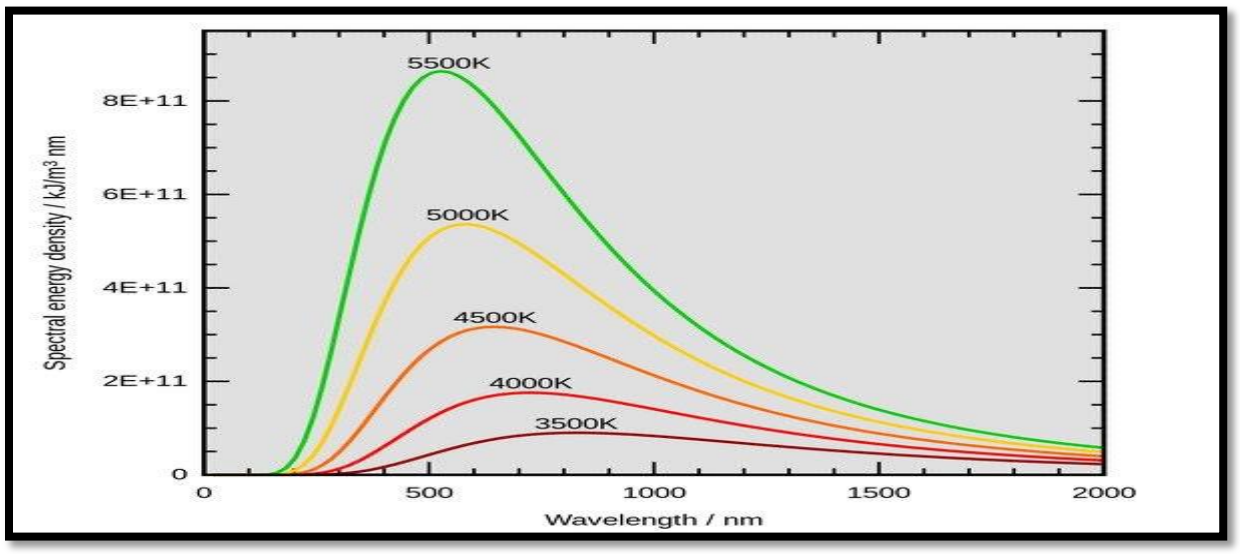

Figure (1-3): Planck's law from frequency to wavelength [47].

This law can be expressed as follows for radiation into a vacuum or a material with a refractive index of unity [48].

$$M_{\lambda} = \frac{2\pi hc^2}{\lambda^5(\frac{hc}{e^{\lambda kT}-1})} \quad \textbf{(1-3)}$$

Where:

$\mathbf{M_{\lambda}}$ =Spectral radiant existence (W/ (m2 .rad.µm)).

h = The Planck constant (6.626×10^{-34} J s).

c = light speed (2.9979246×10^{8} m/s).

k = Boltzmann constant (1.3806×10^{-23} J K^{-1}).

T = literal temperature (K).

λ =wavelength (µm).

1.6 Stefan-Boltzmann law

Law of Stefan-Boltzmann entropy [49] gives a relationship between the absolute temperature and region under the radiation curve, which is sum of a black body's radiated electromagnetic waves. It is the sum total of energy discharged by a blackbody at all wavelengths for a given area of its surface. The following equation provides a mathematical explanation of Stefan Boltzmann's law, which states that molten solid iron emits energy at rapid rates [50].

$$T_{Radbb} = \sigma T_{kin}^4 \quad \textbf{(1-4)}$$

Where

$\mathbf{T_{RadBB}}$ = blackbody radiation flow (W/ m²).

$\mathbf{T_{kin}}$= Thermodynamic absolute temperature (K).

σ = the Stefan-Boltzmann constant (5.6697×10^{-8} W m^{-2} K^{-4}).

1.7 Wien's Displacement Law

The Wien's displacement law elucidates correlation between heat and peak wavelength which is also the spectral maximum of the radiation spectrum. When plotted as a function of wavelength, the peak of the spectral radiant density curve moves as the temperature rises, light shifts toward shorter wavelengths. Planck's law is typically stated in terms of wavelength rather than frequency.

The following equation describes this phenomenon [51]:

$$\lambda_{max} = \frac{A}{T} \qquad \textbf{(1-5)}$$

Where

λ_{max} = is the wavelength at which the spectral radiant existence is most intense (μm).

A = means Wien's constant (2897.8 μm K).

T= in terms of its absolute value (K).

Maximum existence (max) changes for an entity as its temperature increases.To shorter wavelengths. However, although the Earth's maximum emission occurs in the (TIR), the Sun's occurs in the visible (VIS) area of the spectrum at temperatures averaging 5,778 K (or, roughly, at green 0.55 m).

1.8 Emissivity and Kirchhoff's Law

Emissivity of the land surface (LSE), a characteristic of the earth of material composition, must be precisely known to make an attempt at Land Surface Temperature Estimation. Since the land surface is uneven, its emissivity range varies with land cover type, surface moisture, roughness, and viewing angle. It is larger than that of the oceans. In the LST retrieval process, surface emissivity is a crucial metric for separating the effect of the surface from that of the atmosphere. Physical characteristics of the surface, such as its density or water content see Table (1-1) .

Table (1-1) Emissivity averages for some materials [52].

Materia	Average Emissivity(μm)
Clearwater	0.98-0.99
Green vegetation	0.96-0.99
Dry-vegetation	0.88-0.94
Asphaltic concrete	0.94-0.97
Basaltic	0.92-0.96
Granitic	0.83-0.87
Dry mineral soil	0.92-0.96
Polished metals	0.06-0.21

1.9 The Climate Parameters

The climate has a significant impact on human life, and all of its components have an impact on how the land surface changes temperature, some of which are inverse relationships and some of which are direct relationships.

1.9.1 The Air Temperature

Despite the fact that air temperature varies seasonally and geographically due to natural fluctuation, it is a reliable indication of local, regional, and global climate change [53].That the LST should be proportional the radiometric equivalent of the atmospheric temperature. Of the ground or vegetation canopy, as opposed to T_{air}, which is the surface temperature you would feel if you put your hand on it. From the ground or from space, the quantity of heat radiated from the earth can be measured with the help of a radiometer .The heat given out by the planet's crust (or "skin"), where solar energy interacts with the earth to warm it, or the surface of the canopy in wooded areas, is what LST measures. LST is an effective predictor of energy partitioning at the land surface-atmosphere interface because of its sensitivity to change in surface conditions. In a classic diurnal cycle, LST is significantly warmer during the day than T_{air}, but similar to T_{air} at night [54]. The LST-T_{air} association can be caused by a number of major variables. Cloud cover [55] season, and latitude variations in solar radiation can alter the distinction between LST and T_{air}. For instance, increases in cloud cover can have an almost immediate impact on the relationship between the midday T_{air} and LST, making the two variables more comparable as

shown the Figure (1-4).Variations in the type of land cover, the density of the vegetation, and soil moisture also have a significant impact on the link between T_{air}

and LST since LST is more closely related to the biophysical properties of the land surface.

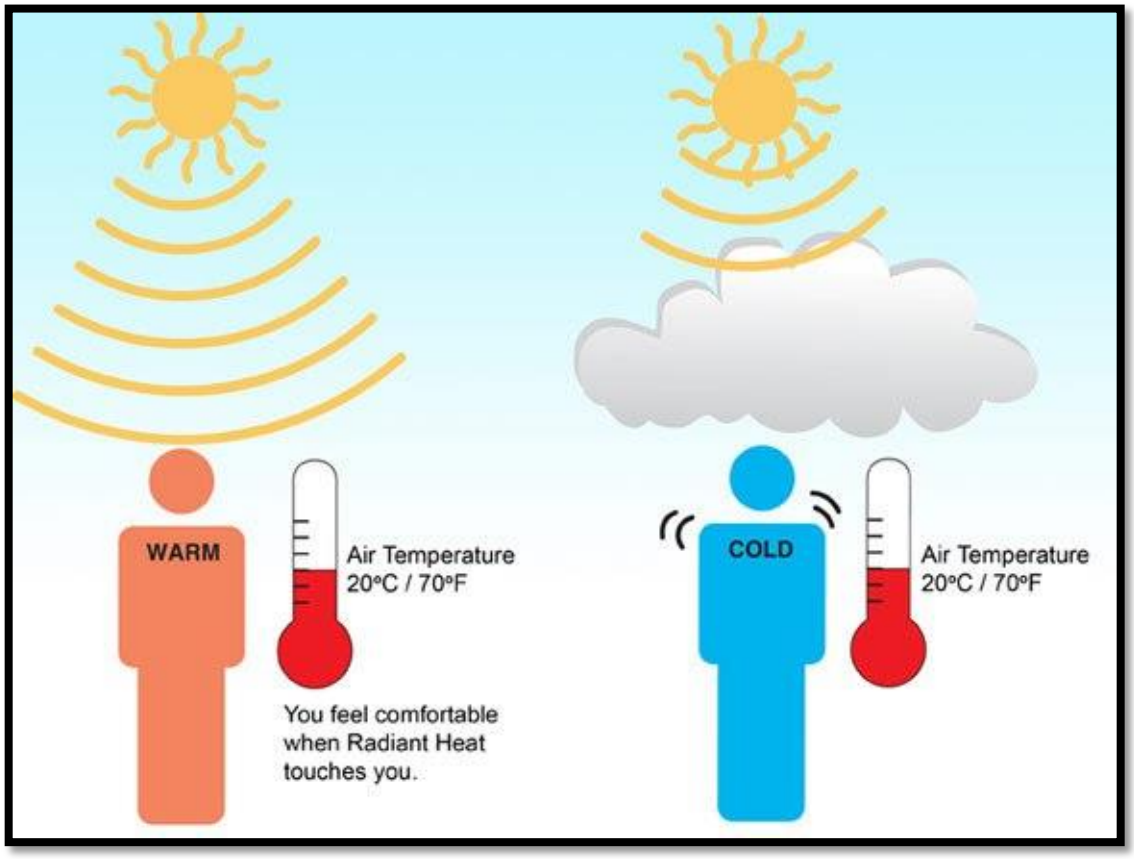

Figure (1-4): Clarifying the difference between radiant temperature and air temperature [56].

1.9.2 The Relative Humidity

The amount that is most frequently utilized for general applications, including agriculture, hydrology, water resource management, and human comfort. In addition to wind speed, it is the deciding factor that impacts the amount and rate of evaporation, making it crucial to assess the rate of moisture loss by soil, plants, water reservoirs, etc. Other moisture parameters are qualitatively and quantitatively

different from relative humidity. It can be changed by altering water vapor concentration in the air (for example, through evaporation) or the air's ability to hold moisture (for example, by changing the temperature) the atmosphere [57]. Relative humidity and water vapor pressure can be thought of as two separate characteristics of the humid atmosphere, which is a system made up of two components: dry air and water. The radioactive effect is also closely connected to relative humidity. There are three types of humidity, namely: 1- Absolute humidity, which represents a mass of water vapor that is present in certain proportions in the air and has an effect on air temperature. At normal temperature 3- It is the last type and represents the difference between compared to the saturated vapor pressure, the vapor pressure when exposed to air is lower. The device that is used to measure humidity is (hygrometer) [58].

1.10 The Remote Sensing (RS)

Since technological advancements in remote sensing, the majority of studies on urban meteorology have relied on point samples of air temperature at fixed points in the city. Due to their ability to record spatially continuous data over a vast area, remote sensing techniques have proven to be superior in gathering data on land surface temperatures.

The sensors' increased re-visit times (temporal resolution), in addition due to their great spatial resolution, time series data for significant biophysical processes happening at or near the Earth's surface may now be evaluated. Operational Land Imager, Landsat Thematic Mapper/Enhanced Thematic Mapper(TM/ETM+, OLI), Plus, Advanced Space-borne Thermal Emission and Reflection (ASTER), and the Advanced Very High Resolution Radiometer (AVHRR) are all examples of such instruments. Geostationary Operational Environmental Satellites (GOES), while more,and Satellite Pour [59],used to study variations in surface temperature while

remote sensing is known to collect massive amounts of data at relatively low cost, issues with data retrieval, poor data quality, and temporal accuracy are all quite pervasive. For example, it is important to collect information on certain regions of the Earth at a distance, particularly in the tropics because of difficulties with cloud cover and high humidity, which is difficult quality is tough. They point out that many due of the difficulty in obtaining accurate ground-based measurements of the LST, fewer studies have been conducted to validate the satellite derived LST, which is resolution of satellite images [60]. However, data retrieval and gathering from the LST is anticipated, and use will progress with the launch of Landsat 1, Landsat 2, and Landsat 8, as well as with potential future developments in space science and technology. Predicting how climate change will influence metropolitan areas is crucial, especially in light of the dangers posed by a potential rise in LST. This is why the current study is so important. The present study processed cloud-free (less than 10% cloud cover) LST and NDVI data sets as a result of the expanding urbanization. Pictures taken by Landsat in the section (2-2) titled "Methods and Data more information is given regarding the data and analytic techniques. Figure (1-5) shows the remote sensing process.

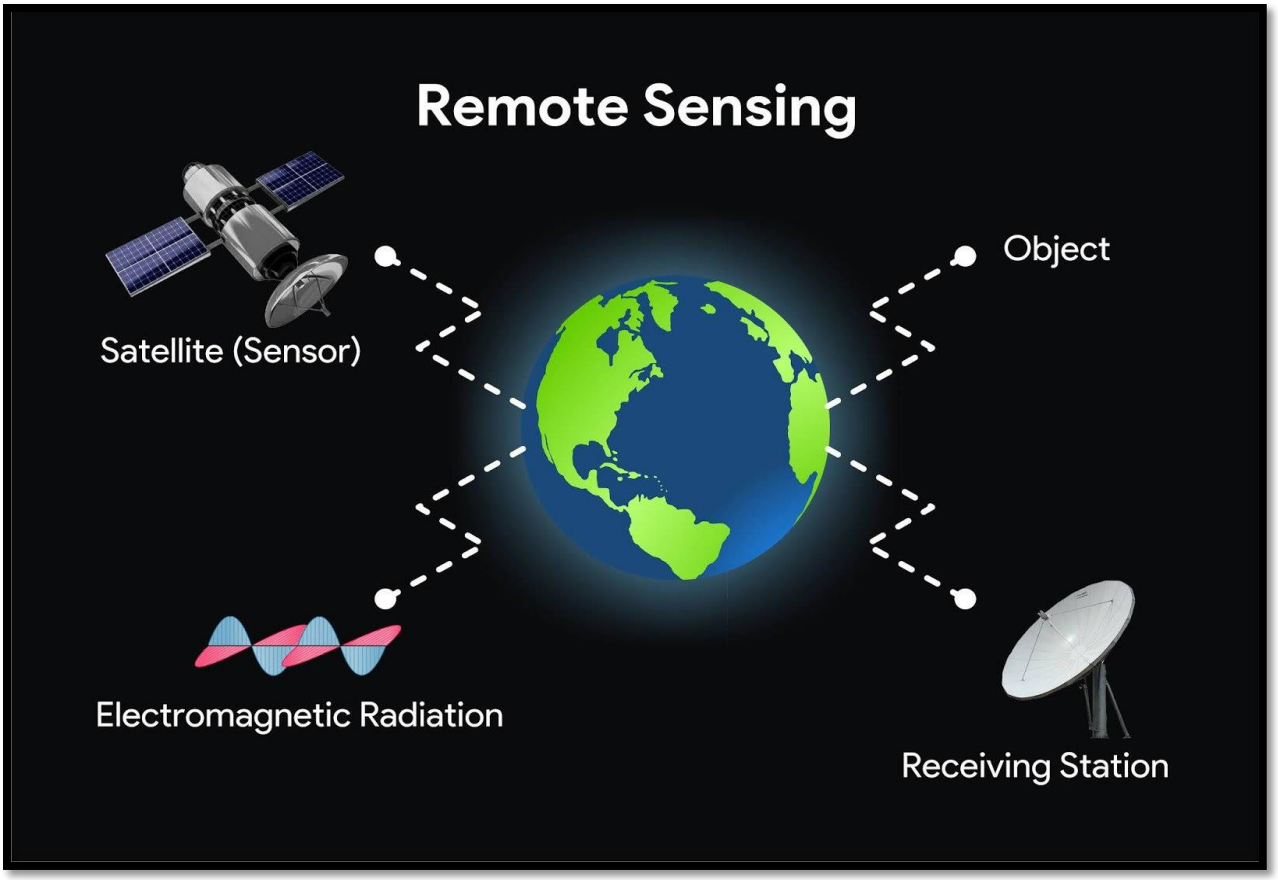

Figure (1-5): Understanding remote sensing and the technologies involved [61].

1.11 Geographic Information System (GIS)

The GIS, which stands for "geographic information system," (GIS) is commonly used to refer to regionally focused integration of computer systems and technologies used in practical variety of other applications, and more, a new field that is garnering significant interest on a worldwide scale. The GIS is more challenging to define than initially thought for a variety of reasons. It is obvious that GIS is a relatively new phenomenon, even though there has been some controversy about the term's definition and the time when development in the subject first began [62]. Geographic information systems are information systems that created to interact data that makes use of spatial or geographical references. For another way of putting it, a database system designed specifically for

geographically linked data, GIS also includes a suite of data-processing tools. [63].Another feature that sets the GIS sector apart is the variety of applications. Geography, of course, but also agriculture photogrammetry, surveying, and zoology, as well as the fields of botany, computing, economics, mathematics, and more are just a few of the disciplines that are integrated into the GIS. Differentiating between the competing demands of many organizations and individuals who all want to be represented in a growing and lucrative profession is necessarily difficult. Because there are many various methods to define and categorize things and themes, it is equally challenging to define GIS. Not unexpectedly, to handle dereferenced data, the GIS can offer four kinds of capabilities [64]:

1. Gathering and preparing data.
2. Data management encompasses maintenance and storage.
3. Analysis and data processing.
4. Information Display.

1.11.1 GIS and Other Information System

The GIS and other information systems understanding how GIS functions in relation to database management, computer-aided design, computer mapping, and remote sensing information systems is essential. They assert that examples include the fact that almost any system capable of putting a map on screen on a CRT these days calls itself GIS. is sometimes described as a subset or superset of such systems. Systems for computer-aided design (CAD) are created to generate product result and draft new items. It is graphic-based and bases the representation of elements in the interactive design process on symbols. Only basic linkages to databases that typically contain incomplete listings or inventory reference numbers

are present in CAD systems. They deal with comparatively less data. CAD systems often have limited analytical capabilities and do not allow users to automatically assign symbols based on user-specified criteria. Computer mapping systems concentrate an emphasis on automatically locating, classifying, and coding data. Presentation is prioritized over retrieval and analysis [65]. Computer mapping systems employ straightforward data structures that are devoid of topology-related details. Although they can be connected to a database management system, they typically just execute straightforward callbacks. Computer mapping systems often provide a wide range of tools for creating high-quality vector output and constructing maps. The capacity of GIS to analyze spatial data is frequently viewed as a crucial component of its definition and is frequently used to set GIS apart from systems whose main goal is map generation as shown in the Figure (1-6). The only two GIS-specific procedures are spatial search and overlay [66].

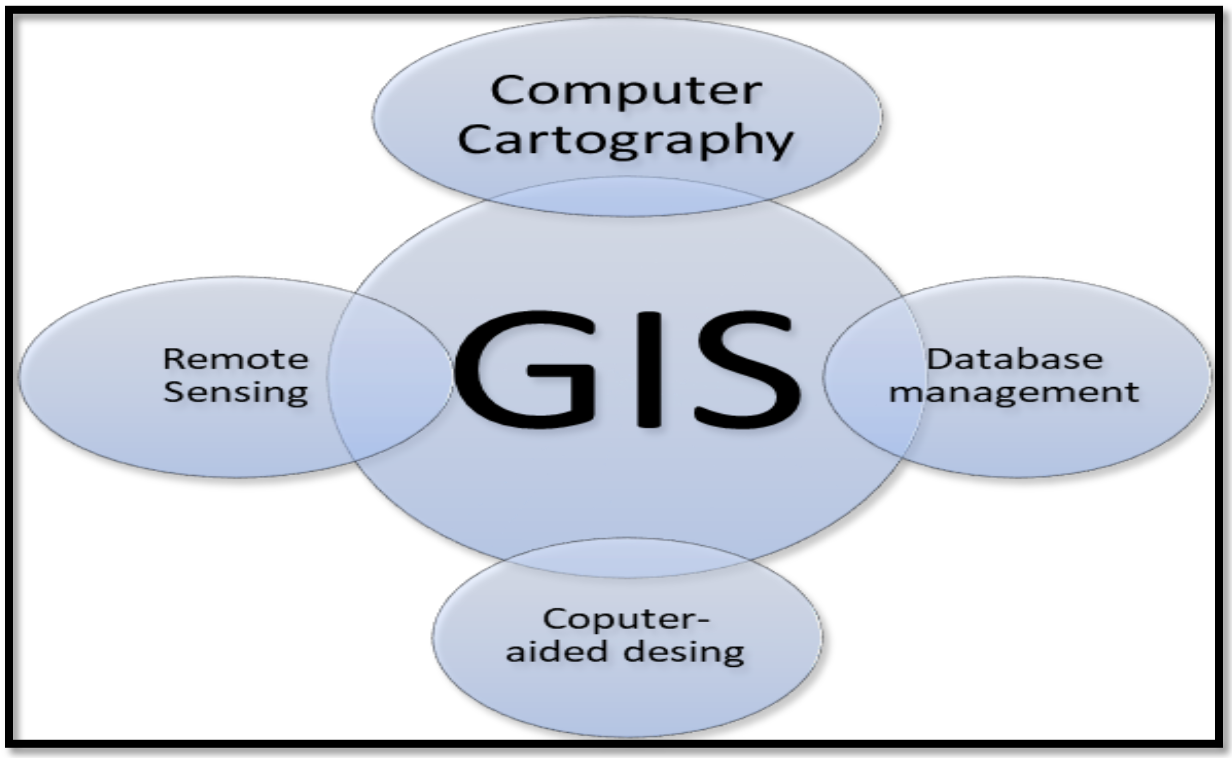

Figure (1-6): Application of GIS.

1.11.2 Data Types Used in the GIS

(a) Spatial data: is a collection of datasets (both vector and raster) that have been created using field surveys or remote sensing data and are based on the surface of the earth. These datasets are made up of satellite photos, coordinates, and other data that are analyzed to create themed maps that can help with agricultural planning for the sustainable use of finite resources. Coordinates are used to represent geospatial data. Points, polygons, and lines (arcs) are the three fundamental spatial informational elements of data in the form of vectors. In the same way that a polygon is made up of connected lines, a line is made up of connected points. Each of these components comprises, in the simplest terms, just a string of coordinates as shown in the Figure (1-7).

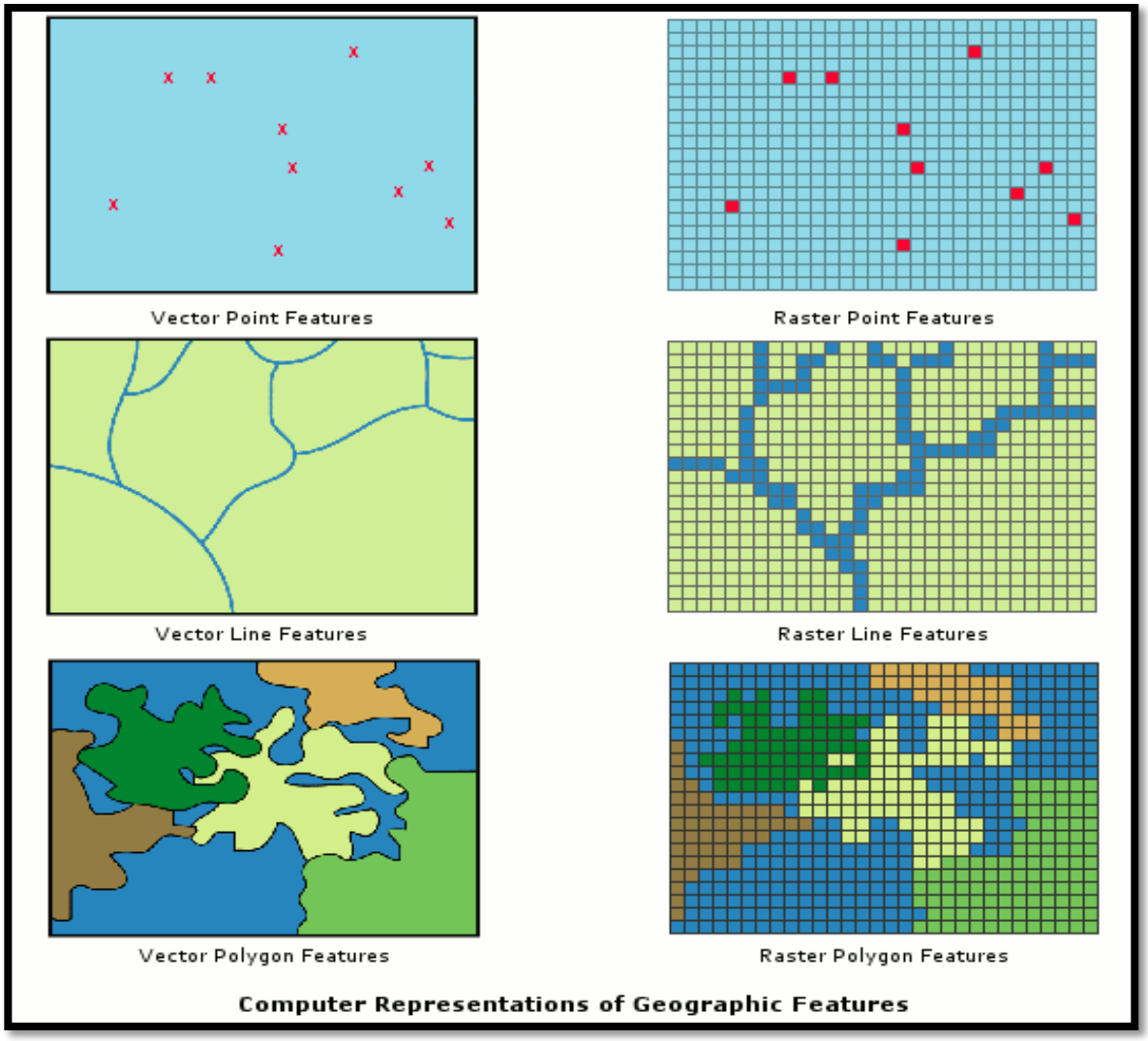

Figure (1-7): The GIS data (Raster and Vector data models) [67].

- **Co- ordinate**: a coordinate in an n-dimensional space expressed as an n-number along an n-axis, or paired numbers expressing orthogonal axes' horizontal distances, or triplets of numbers measuring both axes' vertical and horizontal distances. Co-ordinates are commonly used to depict locations on Earth's surface in relation to other locations.
- **Point:** a solitary, non-physical entity that can be located only in two-dimensional space. Small-scale maps sometimes employ points to indicate

the position of buildings or towers because these elements are too inconsequential to be represented by lines or regions.

- **Line:** A set of ordered coordinates displays the form of geographical features that are either linear (like county boundary lines) or too thin to be presented as an area at the requisite scale (such stream contours, roadway centerlines, or contours). Lines and arcs have the same properties.
- **Polygon:** something that represents a space. A polygon is defined by the set of lines that make up its boundaries and a single identifying point inside those lines. The properties of polygons, such as forest and district, describe the geographic feature they represent.

(b) Non- spatial data: The non-spatial qualities explain what is at a point, along a line, or in a polygon, as well as socio-economic aspects from other sources. They are complementary to the spatial attributes. The depth of the soil, the texture, the drainage, and erosion are examples of a soil category's characteristics as shown in Figure (1-8).

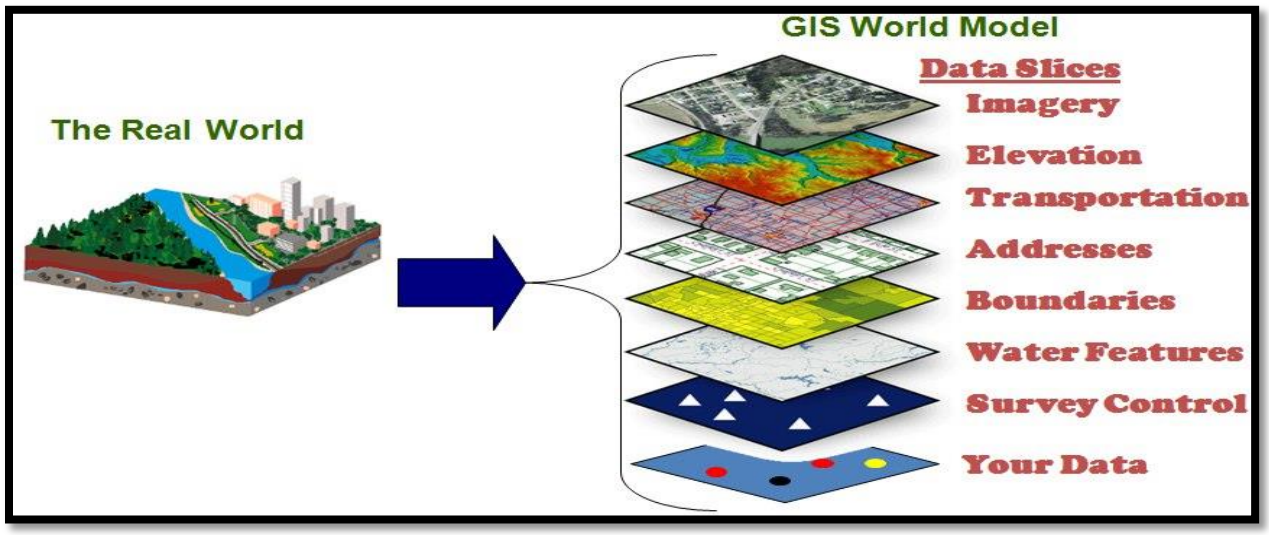

Figure (1-8): A diagram illustrating the many layers that may be applied to a GIS [68].

1.11.3 The Element of GIS

Computer hardware, computer software, data, and liveware are the four fundamental components of the GIS that work in an institutional setting. Almost any sort of computer platform, including relatively basic personal computers, high-performance workstations, minicomputers, and mainframe computers, can serve as the hardware element.

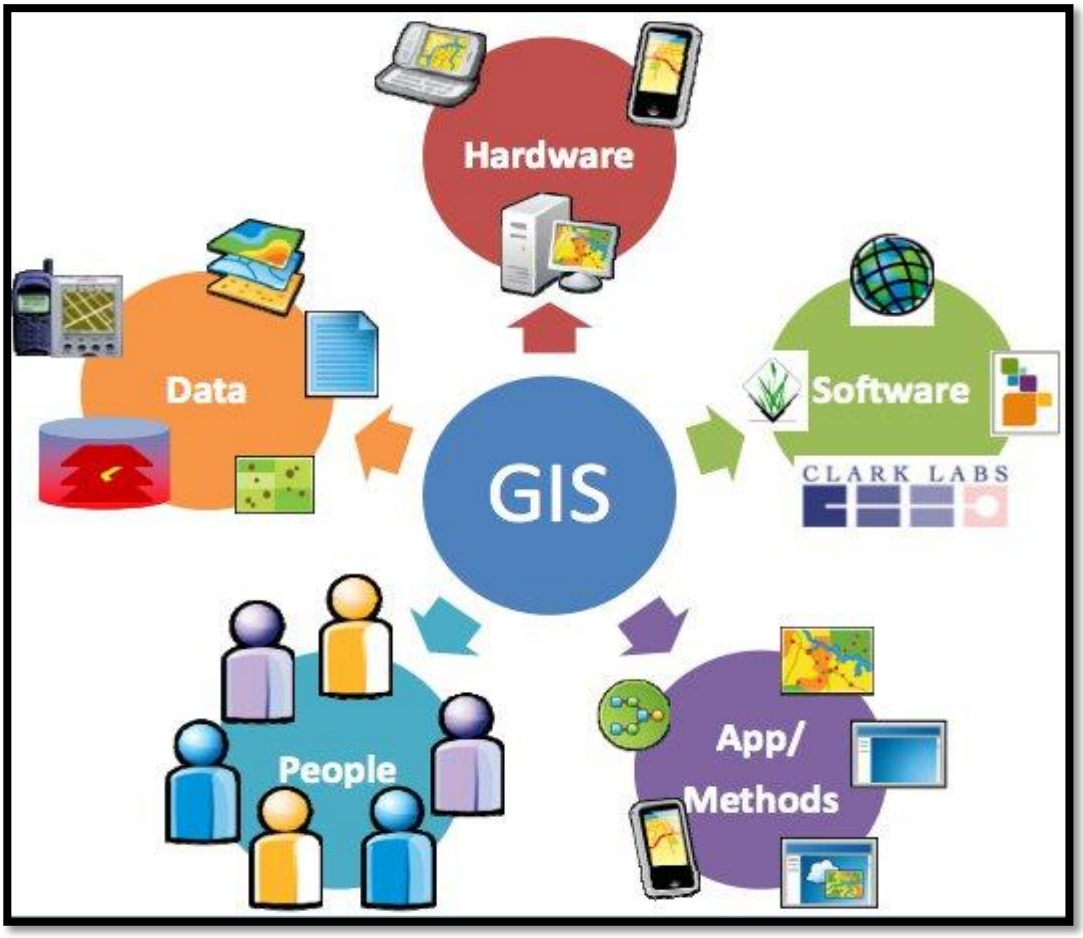

Figure (1-9): The element of GIS [69].

- **Hardware:** The machine on which a GIS runs is called hardware. A broad variety of hardware, including stand-alone PCs, networked desktop

computers, and centralized computer servers, can run GIS software. Hardware refers to consumer electronics like scanners, plotters, and graphic devices. An assortment of processors is used for data storage and manipulation. The range of hardware options includes supercomputers and personal computers with 300 MHz. The computer, which is the heart of the GIS hardware, receives input from a digitizer board or a scanner. A scanner turns a physical image into a digital one for processing. Scanner output can be stored in a variety of formats [70].

- **The software:** GIS programs equip users with the means for gathering, analyzing, and displaying geographical data. Analyzing, and displaying spatial information. The foundational components of GIS software include [71].

- Instruments for entering and modifying geographic data
- Database management system, (DBMS).
- Applications that facilitate geographic analysis, visualization, and query
- An easy-to-use graphical user interface (GUI) for utilities

- **Data:** The data are the backbone of every geographic information system. You can collect geographic information on your own, or you can purchase it and related tabular information from a commercial data provider. The GIS can take advantage of a database management system (DBMS), which is used by most enterprises for data administration and storage, to link spatial data to other data sources. One of the main obstacles to GIS adoption is the expense of collecting and storing relevant data. All GIS information consists solely of either geographic information or attributes details [72].

- **People:** GIS technology would be of limited utility and ineffectual without the people who manage the system and establish plans for using it to solve problems in the real world. The Geographic Information System (GIS) has a wide variety of users, from the technical professionals who build and maintain the system to the regular folks who rely on it to get their jobs done.
- **Methods:** A good GIS follows business rules, or the models and operating procedures unique to each company, developed after careful consideration. GIS stands for Geographic Information System and is the method through which people formally measure geographical processes and events. To better illustrate geographical themes, entities, and relationships, represent them in a computer database .Utilize these representations to generate more measures and find novel associations by fusing several data sources .Transform these representations to match other entity and connection frameworks [73].

1.12 The Landsat

The first Landsat satellite is successfully launched by NASA in 1972, and since then, five more have been launched. Since the 1990s, NASA has been responsible for manufacturing and launching the satellites, while the U.S. Geological Survey (USGS) has supervised the missions. Despite providing a near-constant record of images, the Landsat program is plagued by variations between satellites and sensors that make it difficult for both specialists and the general public to use the data [74]. Landsat (1–3) are equipped with the Multispectral Scanner (MSS), which captured data in four spectral bands (two visible and two near-infrared). After the MSS, the next series of satellites, Landsat 4-7, carried sensors with higher radiometric resolution and spatial resolution (i.e. pixel size)

that is superior to that of the MSS. This category's spectral range is widened by the addition of mid- and thermal-infrared-operating bands. Shortwave infrared (SWIR) replaces the older term "middle infrared" (NIR). The relevant Landsat bands are located inside the region where the spectral ranges of middle-infrared and shortwave infrared (SWIR) overlap. For these reasons, we have decided to employ SWIR[75]. Landsat 8, with its thermal infrared sensors (TIRS) and operational land imagers (OLI), is currently part of the third class. A second thermal band is added by TIRS, but the spectral resolution of the TM array is improved by OLI, which also includes a dark blue band and a cirrus band. The sensors and calibration methods used by these devices are also vast improvements over those used by past Landsat missions. Landsat 9, the third member of the group, and a reconstructed version of Landsat 8 are both scheduled for release in 2020 and 2021, respectively as shown in Figure (1-10).

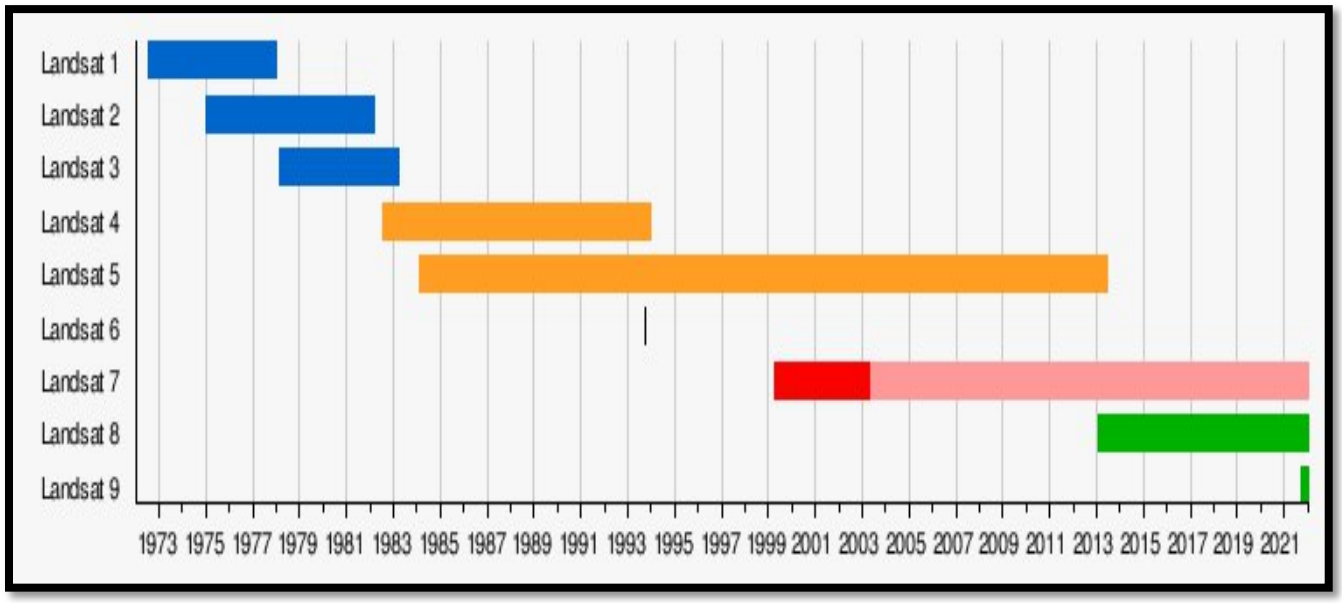

Figure (1-10): Landsat Program history and importance [76].

1.12.1 The Landsat 8

The Landsat 8 covers the Operational Land Imager's (OLI) measurements of nine spectral bands in the visible and short-wave infrared spectrum. It is complemented by a Thermal Infrared Sensor (TIRS) [77]. The major objective of the Landsat 8 mission is to continue recording future Landsat and to provide continuity of observation, so that data from Landsat 8 may be reliably compared to data from earlier Landsat systems. Operational Land Imager (OLI) measurements span nine different spectral bands, from visible to short-wave infrared. The last component is the Thermal Infrared detector or TIRS for short [78]. In order for the data from Landsat 8 to be consistent and comparable with those from earlier Landsat systems, the fundamental goal of the Landsat 8 mission is to keep collecting data and making observations into the future. Landsat supplies the worldwide data and information needs of the NASA Earth Science program in order to improve climate, weather, and natural hazard prediction. The goal of Earth Science is to increase scientific understanding of the Earth system and how it reacts to both natural and human-made disturbances [79]. Landsat 8 is a scientific mission, unlike previous Landsat systems. Without an operational purpose. This specifically indicates that there won't be a quick switch to another Landsat if the existing Landsat 8 equipment malfunctions.

- **Landsat 8 sensor overview**

On February 11, 2013, Landsat-8 is launched into space with two new Earth imaging sensors to complement the previous Landsat's continuous data record. Push broom technology is used for Landsat-8.Moreover, the thermal and reflecting scopes are separated into their own devices. An operational land imager (OLI) is a thermal and reflective range sensor. Is a thermal infrared sensor Bands have been added, spectral band passes have been enhanced, and dynamic range and

data quantization have been increased, among many other enhancements, in addition to these core modifications. As with all previous Landsat missions, NASA and the United States Geological Survey (USGS) jointly developed, launched, and managed the Landsat-8 project. Instrument and data characterization and calibration were essential components of this partnership. This special issue describes the combined USGS-NASA calibration teams and its affiliates' efforts to describe new sensors and their data for scientific and practical Landsat archive users. The TIRS only has two spectral bands (10 and 11), but the OLI sensor has (1-9) .The TM and ETM+ sensors work with seven different OLI frequencies (from 2 to 8). Two of these are the 1st and 9th bands. New spectral bands that increase cirrus cloud identification and water resource assessment and coastal region realization, respectively. Evapotranspiration rates for water management can be determined with the help of thermography imaging of TIRS activities [80].

Table (1-2): The characteristic of bands which observed by the sensors [81].

Band	Resolution(m)	Wavelength(µm)	Description	Sensor
1	30	0.43 - 0.45	Coastal/Aerosol	**Operational Land Imager(OLI)**
2	30	0.45 - 0.51	Blue	**OLI**
3	30	0.53 - 0.59	Green	**OLI**
4	30	0.64 - 0.67	Red	**OLI**
5	30	0.85 - 0.88	Near Infrared	**OLI**
6	60	1.57 - 1.65	Short wave Infrared	**OLI**
7	30	2.11 - 2.29	Short-wave Infrared	**OLI**
8	15	0.50 - 0.68	Panchromatic	**OLI**
9	30	1.36 - 1.38	Cirrus	**OLI**
10	100	10.6 - 11.19	Thermal Infrared	**Thermal Infrared Sensor(TIRS)**
11	100	11.50 - 12.51	Thermal Infrared	**TIRS**

➢ **Band types for Landsat 8 [82].**

- **Band (1):** Near coastal areas, a blue band (range 1) is used to measure the color of the water. The chlorophyll concentration, or ocean color, will be measured in coastal areas by means of this scope. Dubbed the Coastal/Aerosol, it has a wavelength range of 0.433 to 0.453 m with a resolution of 30 m.
- **Bands (2, 3, 4):** Bands 2, 3, and 4 are blue, green, and red, respectively. (Visible) is the name of these bands. These bands have wavelengths between 0.45 and 0.515 m, 0.525 and 600 m, and 0.630 and 0.680 m, respectively; their resolution is 30 m.
- **Band (5):** Because the water in healthy plants' leaves scatters the Near Infrared (NIR) wavelengths back into the atmosphere, this region of the spectrum is unique and crucial for researching ecology. The NDVI values indicate the health of the plants more accurately than their apparent greenness when the NIR is contrasted with other bands. Band (5) has a wavelength of (0.845-0.885) m with a resolution of 30 m.
- **Bands 6 and 7:** These bands cover several SWIR (Short Wavelength Infrared) slices. They are notably helpful for geology (rocks and soils that appear identical in other bands frequently and show strong contrasts in (SWIR)) and for separating and studying soil from dry soil. These bands have a resolution of 30 m and cover wavelengths (1.560-1.660 m, and 2.100-2.300 m, respectively).

- **Band 8:** Black and white bands called panchromatic bands mix the energy of the visible spectrum. The photos are sharp, with a

resolution of 15 m, as collated aids in more light collection. These are employed to pan brighten lower resolution images, and the wavelength range for this band is from 0.500 to 0.680 m.

- **Band 9:** Satellite photos make it difficult to see thin high clouds. The shadows cast by the clouds and the clouds themselves can skew measurements. Band 9 of OLI's new shortwave infrared sensor will be able to detect cirrus clouds more accurately than earlier Landsat instruments because of the way it analyzes light. The wavelength for this band is (1.360 - 1.390) m, and the resolution is 30 m.

- **Band 10, 11:** The temperature of the ground itself is measured using thermal infrared (TIR) bands. Urban heat islands can be located by analyzing these bands. Both bands exhibit a stripping effect; however band (11) exhibits greater value instability than band (10). Both bands have a resolution of 100 m and have wavelengths between 10.30 and 11.30 and 11.50 and 12.50 m, respectively.

1.13 The Study Area

In the current study, the spatial distribution of LST in the Babylon province has been examined. The latitudinal and longitudinal extensions of Babylon are 32° 06′ N to 33° 08′ N and 43° 57′ E to 45° 12′ E, respectively. Babylon is located in the middle of Iraq, as shown in Figure (1-11). The city is about 37 meters above sea level. The total area of Babylon is about 5119 km^2. The climate of Babylon governorate is predominantly desert, with minimal annual precipitation and high summer temperatures that sometimes approach 50 C^o. While warm weather

prevails in the dead of winter. Summertime (July and August) and wintertime (December and January) are the warmest and coldest months, respectively.

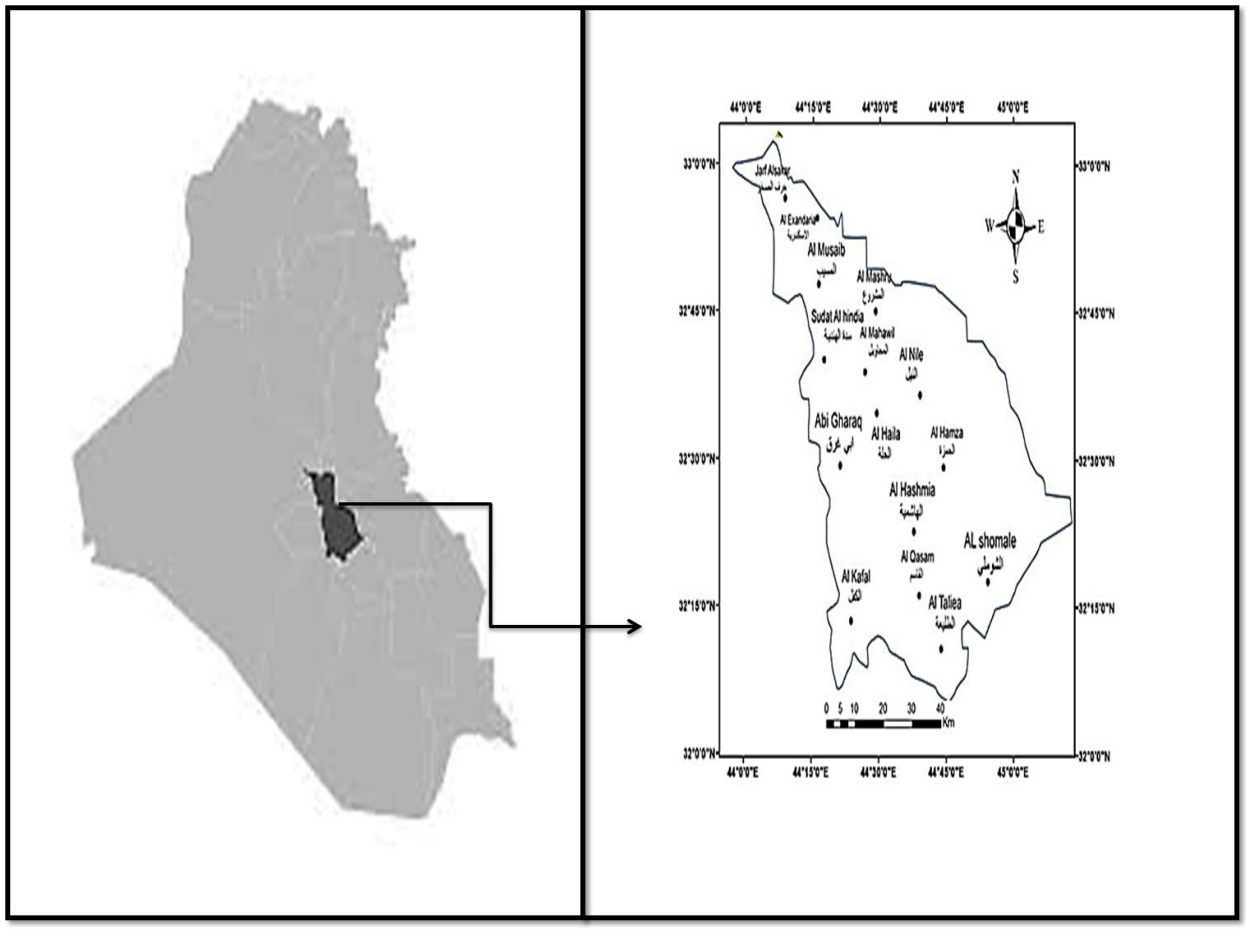

Figure (1-11): The map of Babylon government that shows all the important regions.

1.14. Steps to Calculate the Land Surface Temperature (LST)

1. In order to get Spectral Radiance L (ʎ) readings from a sensor, first plug the DN values into the following equation [83].

$$L\lambda = M_L * B10 + A_L - Oi \qquad \textbf{(1-6)}$$

Where

L (ʎ) = Spectral radiance.

$\mathbf{M_L}$ = Radiance multiplicative band.

$\mathbf{A_L}$ = Radiance add band.

$\mathbf{O_I}$ = Correction Value.

2. Converting radiance to brightness temperature (BT) by using the equation below [83].

$$BT = K_2/(ln\, K_1/L_\lambda + 1) - 273.15 \qquad \textbf{(1-7)}$$

Where

K1,K2 = Constant for band .

(273.15) = to conversion of (BT) in Kelvin to Degree Celsius scale.

3. Use the following formula to determine the Normalized Difference Vegetation Index (NDVI) in section (1.11).

$$NDVI = (NIR - RED)/(NIR + RED) \quad \textbf{(1-1)}$$

Where

Infrared (NIR) = Band 5 RED =Band 4

4. Calculating the percentage of plant life (PV) with the help of the given equation [84].

$$PV = \left(\frac{NDVI - NDVI_{Min}}{NDVI_{Max} - NDVI_{Min}}\right)^2 \quad \textbf{(1-8)}$$

5. Determination of ground emissivity (E) by using the equation below [85].

$$E = 0.004 x P_V + 0.986 \quad \textbf{(1-9)}$$

Where

0.004= is the standard deviation.

P_v =is vegetation percentage (vegetative variation value).

0.980= Average radiation power.

6. Estimate LST by using the equation below [86].

$$LST = \frac{BT}{\left(1 + \frac{\lambda BT)}{\rho} ln\, E\right.} \quad \textbf{(1-10)}$$

Where

λ = Wavelength of emitted radiance equal =11.5μm
ρ= h x c /σ = (1.438 x 10^{2} (m K)).
h=Planck constant (6.626x 10^{-34} (Js)).
C=Light's speed (2.998 x 10^{8} (ms^{-1})).
σ = Boltzmann constant (1.380649x 10^{-23} (JK^{-1})).

1.15 Urban Heat island equations

1.15.1 The following equations is used to determine UHI and non-UHI [87]

$$\mathbf{LST} > \boldsymbol{\mu} + \mathbf{0.5} * \boldsymbol{\delta} \qquad \textit{(1-11)}$$

$$\mathbf{0} < \mathbf{LST} \leq \boldsymbol{\mu} + \mathbf{0.5} * \boldsymbol{\delta} \qquad \textit{(1-12)}$$

Where

The mean LST and standard deviation for the study area are denoted by μ and δ, respectively.

1.15.2 Urban Hot Island (UHS)

The formula used to determine these spaces is as follows [88]:

$$\mathbf{LST} > \boldsymbol{\mu} + \mathbf{2} * \boldsymbol{\delta} \qquad \mathbf{(1\text{-}13)}$$

Where

μ and σ represent the mean value and standard deviation of the LST.

1.15.3 Urban Thermal Filed Variance Index (UTFVI)

The formula used to determine these spaces is as follows [89].

$$\mathbf{UTFVI} = \frac{\mathbf{T_s} - \mathbf{T_{mean}}}{\mathbf{T_{mean}}} \qquad (\mathbf{1-14})$$

Where

T_s represent the LST in (C°). T_{mean} refers to the mean LST in (C°). UTFVI represents the variance index for urban thermal fields.

1.16 Literature Survey

- **Li *et al.*, 2013 [90].** In this work, various existing remote sensing techniques for deriving LST from thermal infrared data are assessed. DATUM (TIR). A brief theoretical introduction is provided, as well as a summary of the algorithms that can be used to get LST. The topic centers on TIR data received from polar-orbiting satellites because of its extensive use, worldwide applicability, in addition to better spatial detail compared to geostationary satellites. The techniques for confirming the LST derived from satellites are next studied, after which the theoretical basis and methodology for calculating the LST from the data are discussed. After that, satellite-derived LST is made more precise, and new areas of study are suggested.
- **Juanc *et al.*, 2014 [91].** Methods for using data from Landsat-8 Thermal Infrared Sensor to determine surface temperature. The surface temperature may be determined with a high degree of accuracy using the sensor's data, which is useful in many environmental sectors. In this thesis, they use Landsat-8 TIRS data with SC and SW methods to get LST. They test the algorithms using simulated data from partner foreground operations, emissive spectra that have been gathered, and databases of the side part of the atmosphere. From the spectral archives, extracted. The data also demonstrate that the error rate is often less than 1.5 K for both the SC and SW algorithms, with the SW algorithm achieving better outcomes when compared to the SC algorithm, which is also followed a rise in atmospheric water vapor.

- **Al-Timimi *et al*., 2014 [92].** This research used ETM+ sensor thermal band. Using Landsat 7 satellite and ERDAS 8.4 program to estimate LST for multiple regions in Iraq. Thermal images are used to create temperature-based maps of the landscape. Land surface temperatures in the stations of Al-Basrah, Al-Mousl, ,Taleafer, Al-Ramadi, Heet, Kerbela, and Al-Hai are all within the scope of this statement. From 29.7 to 31.8 degrees Celsius, or 17 to 17.8 degrees Fahrenheit, according to data. And 20.6 to 30.2 C°., respectively. Estimated and observed values are proven to be highly correlated, with a variance of only (1-2) C°.
- **Orhan *et al*., 2016 [93].** Utilizing six Landsat images from 1984, 2011, and 2014, researchers examined the multi-temporal LST and NDVI changes in Konya, Turkey. The findings indicated that the basin's surface temperature rates grew by roughly 5°C throughout the extended period of time between 1984 and 2014.
- **Feng *et al*., 2016 [94].** They looked at how different types of adjacent land cover affected the temperature of various construction materials' exteriors. The LST pattern study considered the different types of building heights as well as the surrounding land cover when drawing conclusions. Topography and vegetation affected a building's land surface temperature.
- **Mushore *et al*., 2017 [95]**. They sought to determine how the microclimate influenced changes in land use and land cover (LULC) in the diverse Harare Metropolitan City, Zimbabwe, between 1984 and 2015. This goal will be accomplished through the transformation of major.
- **Salih *et al*., 2018 [96].** Suggested a method for deriving the LST in Babil, Iraq, by combining information from the satellite's two thermal bands. Two images are utilized to determine LST and compare it to data gathered on the

ground with an infrared thermometer camera. The results show that water has a higher LST value than other land cover types.

- **Beg, 2018 [97].** Conducted a study on Rusafa (Baghdad, Iraq), where the population is growing, which has caused a deterioration in municipal services and an increase in LST. Using ERDAS software and several dated satellite pictures, the regional temporal variance of LST. is evaluated The increase in built-up area by 23% and the decrease in open space and vegetation cover by 16% and 6% respectively, suggest that the environment of the study area is likely to be warmer.
- **Anna Maria Jönsson *et al*.,2019 [98].** The observable land surface temperature (LST) in the research area from 2000-2016 is compared to NDVI measurements to determine the accuracy of the LST calculation.The magnitude of the UHI for the time period was calculated, as is the spatial distribution and direction of the LST. With Global Moran's I index values larger than 0.6 and standardized scores greater than 220 in all cases at p 0.001, the results reveal a statistically significant variation of LST values throughout all inquiry periods. After explaining between 50% and 71% of the variance in the LST between 2000 and 2002, the NDVI became a less significant explanatory variable for the LST in 2016, accounting for only 29% to 49% of the variance. Seasonal and annual regression coefficients The negative NDVI results for the study area show that NDVI has a negative correlation with LST. The search revealed a decrease in UHI density from the beginning of the wet season until the end of the dry season.
- **Suroor Fawzy Najy *et al*.,2021 [99].** Emissivity calculated using normalized difference vegetation index**.** Images from the USGS website that houses the ETM+ sensors, OLI) from the cloud-free Landsat 7 and Landsat 8 are used for this. The study region (University of Baghdad) has

been cropped from photographs once they are geographically recognized. To estimate the LST for the winter and summer seasons, Landsat photos underwent pre-processing. In addition, the fieldwork is completed over the course of four days: February 4, 2020, February 12, 2020, July 29, 2020, and August 6, 2020. 12 data points are collected for four different types of land: dirt, asphalt, vegetation, and construction. The study compares the appropriateness of Landsat 7 and Landsat 8 thermal accuracy bands for measuring Earth's surface temperature. The findings demonstrate that (LST) depends on Landsat 8 photos for band 10 and band 11/winter and summer. When combined with terrestrial data, the error range for Landsat 8 band 10 for winter and summer is (0.4-0.7) and (0.7-1.4), respectively, while winter and summer straight errors for range 11 are (0.9-1.9) and (1.8-2.4), respectively.

1.17 The Aims of the Project

1. Calculate the land surface temperature by using Landsat 8 for each Season for Babylon Governorate in 2022.
2. Collect information about climate parameters from meteorological stations in Babylon Governorate.
3. Using NASA's Power Project website as inspiration, we are create a network of virtual weather stations for Babil Province.
4. Calculate the values for the urban heat island index (UHI), non-urban heat island index (non-UHI), urban hotspot index (UHS), and urban heat field variation index (UTFVI).

CHAPTER TWO

THE DATA AND IMAGE PROCESSING

2.1 Introduction

In this chapter, I will talk about the methods through which data will be obtained. In my scientific research, data are obtained from three sources:

1. The Landsat 8 satellite

2. Babel meteorological station

3. Power NASA website

Each of these data requires different steps to be completed.

2.2. The Method

The steps for obtaining data and how to benefit from it in my research and linking each other are summarized in the following chart (2-1):

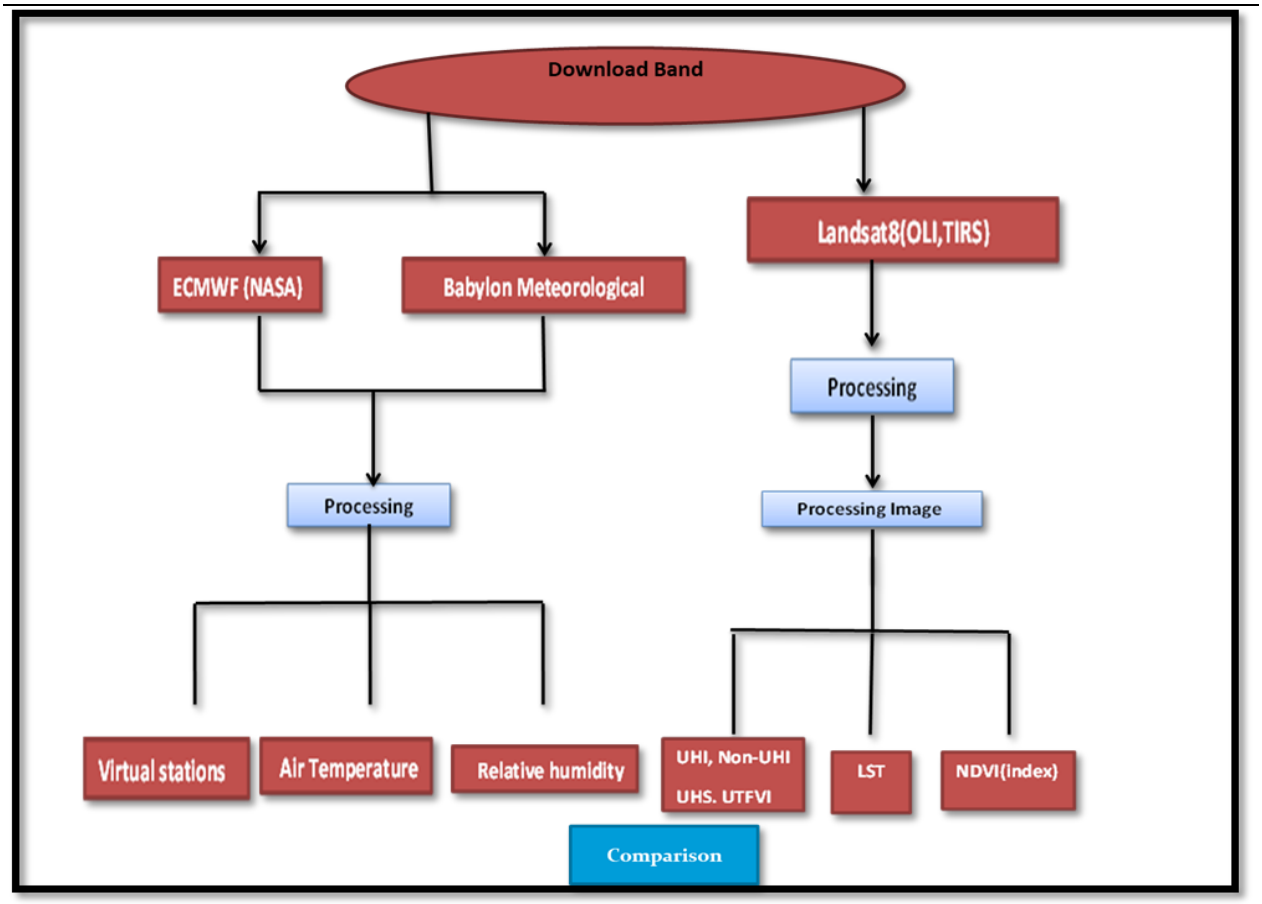

Figure (2-1): The methodology of research.

2.3 The Landsat 8 satellite Data

Two Landsat 8 sensors—operational (OLI) and thermal l infrared sensor (TIRS)—provided LST spatial distribution data. The used bands are Red and Near Infrared (band 4, band 5) from OLI and Thermal Infrared (band 10) from TIRS. These bands are available at the United States Geological Survey (USGS) as images. The USGS is a government website that provides accurate scientific data about detailed information of the earth and this data is free.For example, knowing information about natural disasters that leads to reducing the losses that can occur, as well as providing information that enables us to know geology, mineral resources and

water resources. This information will lead to many improvements in our lives. According to the objectives of the study, Landsat images are downloaded for the months of January, April, August, and October (winter, spring, summer, autumn). For the year 2022 and transfer it to a Universal Mercator (UTM) projection and supplied as floating point power values in Geo TIFF format. Babylon administrative boundary polygon has been downloaded, the polygon is used to visualize the study area on the ESRI-ArcGIS base map, as well as for cropping Landsat data for further analysis [100]. The red, green and blue (RGB) bands are configured from Landsat the Earth's surface temperature is used. LCLU is rating has been highly meticulously verified data obtained from Google Earth images.

2.4 Steps to Download Data from United States Geological Survey (USGS)

1. The first step is to go to the data portal by creating an account on the site (https://earthexplorer.usgs.gov/). Figure (2-2) shows the site of the USGS.

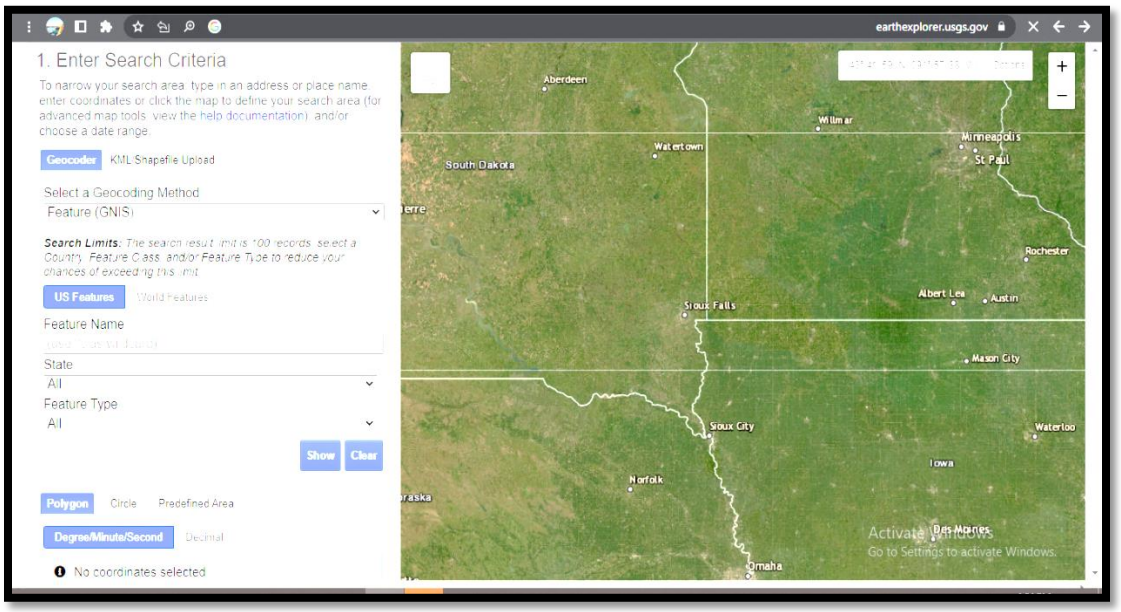

Figure (2-2): The main interface of the website.

2. This phase involves looking for the area to be worked using a website box, utilizing coordinates, or guessing the map's breadth.
3. The next stage, the date range is determined, i.e. the date required to make a specific measurement is added in terms of (year / month / day) .
4. Determine cloud cover by reducing the effect of clouds, to produce a clearer image free of impurities. It is preferable to reach a percentage of clouds that is within (10-20%).
5. Determine the satellite identification according to the requirements of scientific research.
6. The last step is to click on (the results) and I will get several pictures that can be chosen from what suits the coverage of the entire area to be worked on, and sometimes it requires two scenes in order to cover the entire area.

The downloaded Landsat 8-9 OLI/TIRS satellite bands (red, near infrared and thermal infrared) with data specification was listed in Table (2-1) for Babylon governorate.

Table (2-1) : Landsat 8-9 Satellite OLI/TIRS bands (red, near infrared and thermal infrared) with data specification for Babylon governorate.

Season	Scene	Path/Row	The Dates	Scan-time	Sun-azimuth	Sun-elevation	Datum /UTM Zone
Winter	1	168/37	2022-01-24	07:33:47.34	152.30	32.65	WGS84/38
	2	168/38	2022-01-24	07:34:11.23	151.56	33.80	WGS84/38
Spring	1	168/37	2022-04-30	07:33:23.79	129.13	63.60	WGS84/38
	2	168/38	2022-4-30	07:33:47.68	126.34	64.29	WGS84/38
Summer	1	168/37	2022-08-12	07:33:48.05	125.98	62.45	WGS84/38
	2	168/38	2022-8-12	07:34:11.95	123.26	63.07	WGS84/38
Autumn	1	168/37	2022-10-23	07:34:13.49	156.52	42.38	WGS84/38
	2	168/38	2022-10-23	07:34:37.38	155.61	43.59	WGS84/38

2.5 Pre-processing Data

2.5.1 Introduction

Landsat 8 satellite image data are pre-processed with applied radiometric adjustment as research data. The goal of radiometric adjustments is to improve the accuracy of information obtained from satellite imagery data by reducing and correcting errors caused by surface reflectance, sunlight direction, weather, turbulence, and other factors. Multi-temporal analysis is yet another application of correction. The understanding and detection of continuous changes using multisensory data to calculate radio metrically using the tools in the arc map correction can be made.

2.5.2 Step Preprocessing

The treatment that took place is four stages, as shown in the diagram below (Figure 2–3):

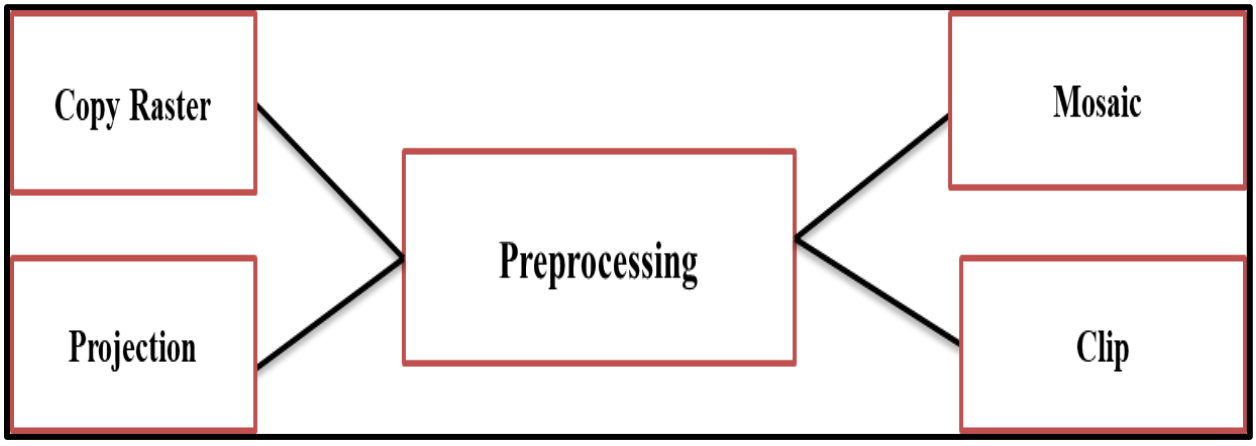

Figure (2-3): Pre -Processing steps applied on the downloaded data.

All the following current steps and images are for Band 4(B4) for the summer season. The following four pre-processing steps are applied on the other bands (B5

, and B10), and the data of the other seasons (winter, spring, and autumn) are treated in the same procedures.

2.5.3 The data Reduction of the Summer Season

- **Mosaic Process**

This step of processing will be done if the required area cannot be covered with one scene, as two or more files are required according to the area of the study area. In the Babylon Governorate case, the Mosaic technique is utilized to combine the two usable data files into a single non-separate data file, which is one tool in arc map. The used instructions in arc map are shown in the Figure (2-4).

Figure (2-4): Instructions to complete the mosaic step.

Some changes are made to maintain the formats between the two data files, where the data is mobilized as a TIFF file to maintain harmony between the two data files, as well as making the UTM Zone 5N projection to insert the panels between the vertical and horizontal axis, and making the pixel type 16 to stay on the same format as shown in the Figure (2-5).

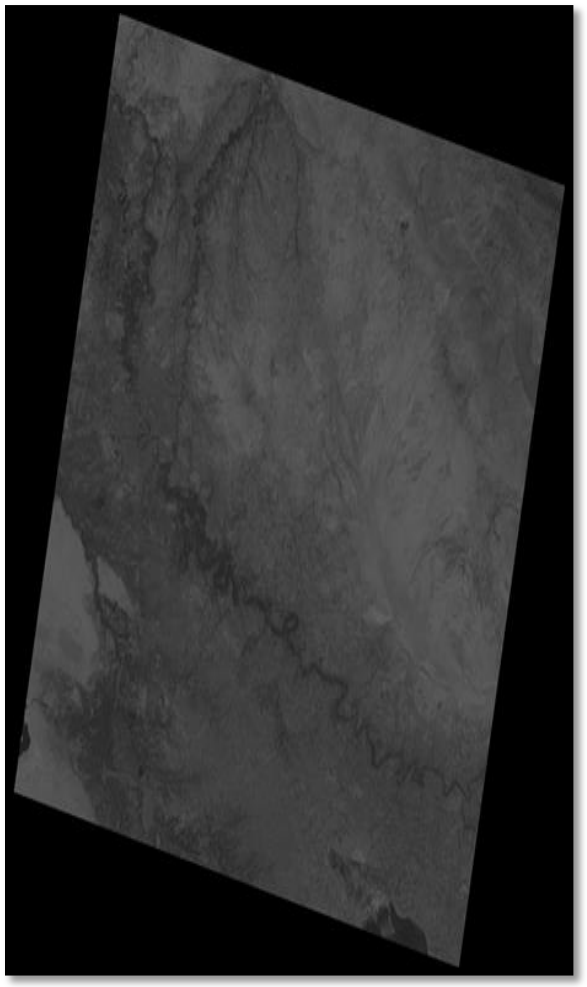

A B

Figure (2-5): (A) Scene data file 1. (B) Scene data file 2.

After the mosaic process, the province of Babylon will turn into one data file covering the entire province. As it presents as seen in Figure (2-6) below.

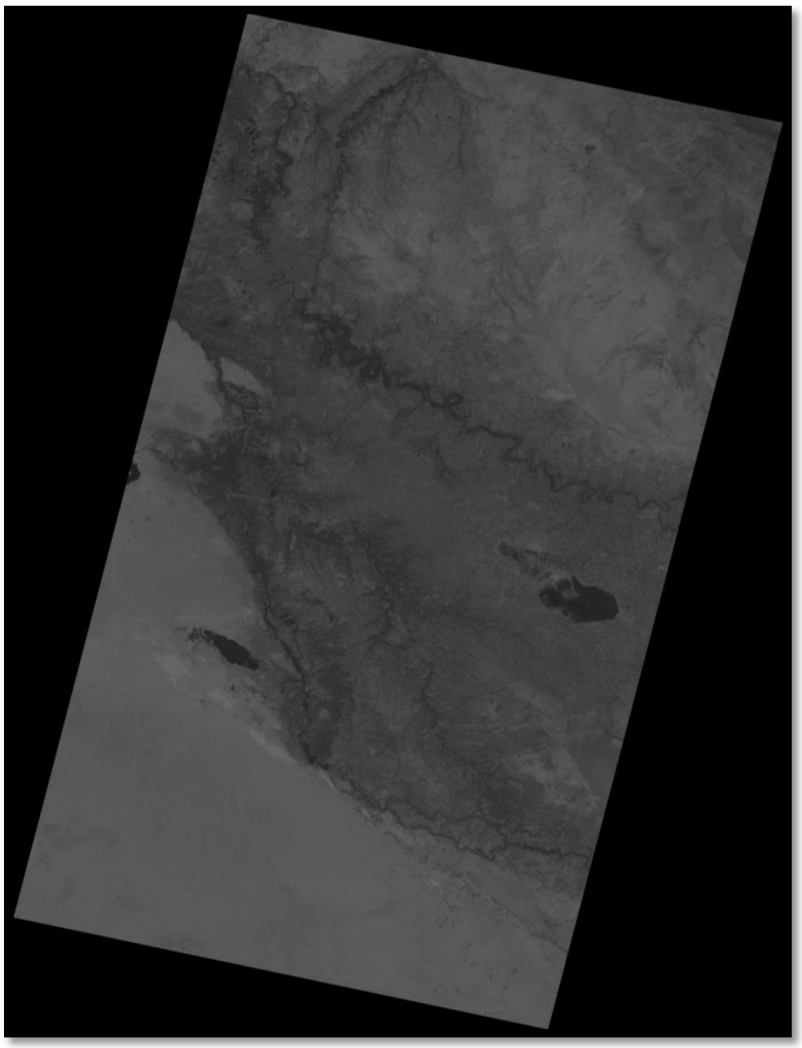

Figure (2–6): Summer mosaic image.

- **The Clip Process**

Before doing the next step of processing ,a necessary step must be done to obtain accurate data, which is the step of eliminating the back ground value shown to us in the data because when performing calculations, the value of the background data will be calculated, which is not required in our calculations. This is done in the following steps as shown in the Figure (2-7).

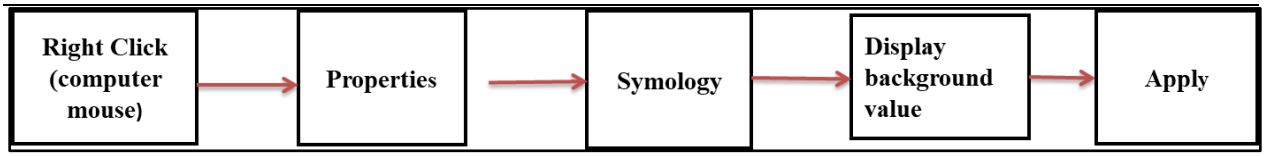

Figure (2-7): The final steps to erase background value.

And that after this step comes the next processing step, called Clip process, which is very important because it will show us the areas surrounding our study area when you download the area data file and when you take the mosaic step and affect the value of the accounts, even though we don't need it because it doesn't belong to our study area. In order for this step to be completed, the Shape File of Babylon Governorate (our study area), which I prepared, must be prepared. Figure (2-8) displays the image following the clipping procedure.

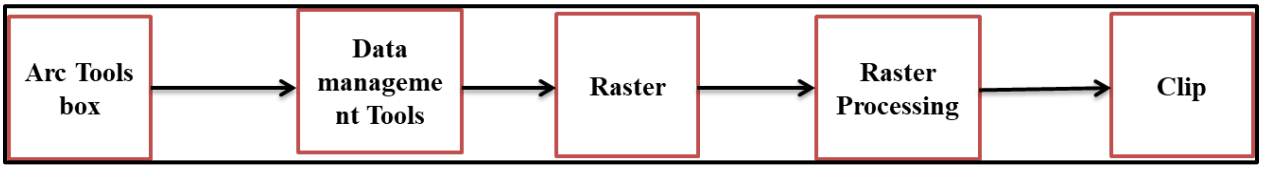

Figure (2-8): Guidelines for the clipping procedure.

Figure (2-9): The image of the Babylon Governorate after the clip process for the summer season.

- **The Projection Process**

The information displayed under the data source indicates that the coordinate system depends on the UTM projection, so changing the projection of the area or defining the projection is a crucial step. If the projection does not already contain coordinates, the coordinates will be defined as shown in the Figure (2-10).

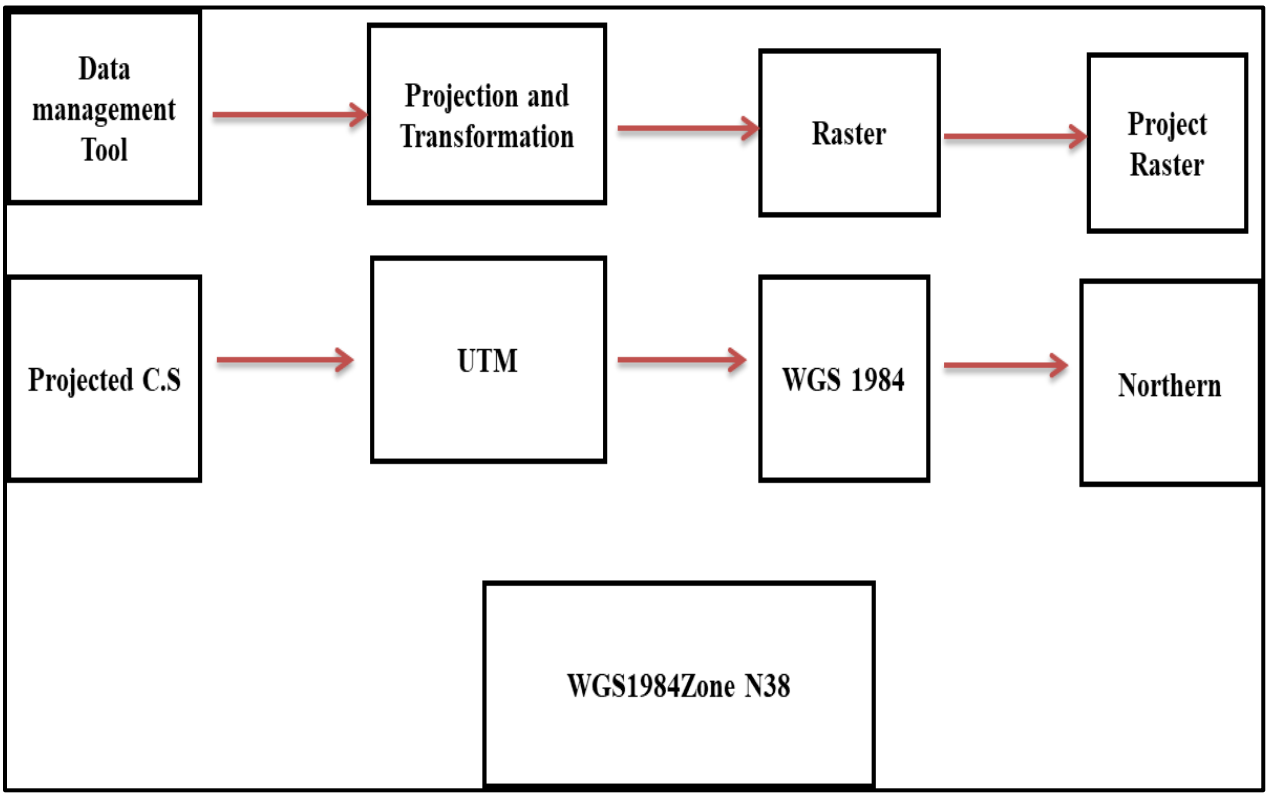

Figure (2-10): Instructions to full Projection the step.

Figure (2-11): The Babylon province map after applying the projection process for the summer season.

- **The Copy Raster Process**

The last step of the processing is called copy raster, and the benefit of this step is to get rid of the random values in the data, and when this step is completed, the data becomes ready to calculations. The used tasks in Arc GIS are shown in Figure (2-12).

Figure (2-12): Instructions to complete the copy raster process.

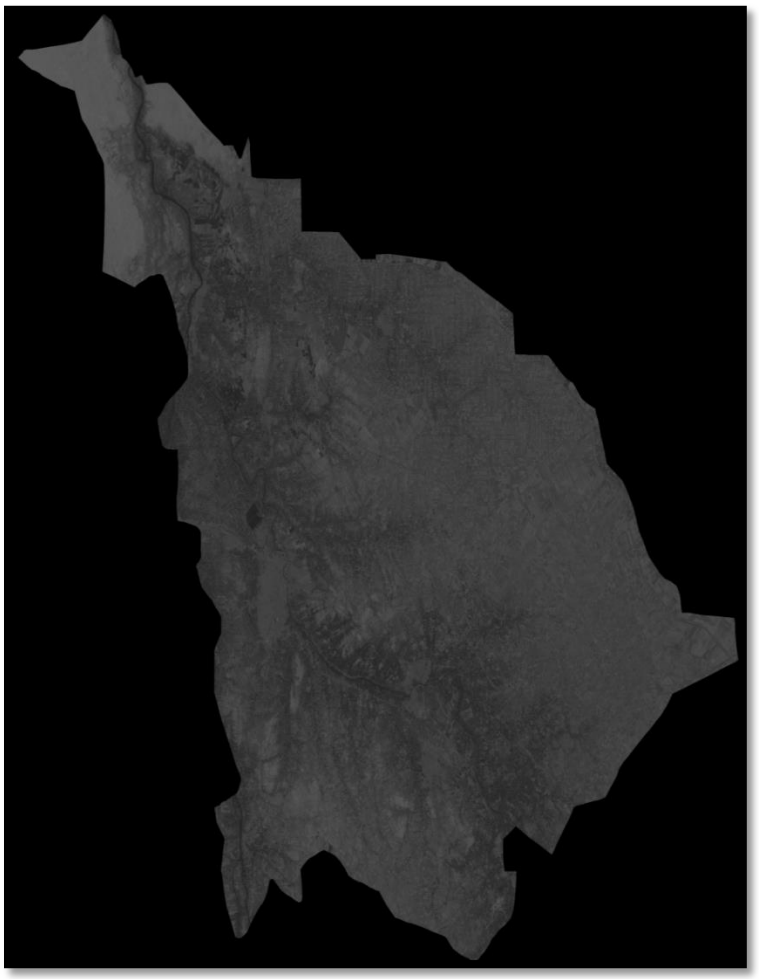

Figure (2-13): Babylon Governorate after performing the copy raster step for the summer season.

2.6 The Climate Elements

2.6.1 The Babel Meteorological Station

The climate elements are collected from the meteorological station, which located in the center of Babylon governorate, which has been in service since 1979 and closed in 1983. The site of the station is located at latitude 32.27º and longitude 44.27º. German and Italian businesses (Kassala and Siyab, respectively) are two of the companies that offer approved measurement devices.

The thermometers are used to measure the temperature. As for the sensors, they are for automatic stations, while the rain is measured with a measuring cylinder and automatic measurement. It is monitored (24) hour every three hours, and eight reports are sent to Baghdad, the recorded data start usually from three o'clock in the morning. In addition to the station of Babylon, there are different stations (Karbala, Ain Tamr, Nakheeb, Diwaniyah, Najaf, Samawah, Salman and Al-Hay) in Iraq, each one at 40 km from the other one to record the international measurements. The recorded climate elements in these stations are rain, clouds, winds, evaporation, and temperatures (maximum and minimum). All these elements are recorded in average daily and monthly.

The study included a large area represented by the province of Babylon. The meteorological station in Babylon is not sufficient to provide us with information about the climate for the whole province to examine the relationship between the LST and climate elements. Therefore, we went to find hypothetical climate stations based on data from the power NASA website. Ten virtual stations are built to cover all the study area.

2.6.2 The Power NASA Site Data

2.6.2.1 Introduction

As we mentioned earlier that the study area (Babylon governorate) is large and therefore it is not possible to deal with ground stations to measure weather conditions. There is only one ground station in the city of Babylon and it cannot reflect the weather in the entire province, but it is used for comparison, thus 10 virtual stations are chosen and shown in Figure (2-14). The Power NASA website provides a range of information about weather variables. NASA-POWER [101],

Meteonorm [102], and Solargis [103] are spatial information-based databases that provide solar radiation data for different places and time periods. The Power NASA website is used for this research to study the relationship between LST and air temperature and relative humidity. The POWER RNASA website was launched in 2003 for public support agricultural demands, renewable energy, and building energy efficiency. The SSE (Surface Meteorology and Solar Energy) is its source. Where the global energy forecast sources are dependent on satellite observations and NASA global solar data is displayed on a 1° x 1° grid of latitude and longitude to extrapolate values for surface insolation. The Solar radiation is calculated as the weighted average of net and cloudy intakes. When aggregated throughout the day, they produce the daily average flow. The POWE RNASA website provides data in different models such as, ASCll format having daily solar radiation. In this section, the measurements of climate components from virtual stations and the POWER NASA website will be introduced. The sole virtual station provides daily, yearly, and monthly climatic parameters like maximum and minimum temperature, relative humidity, rain, and wind velocity. Climate and weather are the biggest factors impacting agriculture, industry, and the environment.

2.6.2.2 Details about NASA Power

Daily, internal, and climatic temporal averages and single point, regional, and global coverage are available through the NASA POWER data access service (https://power.larc.nasa.gov/docs/v1/). A Single point endpoint that generates a time series based on the registered coordinates (one latitude and one longitude). Bounding box time series are available at the regional terminus. Weather parameters include near-surface air temperatures, relative humidity, precipitation, solar radiation, wind speed and direction. All averaged along with the maximum, minimum, mean, and dew point temperatures. It can be applied to a variety of

researches, including studies of climate variability and crop modeling. Many earlier types of research analyzed some global reanalysis data. NASA has created a meteorological dataset created from a model that includes daily maximum and lowest temperatures as well as the total solar radiation for the POWER database.

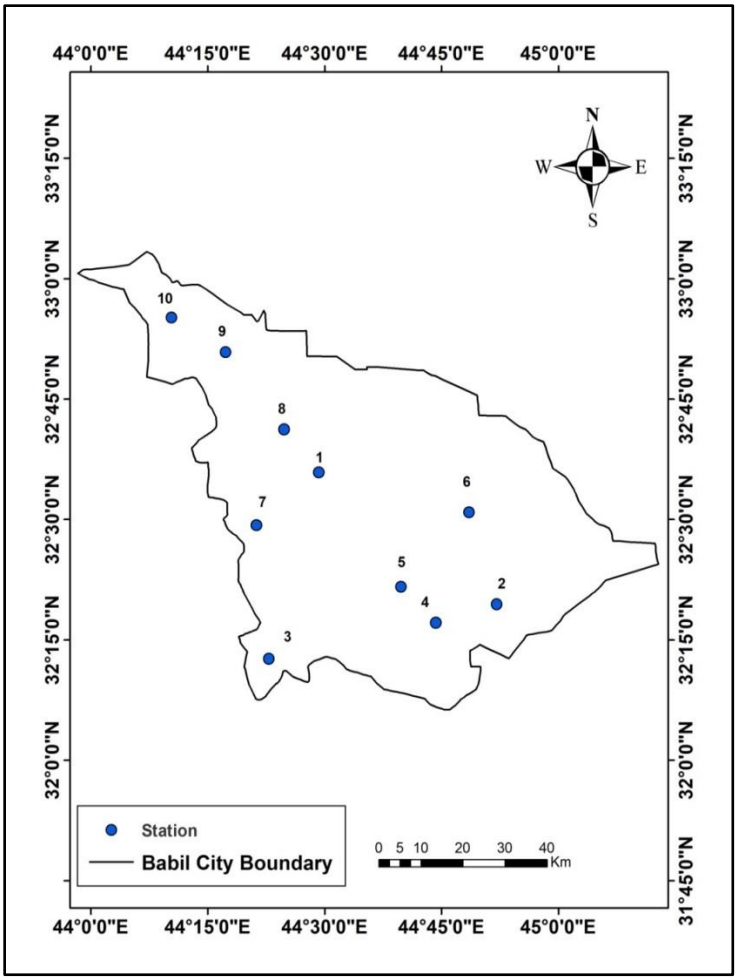

Figure (2-14): Where the virtual stations are located.

After locating the virtual stations we followed the following procedure to obtain the data.

- In this step we will enter the Power NASA website by this link (https://power.larc.nasa.gov/docs/v1/), and the website interface will appear as Figure (2-15).

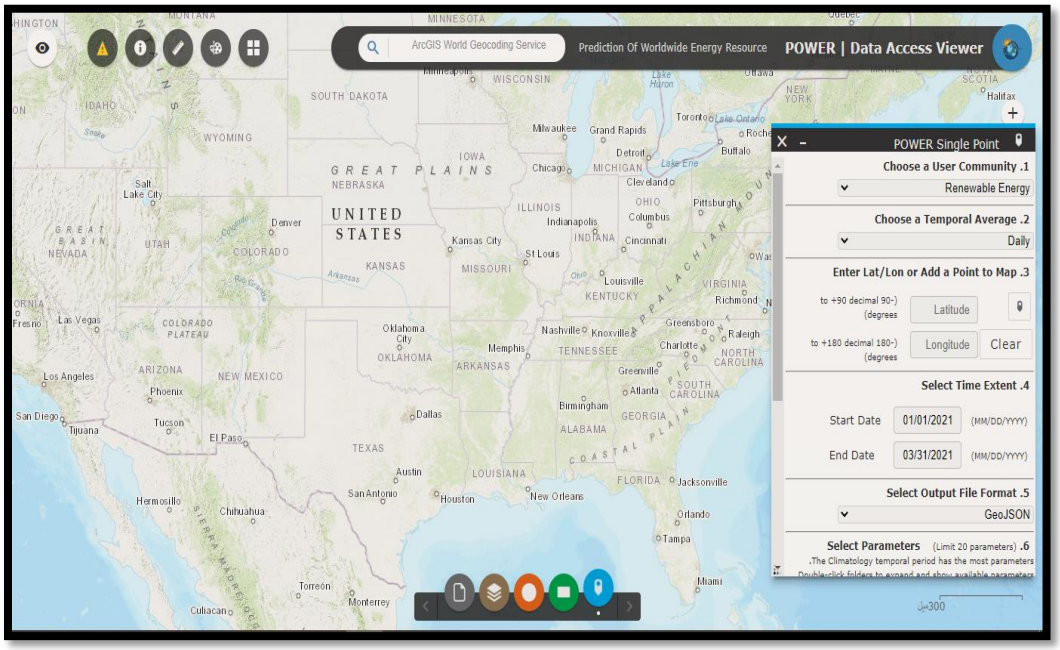

Figure (2-15): The interface of the POWER NASA website.

The next step will be to download the data (relative humidity, temperature, and precipitation, which are downloaded at a daily and monthly rate, as well as determine the latitude and longitude of the location as shown in the Figure (2-16).

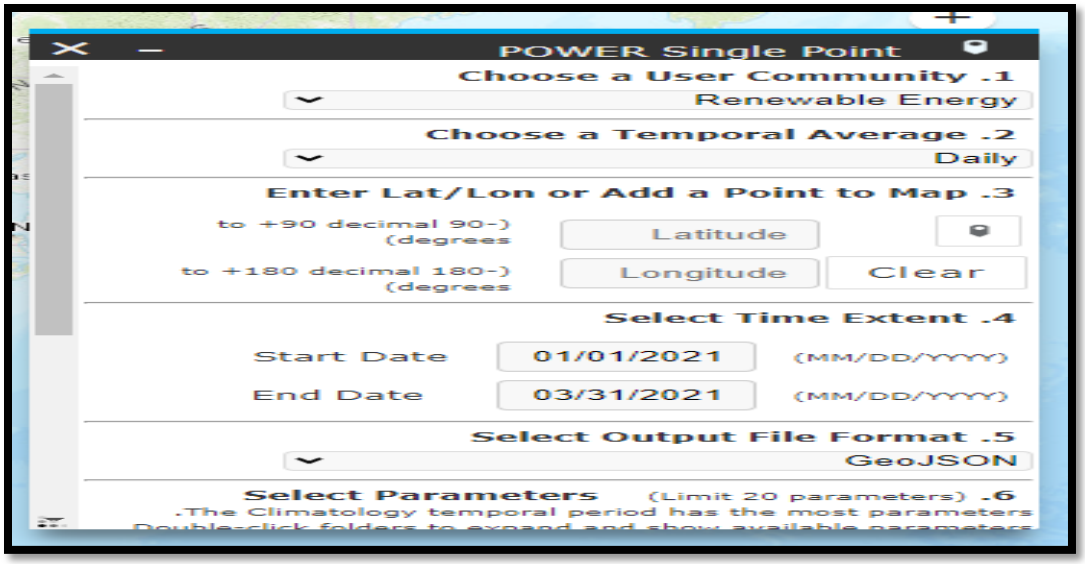

Figure (2-16): Power NASA website interface for selecting the date.

- As for the last step, which is downloading (the daily and monthly maximum and minimum temperature, air temperature, and humidity) as shown in the Figure (2-17).

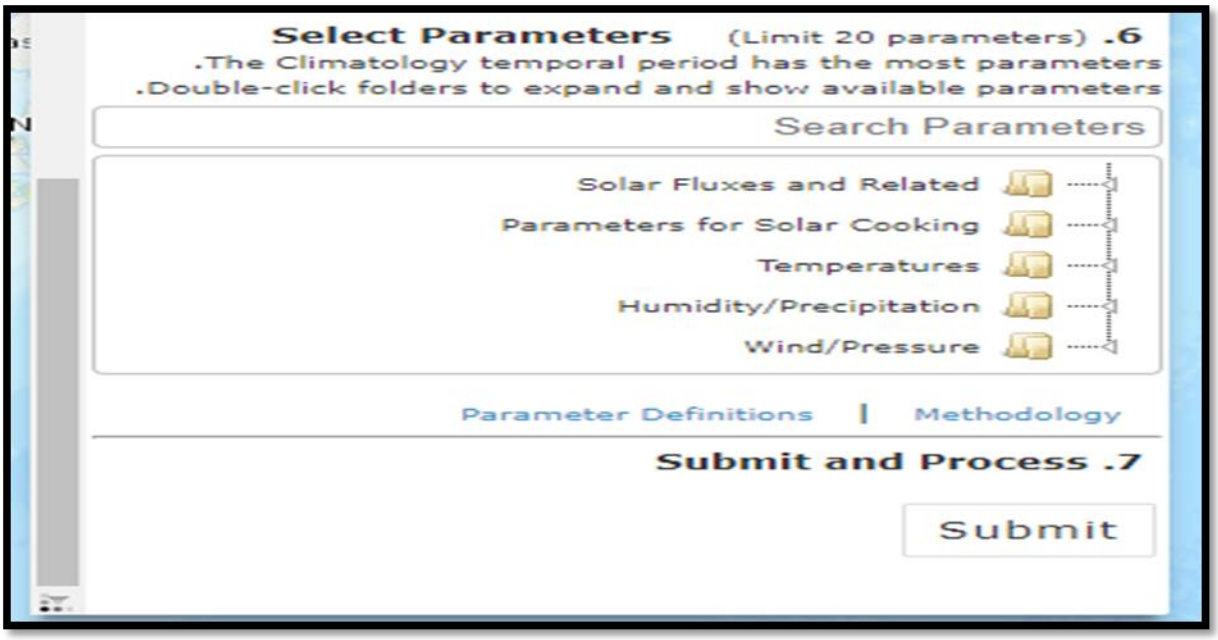

Figure (2-17): Power NASA website interface for selecting the date.

The following Table (2-2) shows the collected data from the Babel meteorological station and the Power NASA website.

Table (2-2): data value of Power NASA and Earth monitoring station

POWER NASA						Earth monitoring station				
Time		Station	Location Latitude/Longitude	LST	T_{air}	Station	Location Latitude/longitude	LST	LST average	T air
1	2022-1-24	Babylon center	32.27 /44.27	7.07	7.72	Babylon center	32.27 /44.27	10.37-12.05	11.21	8.3
	2022-4-30			30.44	28.83			29.6-32.2	30.9	27
	2022-8-12			38.44	37.26			32.6-43.02	37.81	35
	2022-10-23			28.48	29.30			26.9-29.2	28.05	25
2	2022-1-24	Al-Shomale	32.32/44.91	8.01	8.84	Al-Shomale	32.32/44.91	10.3-12.0	11.15	
	2022-4-30			30.6	28.64			32.2-35.0	33.6	
	2022-8-12			39.62	38.31			32.6-43.0	37.8	
	2022-10-23			29.16	29.19			31.3-33.1	32.2	
3	2022-1-24	Al-Kafal	32.22/44.37	6.94	7.56	Al-Kafal	32.22/44.37	10.37-12.05	11.21	
	2022-4-30			30.45	28.66			29.6-32.2	30.9	
	2022-8-12			38.52	37.36			30.4-32.6	31.5	
	2022-10-23			27.9	28.89			26.9-29.2	28.05	
4	2022-1-24	Al- Taliea	32.2/44.73	8.26	8.65	Al- Taliea	32.2/44.73	10.3-12.0	11.15	
	2022-4-30			30.95	28.94			32.2-35.0	33.6	
	2022-8-12			39.77	38.5			32.6-43.0	37.8	
	2022-10-23			29.01	29.26			29.2-31.3	30.25	
5	2022-1-24	Al-Hashmia	32.35/44.6	7.07	7.72	Al-Hashmia	32.35/44.6	10.3-12.0	11.15	
	2022-4-30			30.44	28.83			29.6-32.2	30.9	
	2022-8-12			38.44	37.26			32.6-43.0	37.8	
	2022-10-23			28.48	29.3			29.2-31.3	30.25	

6	2022-1-24	Al- Hamza	32.63/44.9	8.01	8.84	Al- Hamza	32.63/44.9	4.5-10.3	7.4	
	2022-4-30			35.45	28.64			32.2-35.0	33.6	
	2022-8-12			39.62	38.31			32.6-43.0	37.8	
	2022-10-23			29.16	29.19			31.1-33.1	32.2	
7	2022-1-24	Abi- Gharaq	32.50/44.33	7.07	7.72	Abi- Gharaq	32.50/44.33	4.5-10.3	7.4	
	2022-4-30			30.34	28.83			29.6-32.2	30.9	
	2022-8-12			38.44	37.26			32.6-43.0	37.8	
	2022-10-23			28.48	29.3			29.2-31.3	30.25	
8	2022-1-24	Al-Mahawil	32.68/44.41	7.07	7.72	Al-Mahawil	32.68/44.41	4.5-10.3	7.4	
	2022-4-30			30.44	28.83			29.6-32.2	30.9	
	2022-8-12			38.44	37.26			32.6-43.0	37.8	
	2022-10-23			28.48	29.3			26.9-29.2	28.05	
9	2022-1-24	Al- Musaib	32.76/44.28	6.79	7.73	Al- Musaib	32.76/44.28	4.5-10.3	7.4	
	2022-4-30			27.58	28.56			19.7-26.9	23.3	
	2022-8-12			38.12	37.02			32.6-43.0	37.8	
	2022-10-23			28.55	28.05			31..3-33.1	32.2	
10	2022-1-24	Jarf Al-Sakhr	32.90/44.17	6.79	7.73	Jarf Al-Sakhr	32.90/44.17	4.5-10.3	7.4	
	2022-4-30			29.87	28.56			32.2-35.0	33.6	
	2022-8-12			38.12	37.02			30.4-32.6	31.5	
	2022-10-23			28.31	28.5			29.2-31.3	30.25	

CHAPTER THREE
RESULTS AND DISCUSSION

3.1 Introduction

In this chapter, the results will be presented: various factors that are adopted for the calculation of the LST, urban islands, and the climate elements (Babel Meteorological Station, and the virtual stations).

3.2 The Land Surface Temperature (LST) Tests

The method of calculating the LST requires that images need to be applied a number of steps, as images are downloaded from the Landsat 8:

3.2.1 The Determination of Sensor Spectral Radiance (LS)

Numeric values (DN) are converted to absolute radiation. The DN values of pixels in the thermal range (B10) are changed to (LS) using equation (6). The results are shown for each season in Figure (3-1).

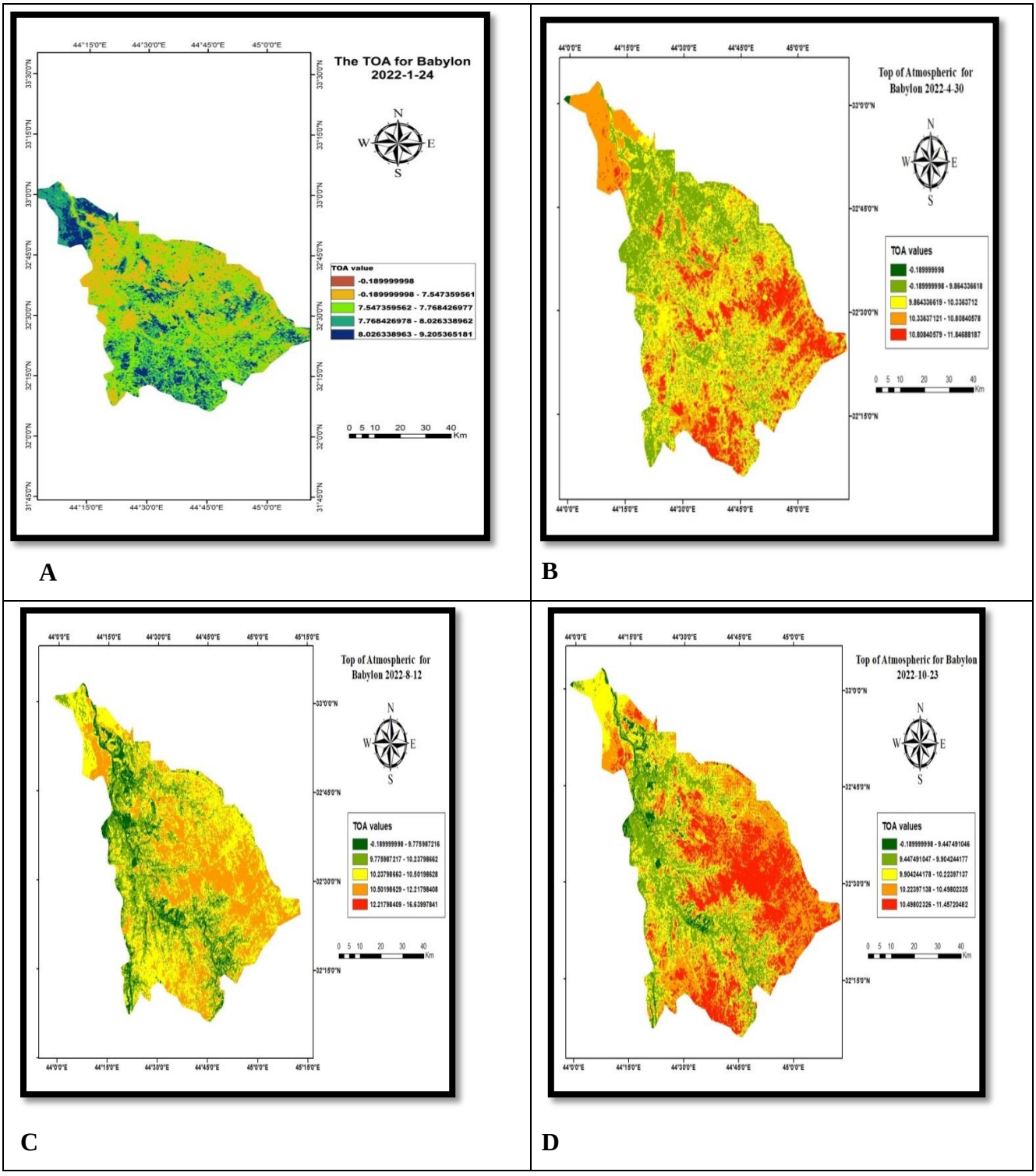

Figure (3-1): The LS values based on Band 10 for (A) winter (B) spring (C) summer (D) autumn seasons.

3.2.2 Conversion of Spectral Radiance to Brightness Temperature (BT)

The brightness temperature (BT) was determined by adopting the LS values using equation (7). The thermal constants of the TIR band 10 (K1 K2) are used in later equation which identify in the metadata file associated with the satellite images. The BT maps of the study area for each season are shown in Figure (3-2**).**

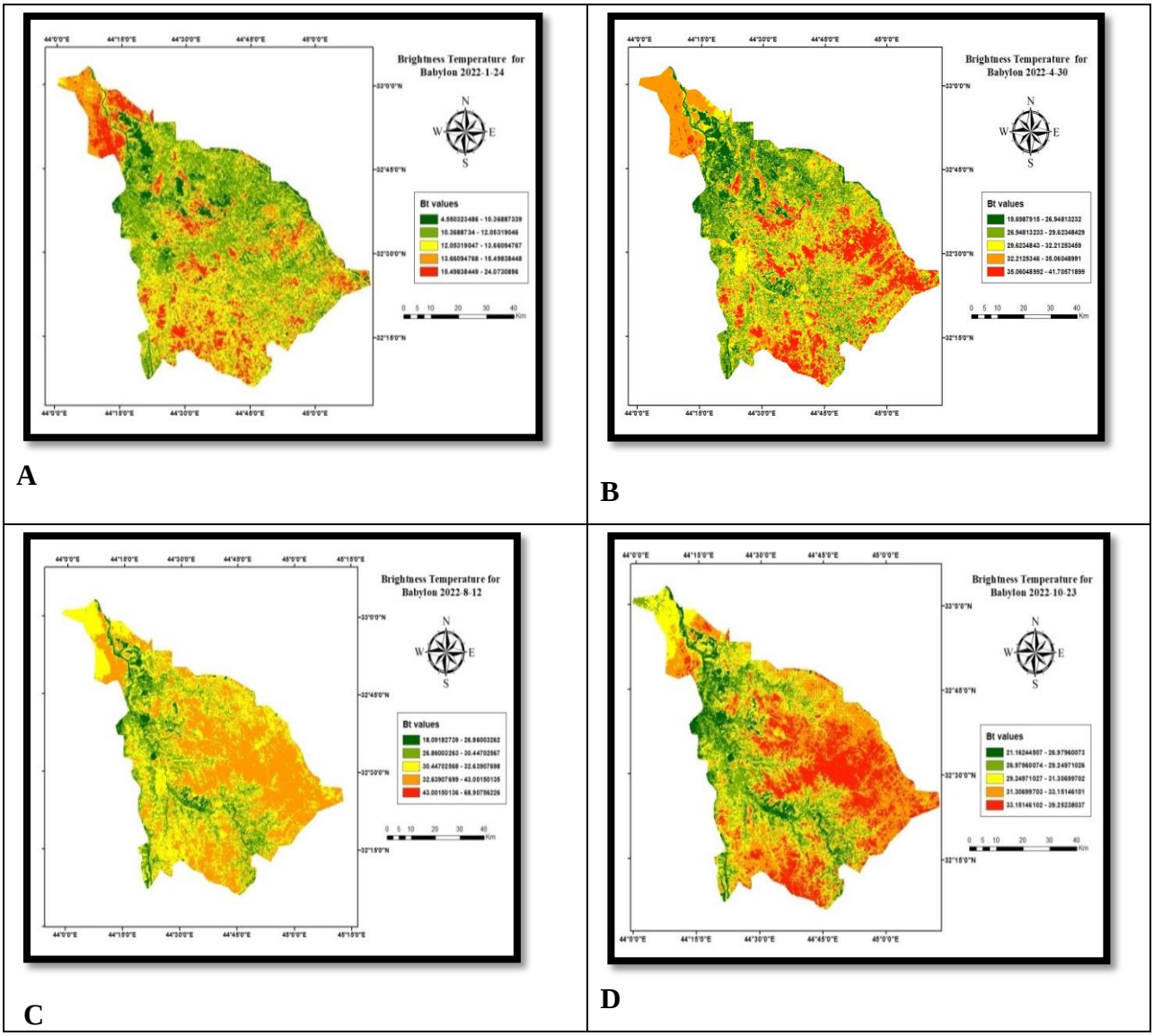

Figure (3-2): BT value for Babylon governorate for (A) winter (B) spring (C) summer (D) autumn.

3.2.3 The Normalized Difference Vegetation Index (NDVI)

Normalized Difference Vegetation Index (NDVI) is a simple numerical index to assess the presence of live green vegetation. The NDVI can be calculated by using Equation (2). For Landsat 8 imagery, the NDVI is computed using band 4 (Red band) and band 5 (NIR), the NDVI results for this study is shown in Figure (3-3).

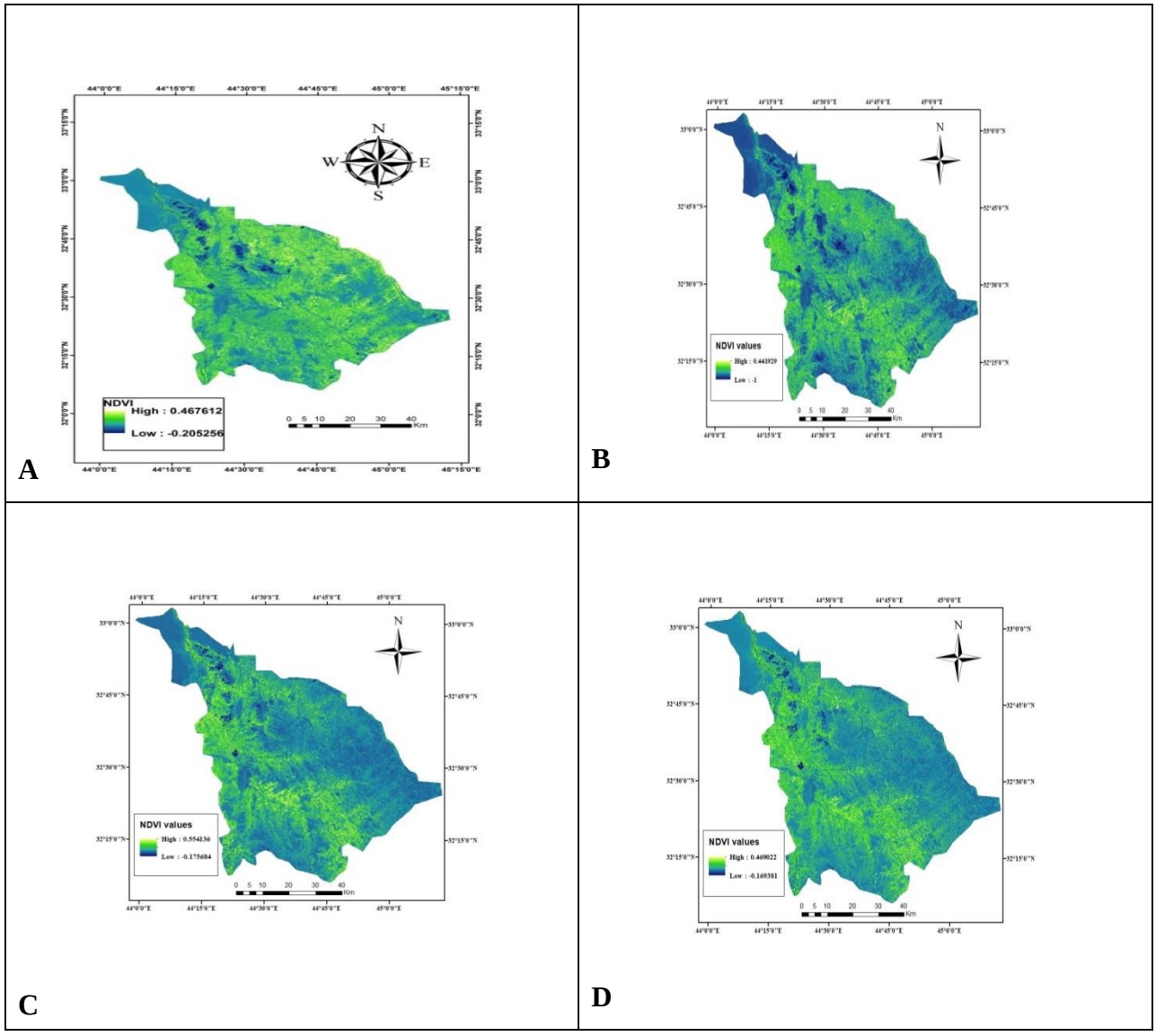

Figure (3-3): The NDVI maps for (A) winter (B) spring (C) summer (D) autumn seasons.

3.2.4 The Proportional Vegetation (PV)

The PV values are calculated based on the NDVI values as shown in equation (8), and the PV values are shown in the following Figure (3-4).

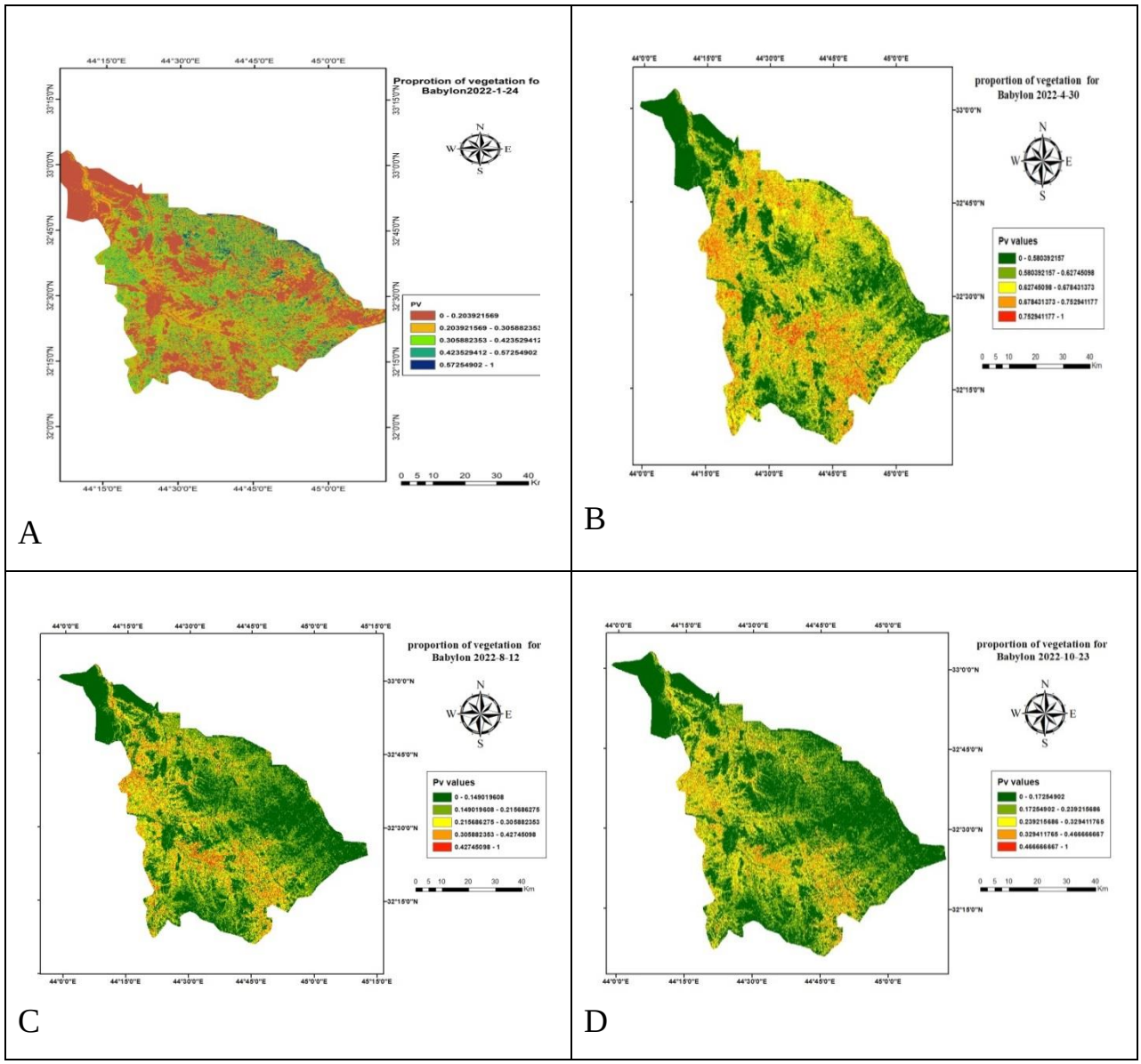

Figure (3-4): The PV maps for Babylon governorate for (A) winter (B) spring (C) summer (D) autumn seasons.

3.2.5 The Emissivity of the Land Surface Cover (E).

The next step is determining the emissivity of the land surface cover by using equation (9), Figure (3-5) shows the maps of the E.

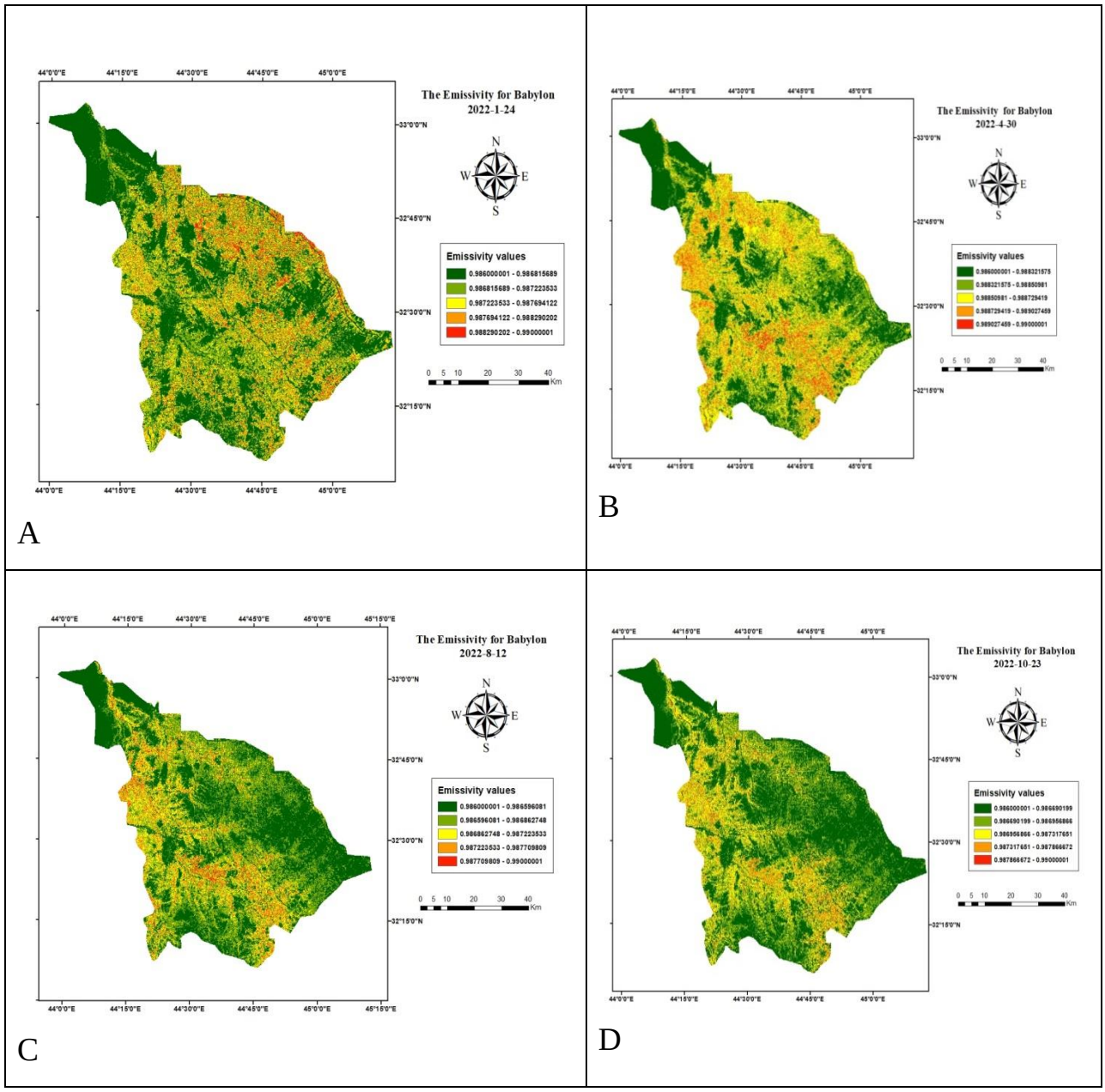

Figure (3-5): The Emissivity maps for Babylon governor for (A) winter (B) spring (C) summer (D) autumn season.

3.3.6 The LST Maps

The calculation of the LST using brightness temperature (BT) of band 10 and emissivity (E) derived from (PV) and (NDVI) by equation (10). The LST is mapped for Babylon government in four seasons in 2022, and shown in Figure (3-6): panels (a, b, c and d) represent the spatial distribution of the LST in winter, spring, summer and autumn respectively.

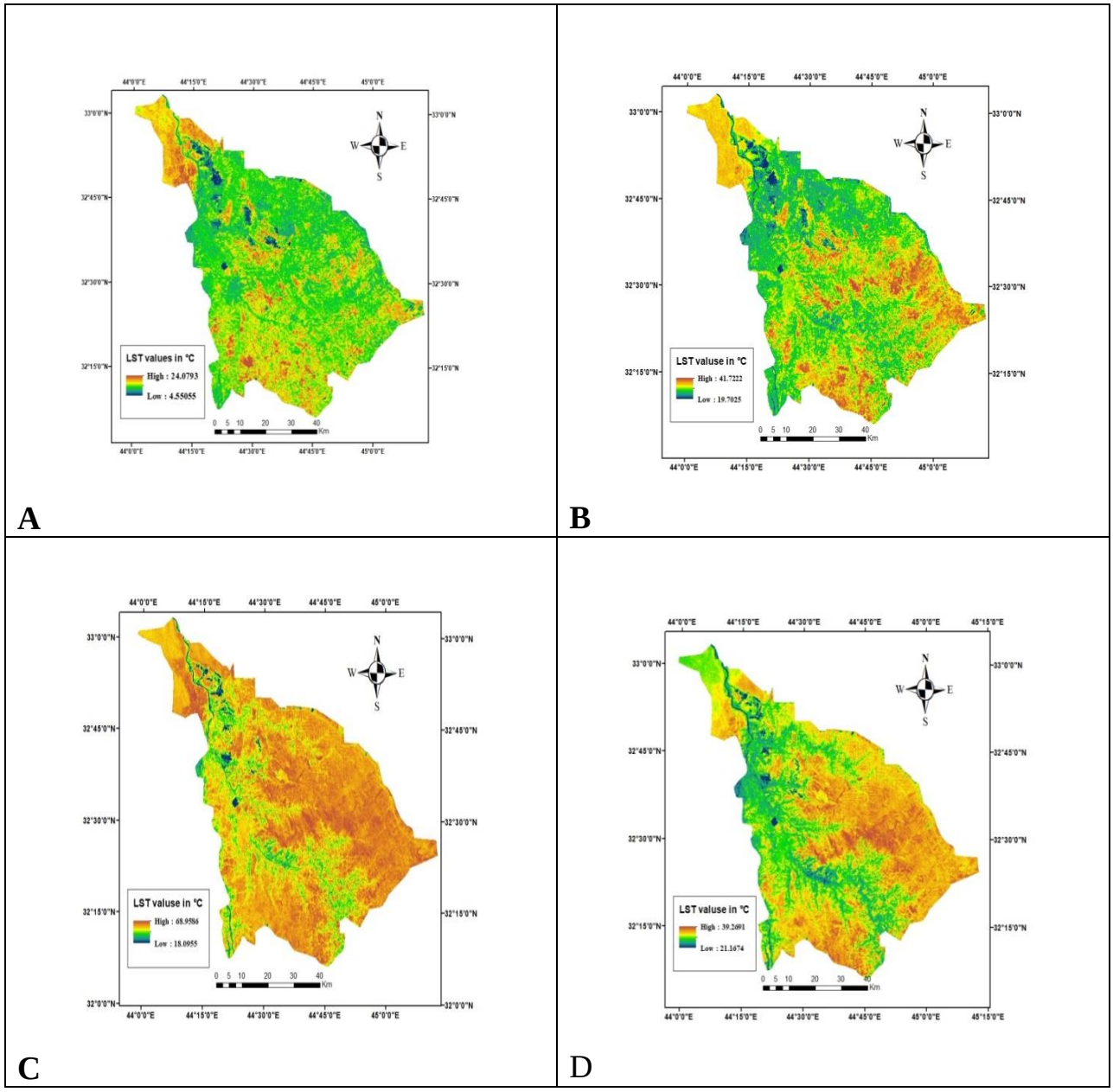

Figure (3-6): The Figure represents the LST distribution of Babylon government in the four seasons. The panel (A) refers to LST in winter, while the panel (B) represents the LST in spring. Panels (C) and (D) characterize the LST in summer and autumn respectively.

Through the results (see Figure (3-6)) there is a great variation in temperatures in different areas within the province of Babylon and during the different seasons of the year, and the reason for this difference is due to seasonal change, as well as the

relationship of temperature to the vegetation index, where the temperature is inversely proportional to the cover index Vegetarian where it turns out that in the summer the temperature ranges between (68.9 - 18.1) Cº. The high temperature is in some eastern areas of Babylon Governorate, such as the administrative area (Hamza), but in the winter, the temperatures range is between (24.1 - 4.6) Cº, the temperatures are medium and tend to decrease.

As for the administrative area (Shomali), in the summer, some places have an average temperature, and the reason lies in the presence of vegetation that affects the low temperature, in other places of the Shomali area, so the temperatures are high, but in winter, the temperatures are somewhat low. As for the southern regions of Babylon Governorate, such as the administrative area (Al-Tali'a), the temperatures in the summer and winter are close, i.e. the temperatures are average. The administrative area (Al-Kifl), which is located in the south of the province of Babylon, the temperature in the summer is moderate and in the winter is low, and the reason for its location is because it is close to the Euphrates River, as the water resources are inversely proportional to the temperature.

As for the central administrative areas of Babylon Governorate (Al-Hilla, Nile, Hashemite and Mahawil), the temperatures are close, where the temperatures in the summer are semi-high and in the winter they are low. One of the areas that are located in the west of Babylon Governorate is the area (Abi Ghark) This area is characterized by being the most areas where the temperature in the summer and winter is low, unlike the northern areas of Babylon (Musayyib, Alexandria and Jurf Al-Sakhar) which are high in the two seasons. In the spring and autumn season, the temperature shakes are (41.7 - 19.7) Cº, (39.3 - 21.2) Cº respectively. The temperatures are almost the same in the two seasons in all areas of the Babylon

province. Except for the northwestern region, there is a decrease in temperature in the spring.

3.3 The Relation between the LST and the NDVI

The descriptive statistics coefficients (minimum, maximum, mean and standard deviation) of the LST and NDVI in each season are listed in Table (3-1). Figures (3-7) and (3-8) show the descriptive statistics coefficients in each season for the period of study: panels (a, b, c and d) characterize the minimum, maximum, mean and standard deviation in January, April, August and October in 2023 respectively.

Table (3-1): Descriptive statistics of the LST and NDVI for Babylon government in each season .

	LST				NDVI			
Seasons	**Minimum**	**Maximum**	**Mean**	**Standard deviation (SD)**	**Minimum**	**Maximum**	**Mean**	**Standard deviation (SD)**
Winter	4.55054	24.07925	12.74871	1.92981	-0.20525	0.467612	0.13883	0.08363
Spring	19.70248	41.72218	31.17165	3.31928	-1	0.44192	0.14145	0.05683
Summer	18.09548	68.95861	31.71405	2.26821	-0.17568	0.55413	0.13349	0.06515
Autumn	21.16742	39.26906	30.97829	2.49600	-0.16938	0.46902	0.11326	0.05272

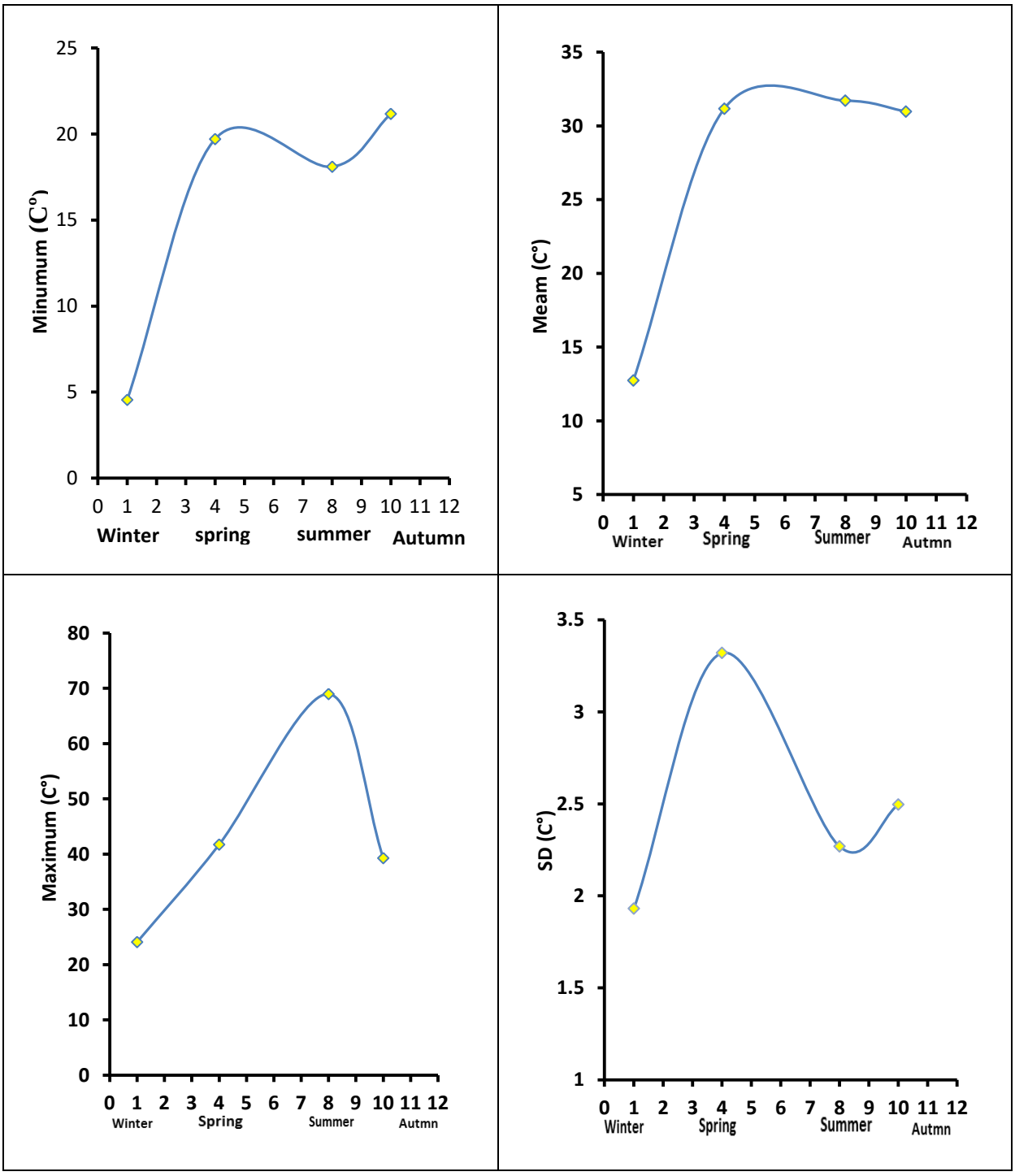

Figure (3-7): The descriptive statistics coefficients of LST in each season for the period of study.

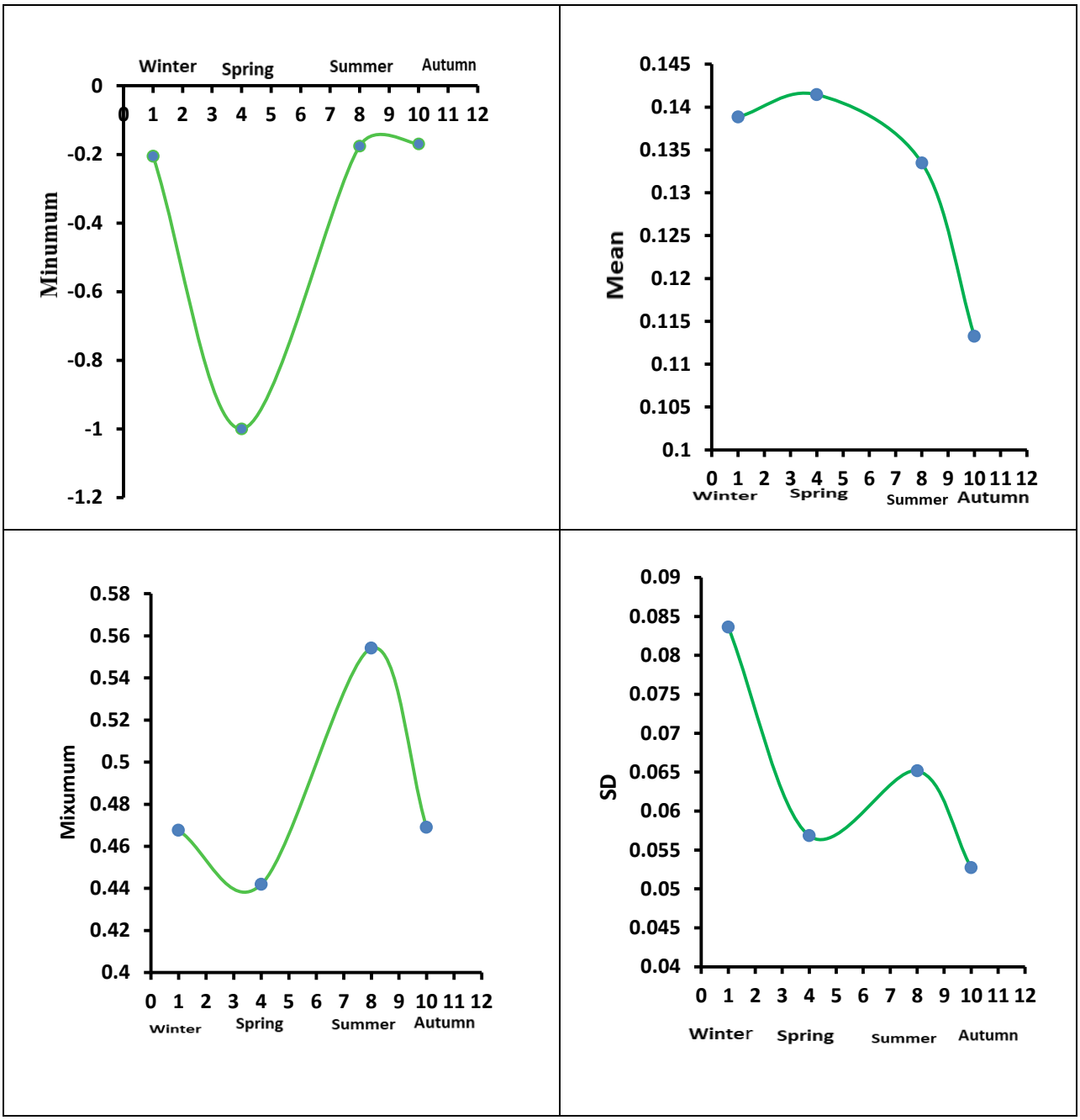

Figure (3-8): The descriptive statistics coefficients of NDVI in each season for the period of study.

There is a relationship between the LST and the vegetation cover, which is an inverse relationship, as when the vegetation cover increases in some areas of Babylon governorate, this will lead to a decrease in temperatures for that region.

Through the results, there are variation in temperature and vegetation cover for all regions of the governorate Babylon during the four seasons of the year 2022.

- **Winter Season**

  The vegetation cover in the northern regions of Babylon government in winter is (0.00847 - 0.10083), so we note that the temperatures in this region are high, i.e. ranging between (15.4253 - 24.07920) C°. As for the northeastern regions, the vegetation cover is good, and it ranges between (0.25915 - 0.46761), so its temperature is rather low, and it ranges between (10.3708 - 12.0556) Cº. As for the southern regions of Babylon governorate, the vegetation cover is dispersed in winter, as some of its regions lack vegetation cover. The percentage of vegetation ranges between (0.00847 - 0.10083) and the temperature of these areas ranges between (13.6639 - 15.4253) Cº. Another part of the areas of the southern part of Babylon government is rich in plants, where the percentage of vegetation ranges in the range of (0.25915 - 17471), so its temperature ranges between (10.3708 - 12.0556) Cº. In the last part of Babylon government, which is the western part, it varies Vegetation. In the area and its percentage is very small and almost non-existent (-0.20525 - 0.00847), the temperature is (15.4253 - 24.079) Cº. As for the rest of the areas of the western part, the percentage of vegetation is fairly good. All of these above values are shown in Table (3-1) and Figure (3-7).

- **Spring Season**

  The vegetation cover in the northern regions of Babylon government in the spring is scarce (-1 - 0.0913), so we note that the temperatures in this region are high, that is, ranging between (32.2234 - 35.0730) C°. As for the northeastern regions, the vegetation cover is good and ranges between

(0.17616 - 0.23836). So its temperature is rather low and ranges between (19.702 - 26.956) C°. As for the southern regions of Babylon Governorate, the vegetation cover varies. - 41.7221) C°, and another part of the regions of the southern part of Babylon government is rich in plants, where the percentage of vegetation cover is within (0.23836 - 0.4419), so its temperature ranges between (19.7024 - 29.6329) Cº, and in the last part of Babylon government, which is the western part, there is a great variation Where plants range from (-1 - 0.23836), temperatures range from (19.7024 - 35.07309) C°. All of these above values are shown in Table (3-1) and Figure (3-7).

- **Summer Season**

The northern regions of Babylon government have a low percentage of vegetation cover, meaning that it ranges from approximately (0.02752 - 0.10765), so the temperature in this region is approximately (30.4622 - 32.656) C°. As for the northeastern regions, the vegetation cover fluctuates in parts of the regions. That is, its percentage ranges between (0.02752-0.25075) and because of this disparity in the vegetation cover, there is a variation in temperatures (26.8718-43.0283) Cº. In the southern and western parts, temperatures and vegetation cover are close in these two regions of the governorate. In summer, Babylon enjoys a high vegetation cover (0.2507 - 0.5541), so its temperature will be somewhat low, ranging between (18.0954-30.4622) Cº. All of these above values are shown in Table (3-1) and Figure (3-7).

- **Autumn Season**

The northern regions of Babylon government have medium vegetation cover (0.02339 - 0.09599), so the temperature is (29.2599 - 31.3185) Cº and the northeastern regions of Babylon government for the autumn season The percentage of vegetation cover in them varies between the limits of (0.023391-0.216164) so there will be a large variation in temperatures in this region (21.1674-39.2690) Cº and the southern part of the government has a vegetation cover ratio (0.21616 - 0.46902) so the temperature is different, i.e. between (26.9883-39.2690) Cº and the last part of the government Which represents the western section of the cover ratio in it (0.14606 - 0.21616) so the temperature in it is (26.988-33.164) Cº. All of these above values are shown in Table (3-1) and Figure (3-7).

3.4 The Impact of the Climate Parameters on the LST

From the stations that we imposed within the government of Babylon, the climatic elements are determined such as humidity and air temperature. The relations between both LST and relative humidity as well as between LST and air temperature are presented in Figure (3-9) to (3-18).

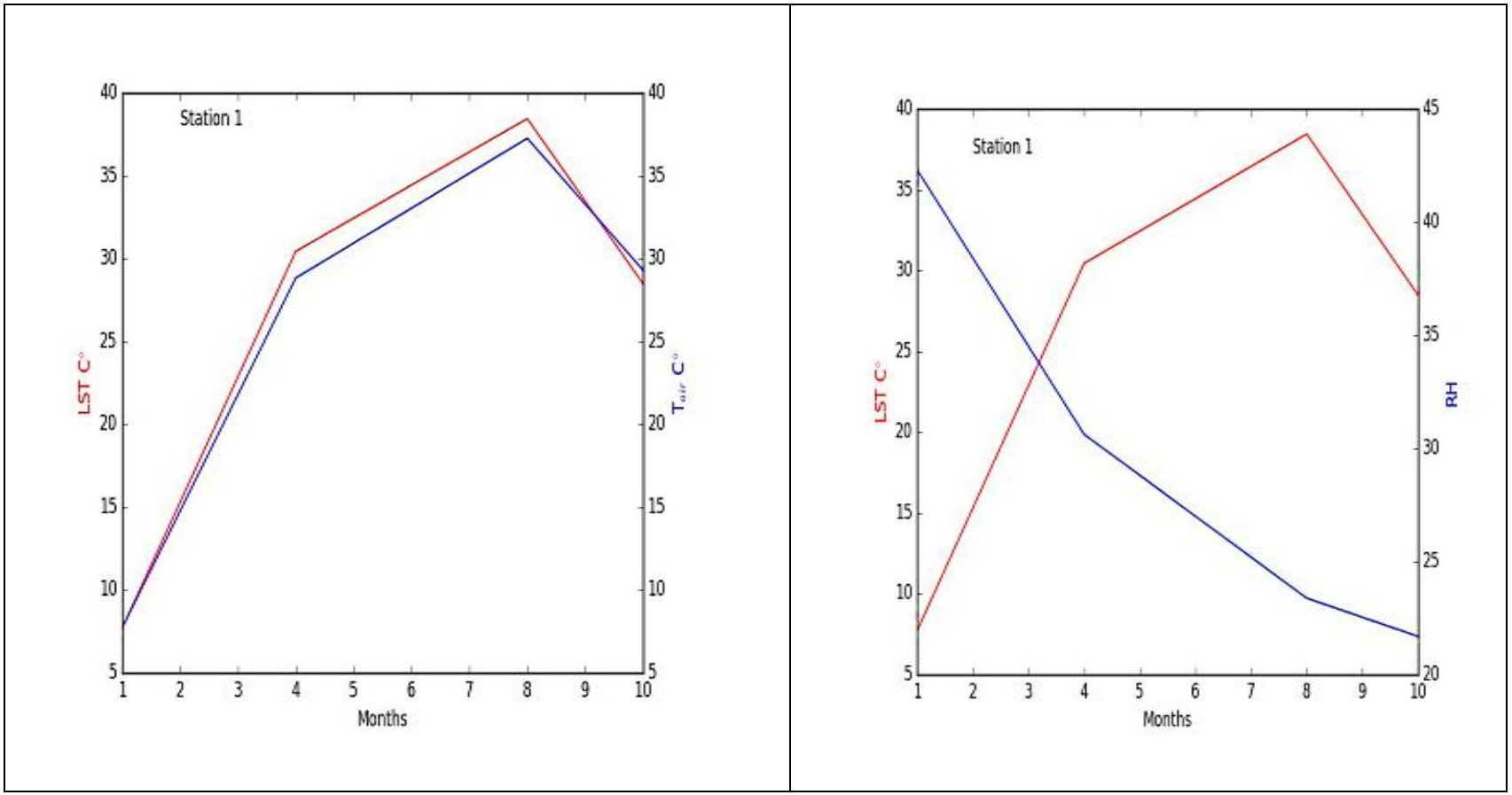

Figure (3-9): The relation between the LST and climate factors: The left panel represents the relation between the LST and RH, the right panel displays the relation between the LST and T_{air}. The labels in the top left corner represent the number of station that labeled in Figure (2-14).

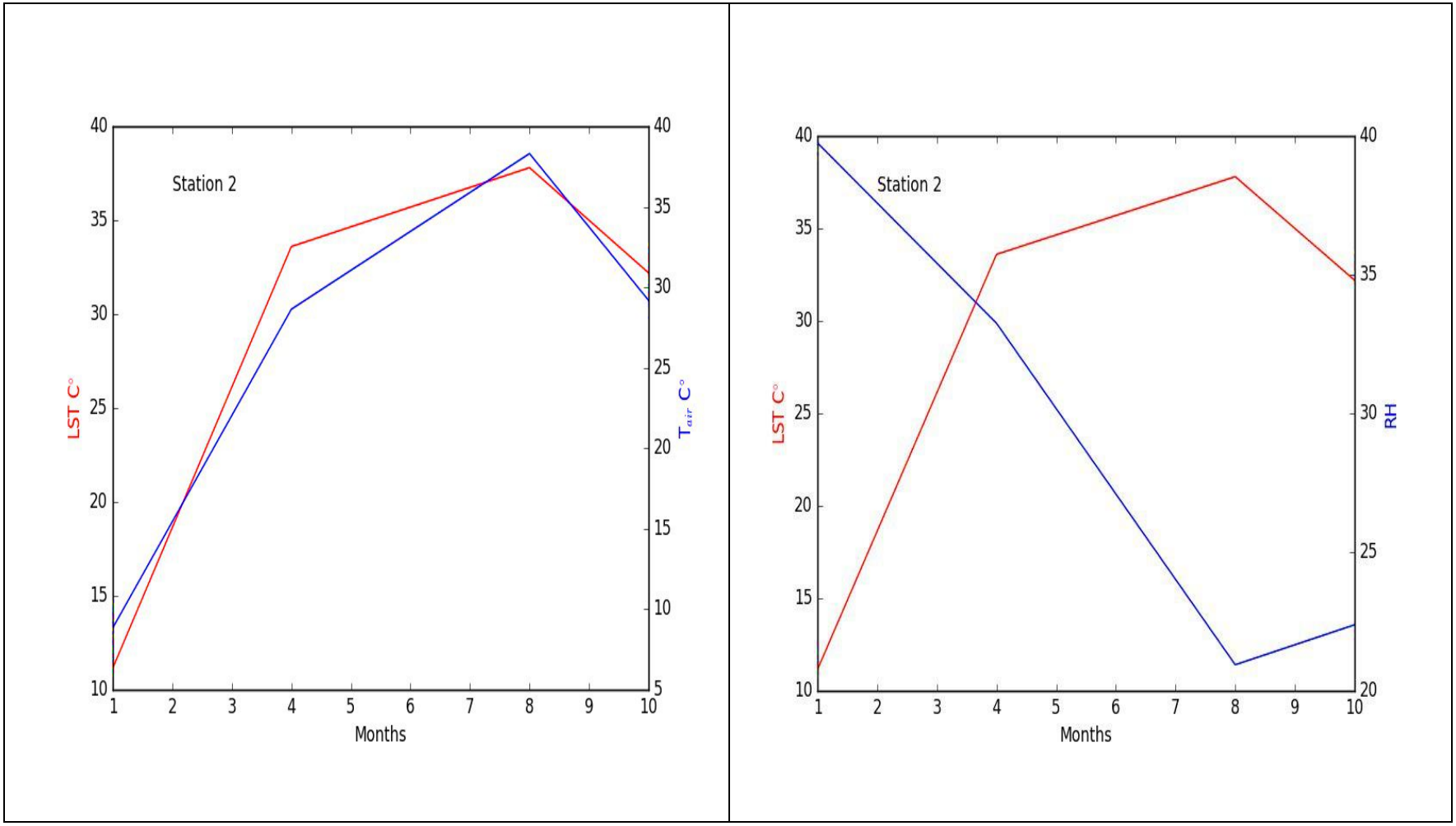

Figure (3-10): As figure (3-9) but for station 2.

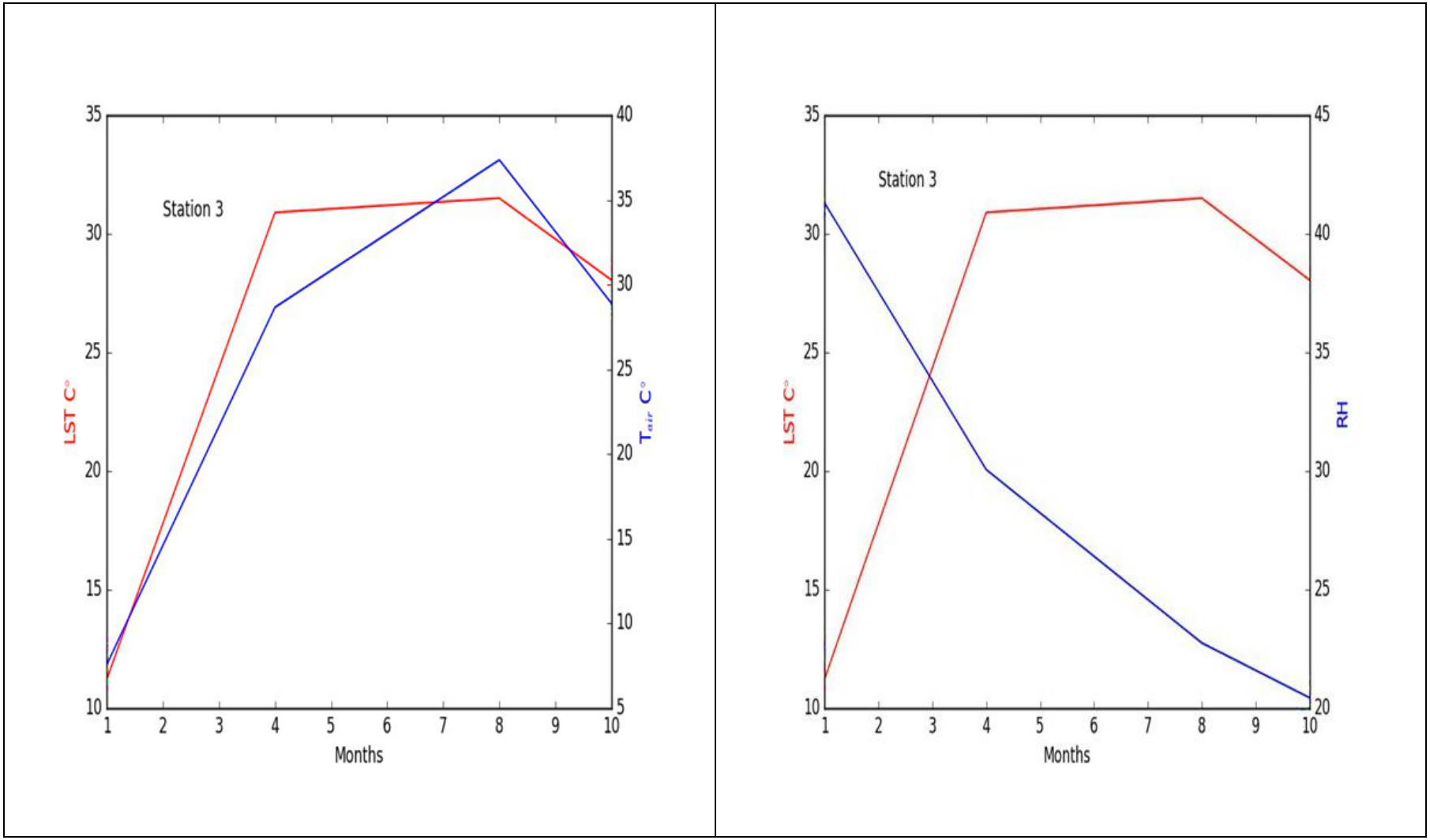

Figure (3-11): As figure (3-9) but for station 3.

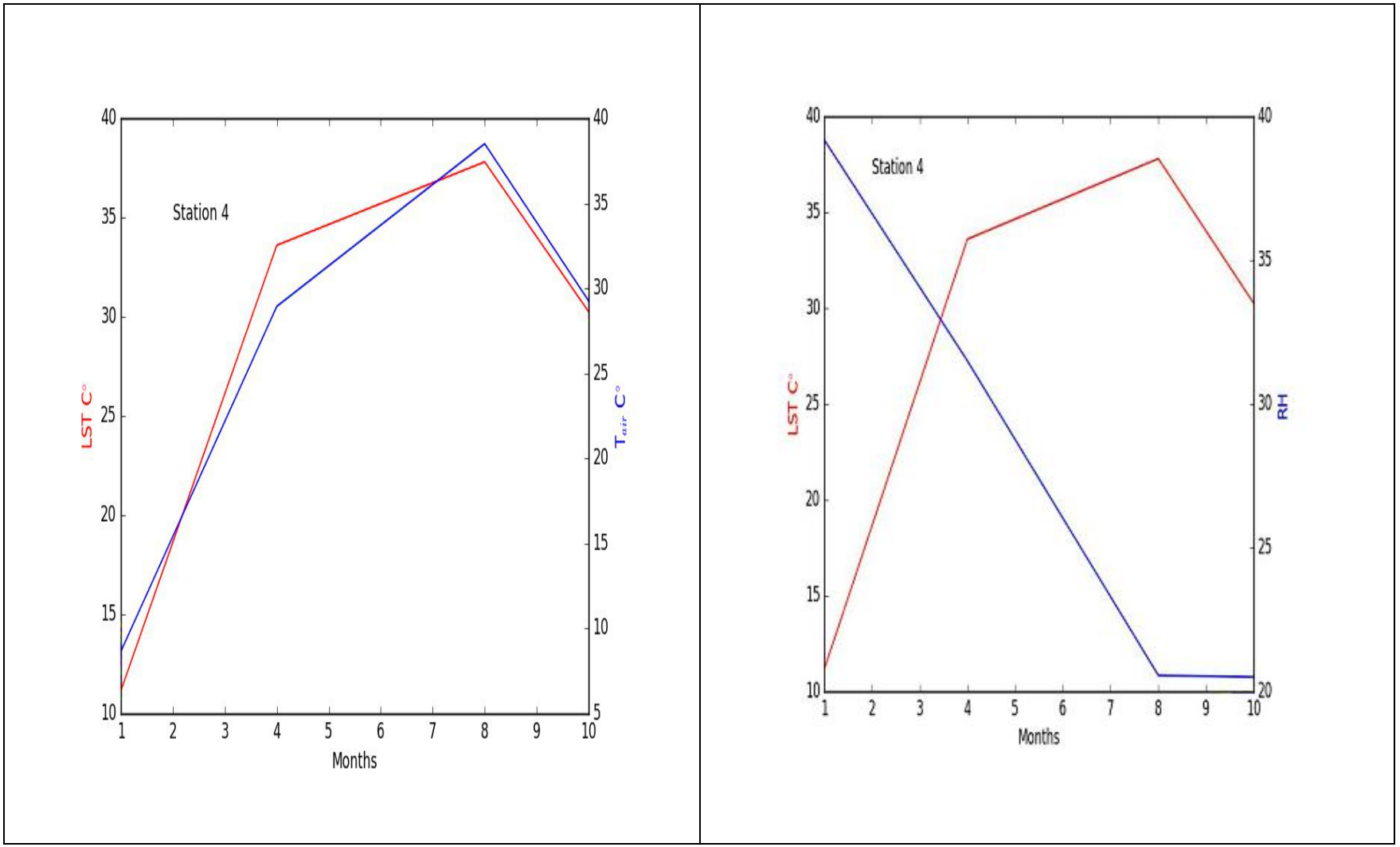

Figure (3-12): As figure (3-9) but for station 4.

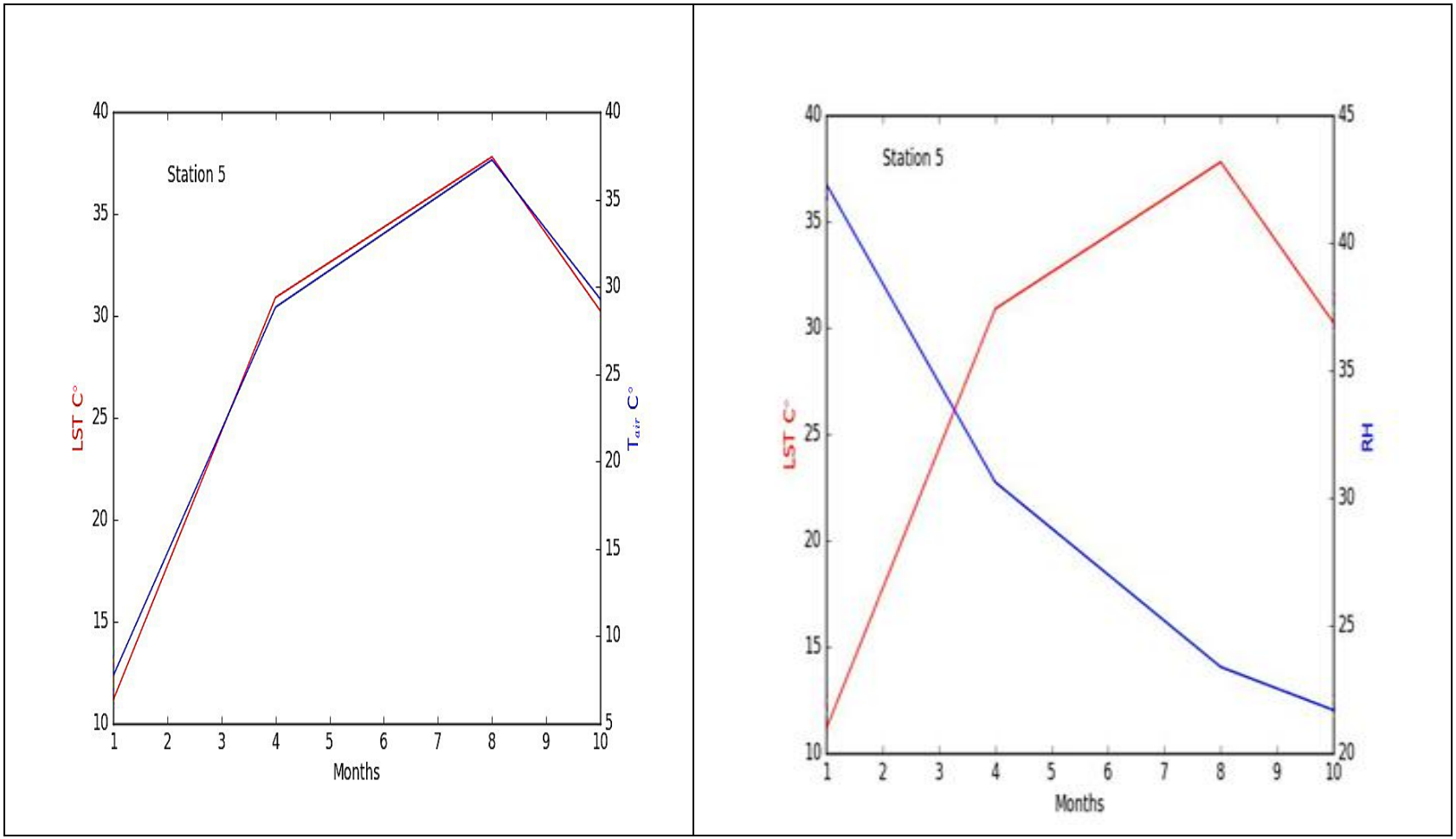

Figure (3-13): As figure (3-9) but for station 5.

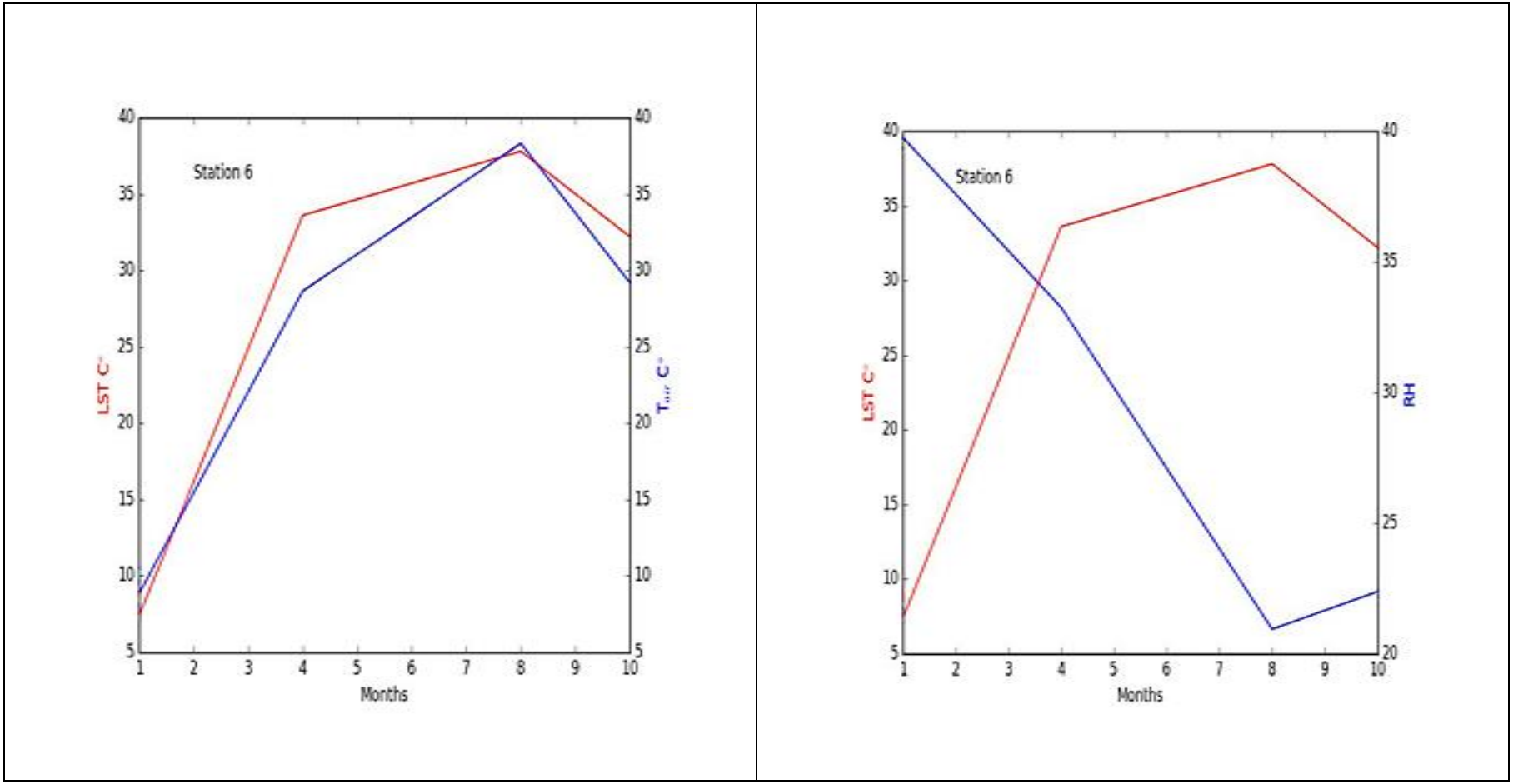

Figure (3-14): As figure (3-9) but for station 6.

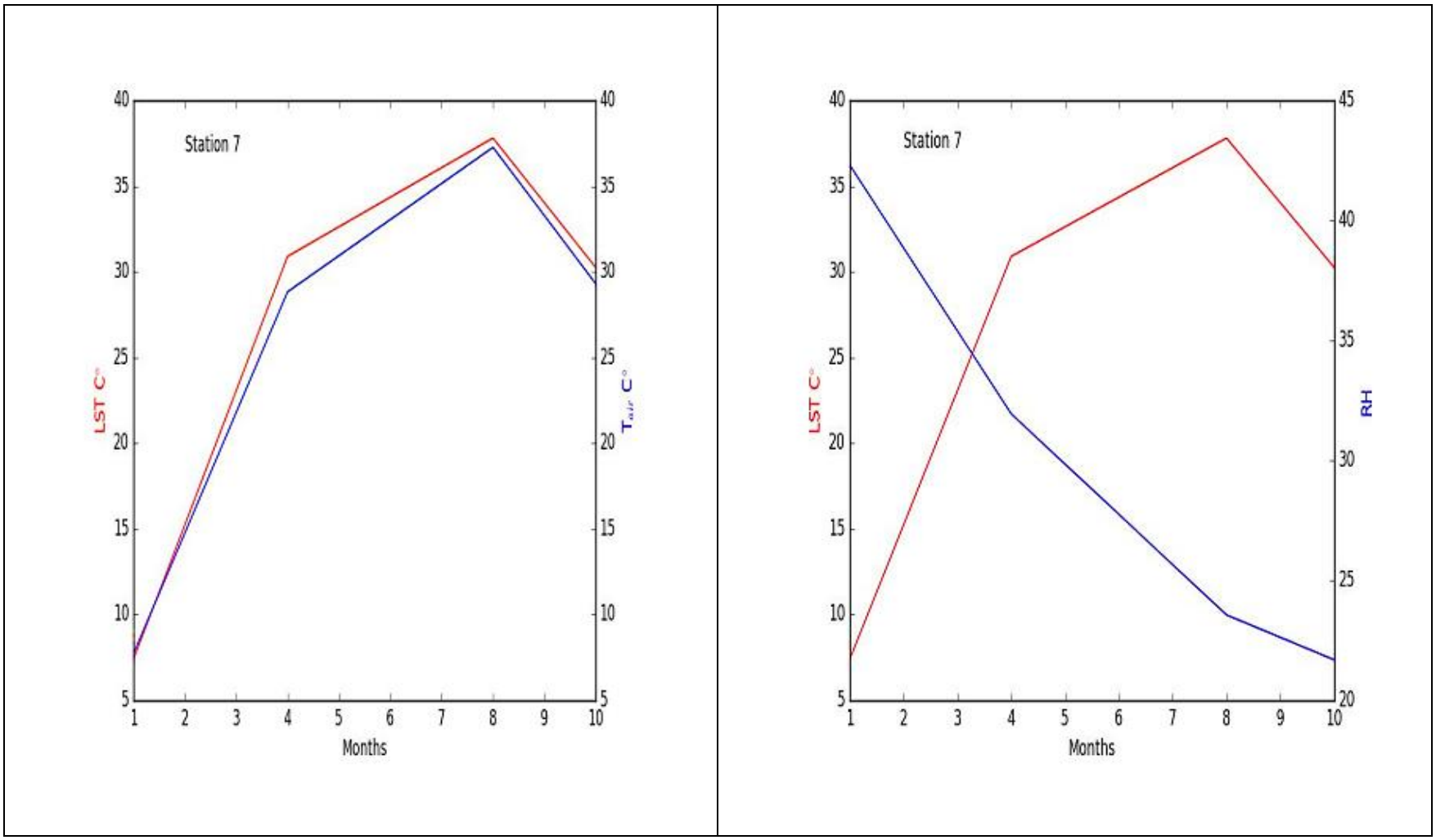

Figure (3-15): As figure (3-9) but for station 7.

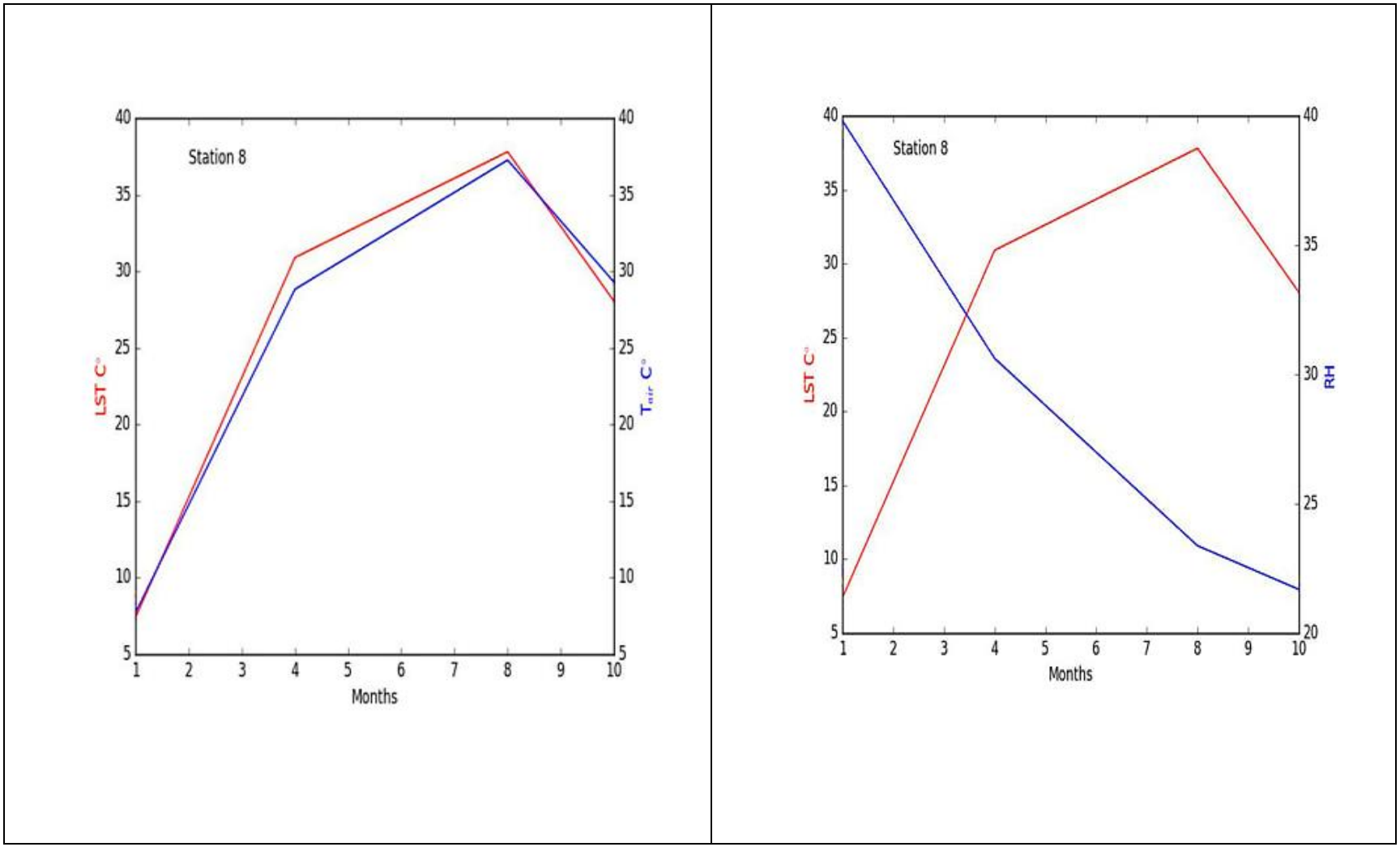

Figure (3-16): As figure (3-9) but for station 8.

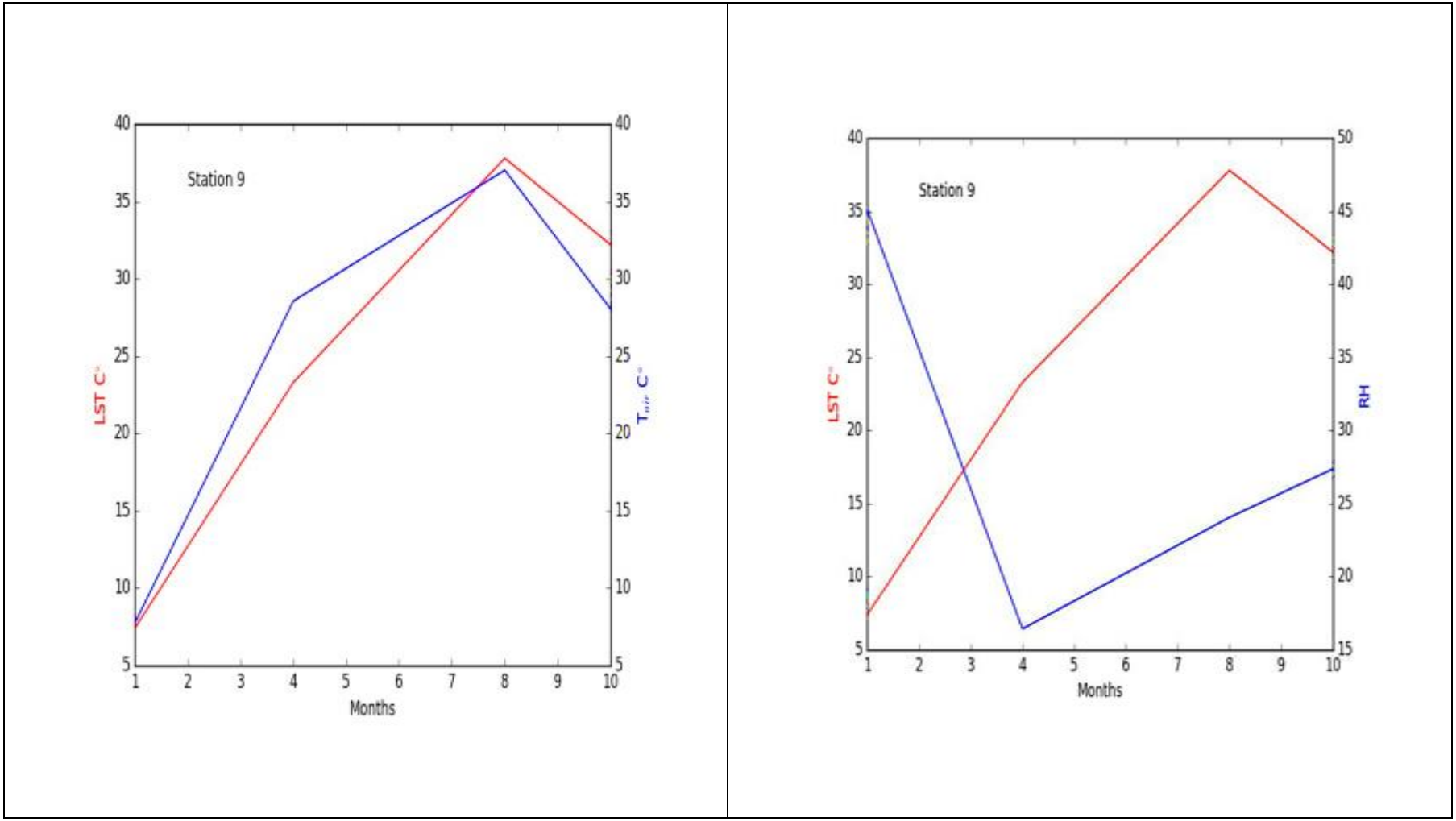

Figure (3-17): As figure (3-9) but for station 9.

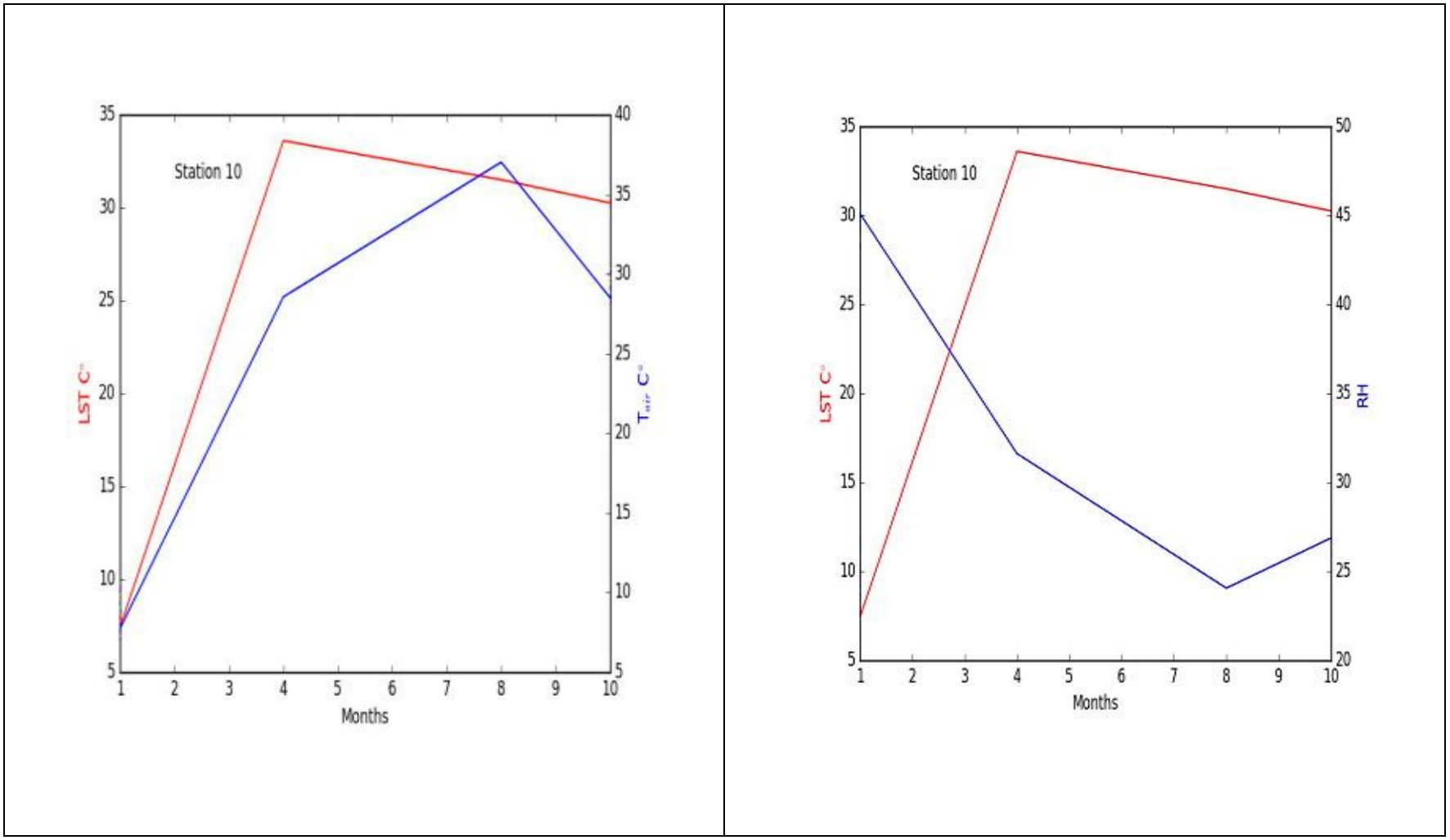

Figure (3-18): As figure (3-9) but for station 10.

All the data obtained from the ten virtual stations showed that there is a direct relation between the land surface temperature and the air temperature, as they have the same behavior during all seasons. While relative humidity behaves differently from that of the land surface temperature behavior.

3.5 The Heat Islands

3. 5 1.Urban Heat Island (UHI) and non-Urban Heat Island (non-UHI)

The urban heat islands and non-urban heat islands are identified throughout Babylon governorate by using equations (11) and (12), respectively.

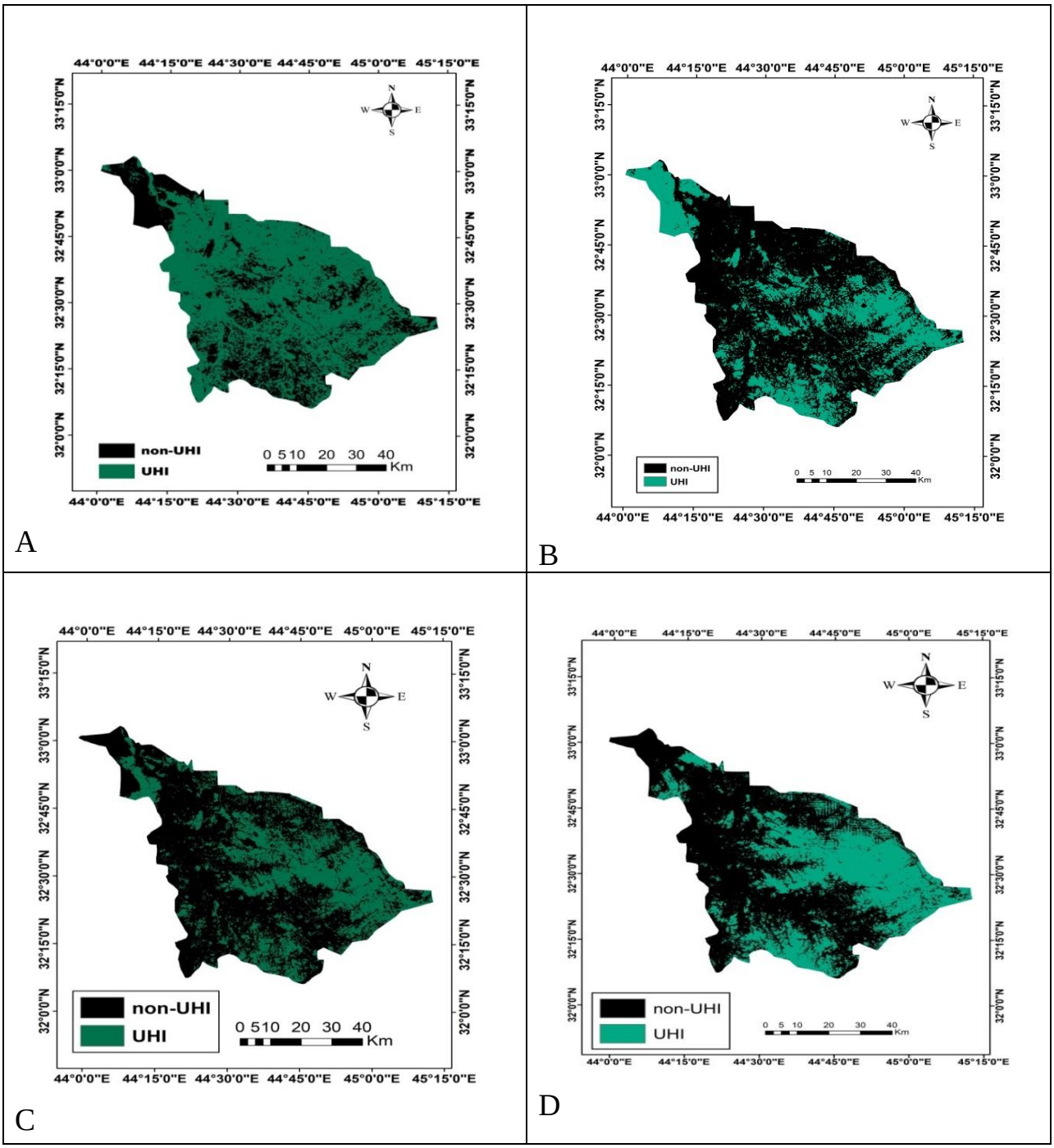

Figure (3-19): The urban heat islands and non-urban heat islands areas are shown within Babylon government in four seasons: (A) Winter (B) Spring (C) Summer and (D)Autumn.

The phenomenon in which heat builds up in urban areas as a result of urban habitation and development is known as the urban heat island (UHI) effect. Admittedly, it is the most public aspect of the capital's climate. There is no doubt that the structure and functioning of urban ecosystems will change due to the warming of the land surface temperature caused by the UHI effect, which will also affect material flow and energy flow. These changes will have an impact on urban temperatures, urban hydrological conditions, and other environmental factors, as we notice through maps that the winter season and the spring season are different and completely opposite to each other, as in the northern regions in the winter we notice that there are non-UHI and in the rest of the regions. The governorate has UHI and UHI is interspersed in some southern regions. In the spring, it is the exact opposite of winter, where UHI is abundant in the northern regions, and non-UHI is present in the rest of the governorate. In some parts of the southern regions, UHI is interspersed. In the summer and autumn, the distribution of UHI and non-UHI are completely identical, as non-UHI is found in the northern and western regions of the governorate, while in the eastern and southwestern regions there is UHI, and the rest of the regions from the southern part contain non-UHI.

3.5.2 The Urban Hot Island (UHS)

The regions of the UHS within the government of Babylon are identified by using equation (13), as shown in Figure (3-20).

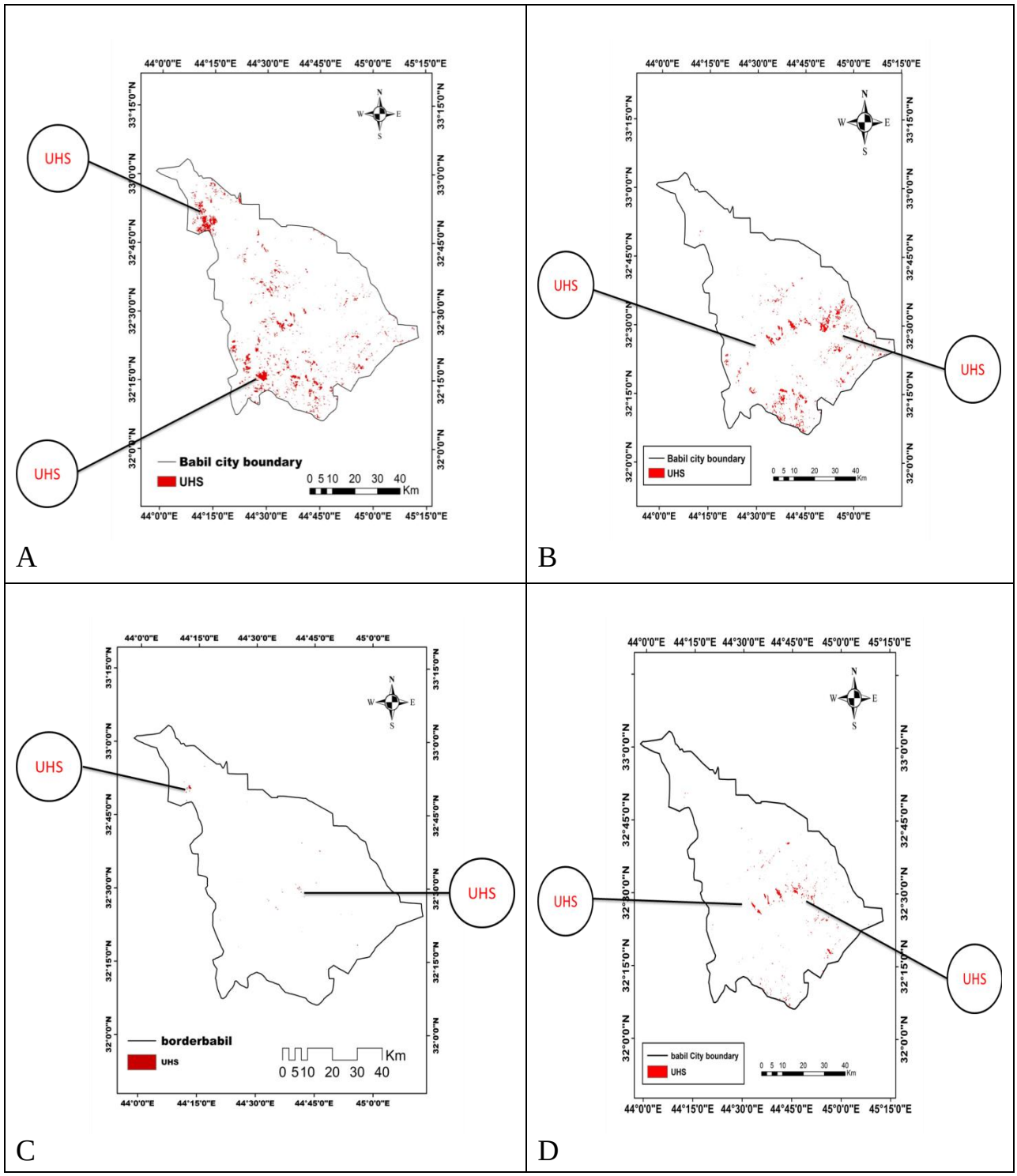

Figure (3-20): The distribution of the UHS regions within government of Babylon in four seasons: (A) Winter (B) Spring (C) Summer (D) Autumn.

Thermal spots vary in distribution in the government of Babylon during the different seasons, as in the winter we notice that most of the spots are located in the northern, western and southwestern regions, while the rest of the regions are present in them, but in very small proportions. Parts of the governorate lack heat spots islands. In the summer, heat spots are present in a very small percentage. In the fall, the concentration of hot spots islands is in the central regions of the governorate.

- **Winter Season**

  The islands of heat spots in the winter appear clearly in the northern part of the governorate, especially in Musayyib, which is located within latitude 32.783 and longitude 44.276 due to desertification in this part of this region as shown in Figure (3-21) as well as it is prominently located in the southwestern part of the governorate, close to the Al-Kifl area, at latitude 32.145 and longitude 44.28. The main reason for the formation of hot spots is desertification, and it is found in the rest of the governorate, but it is randomly distributed.

A **B**

Figure (3-21): Desert areas that cause hot spots in winter (A) the northern regions (B) the southwest region.

- **Spring Season**

  In the spring, hot spots appear clearly in the central and southern regions of the governorate. As for the northern regions, they do not exist except that there is a very small part in the region that contains these spots. The southeastern region of the governorate appears in hot spots due to the absence of any water source or the presence of vegetation cover, where only there are urban areas. As for the central part of the governorate, it appeared in some areas of it, and this region due to the presence of desertification in it and the southern regions as well. The reason for the emergence of it is desertification, specifically Al-Kifl region, while the northern regions do not contain hot spots due to the presence of water sources there. In the figure

below, the urban areas of the southwestern part and the desert areas of the center of the governorate

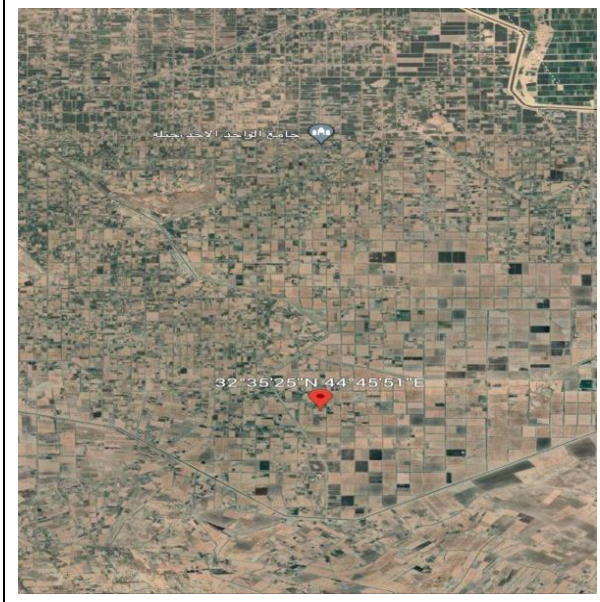

A

B

Figure (3-22): Desert areas that cause hot spots in spring (A) Southeast part regions (B) Central region.

- **Summer Season**

The summer season is the least of the seasons in which hot spots exist, as there are very small spots in the north of the governorate at 32.44 latitude and 44.09 longitudes. Latitude 32.17 and longitude 44.40 and the reason for its appearance are that it is an urban area and the figure below shows the northern and central regions.

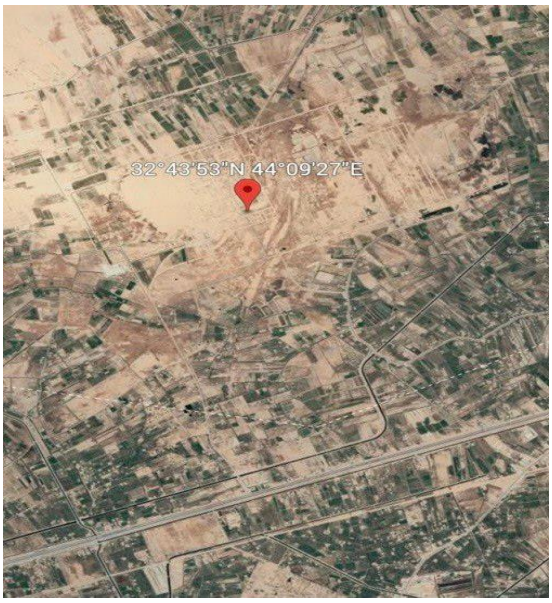

A

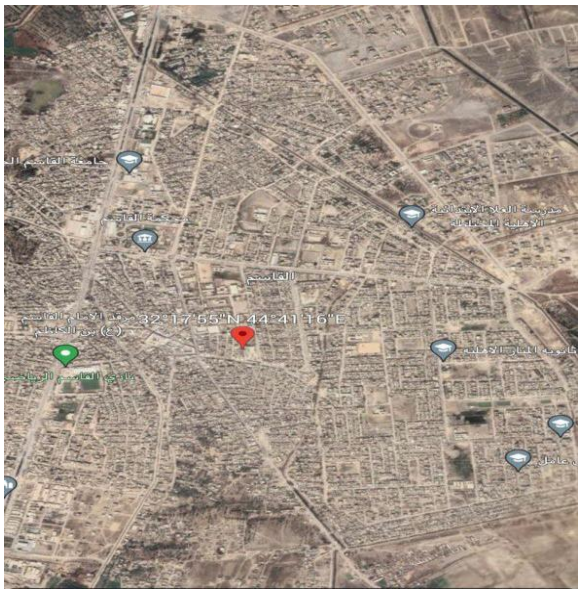

B

Figure (3-23): Desert areas that cause hot spots in summer (A) northern part regions (B) Central region.

- **Autumn Season**

The autumn season is less than the winter and spring seasons, but more than the summer season, as the northern regions of the governorate in this season have no heat spots, but their concentration is in the central regions of the governorate, especially the Medhatiyah region at latitude 32.23 and longitude 44.40 and the Hashemite At latitude 32.21 and longitude 44.36, and its appearance in this region is due to the absence of vegetation coverings, i.e. the areas are urban areas. As for the southern regions of the governorate in the autumn season, it is spread over very small areas, most of which are desert areas. The figure below shows the regions of Madakhtiya and Hashimiya.

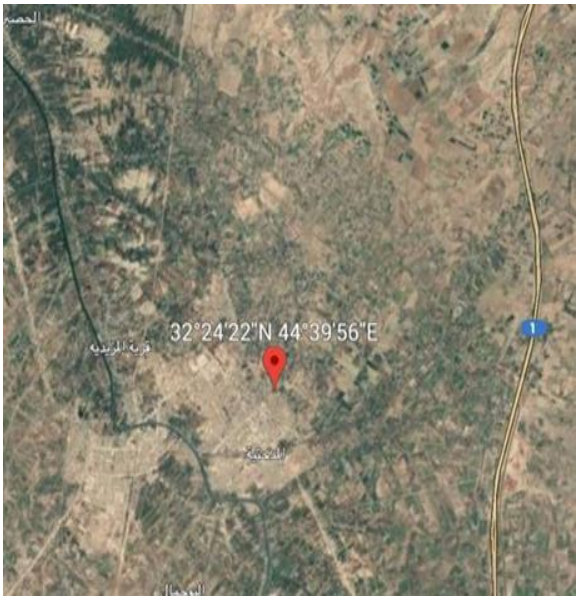

A B

Figure (3-24): (A) Medhatiyah region (B) Hashemite region.

3.5.3 The Urban Thermal Filed Variance Index (UTFVI)

It was calculated using equation (14) and the maps in the following figure show the values

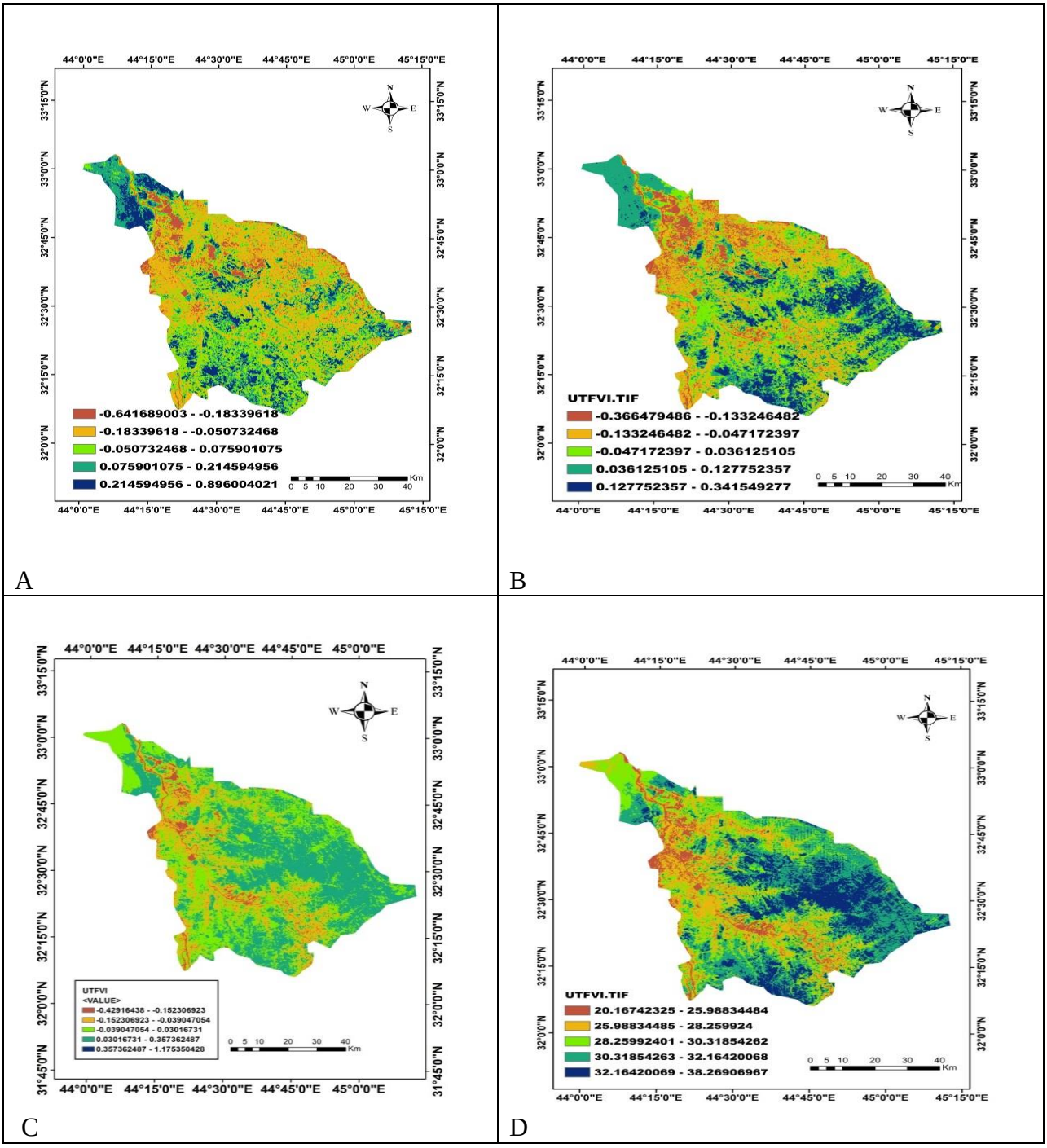

Figure (3-25): UTFVI Values for (A) Winter (B) Spring (C) Summer (D) Autumn.

We notice through the above drawing that UTFVI values vary from one place to another and from one season to another, as we note that the winter season has the highest values in the northern and southwestern regions, where the values range

between (0.214-0.896). As for the central regions of the governorate and the eastern regions, there will be a large discrepancy in values, ranging between (-0.641-0.214). As for the spring season, the lowest values are found in the northeastern and northwest sections, where it ranges between (-0.36- -0.0471). The highest values are found in the southern regions, which range between (0.127-0.341). As for the summer season, we notice that the lowest areas in which it is found are in some parts of the northern and western regions, where its value ranges between (-0.429- - 0.152). As for the rest of the governorate's regions, for example, the southern regions, the values range between(-0.039 -0.0357). As for the autumn season, the lowest values are found in the northwestern regions of the governorate, and values range between(20.6-25.7). As for the southern regions, they have the highest values, ranging between (32.61-38.62), and the rest of the government's regions range between (25.9-30.31). According to the findings, seasonal shifts in UTFVI distribution can be mostly attributed to the growth of the metropolitan area throughout the time period under consideration. Particularly densely populated and industrialized regions are where you'll find the UTFVI hotspot.

CHAPTER FOUR

CONCLUSIONS & FUTURE WORKS

4.1 Introduction

In this chapter, the results of the study will be described, as well as the suggestions for further research.

4.2 Conclusions

By comparing data from many years from Landsat 8, we may get a good understanding of how the weather in Babil province has changed over time. This can provide enough insight into possible changes. The changes in surface temperature index values revealed by this research are indicted on the current state of the planet and have the potential to improve weather forecasting and geolocation techniques. The research can be used as an indicator of high or low temperatures, as well as community activities and climate changes. The following is a summary of the most important results**:**

1. The results show the values of the Earth's surface temperatures and their distribution in the province of Babylon during the different seasons. It showed that the most high temperature regions are the Hamzah region in the summer, but in other seasons of the year the temperature of this district is moderate and the lowest regions in terms of temperature It is the block of Al-Hindiya and Al-Mahaweel in the winter season, but in the spring and autumn seasons, the temperatures are similar in all regions.
2. Our research show the relationship of the Earth's surface temperature with the elements of the climate, where the temperature is inversely related to the relative humidity, as it is observed that places where there is high humidity, such as areas

that contain water resources, the temperatures are lower than the areas where the humidity is low.

3. The results of our research show a relationship between the LST with the vegetation cover, which is an inverse relationship, as it is noticed the areas with high vegetation cover, where the temperature is low.
4. The results of our research show that the urban islands and the urban progress that occurred during the period of previous years are among the most important causes that led to the rise in temperatures.
5. After collecting information from the ground station for meteorological monitoring of Babil governorate and from the POWERNASA website, there is a convergence in the values between the different sources from which the data is obtained (Landsat 8, the ground station for meteorological monitoring and POPWERNANS).

4.3 Recommendations

1. To clearly differentiate between the degrees of the land surface temperature, researchers could employ higher resolution satellites for such a study region (Babylon governorate) or the Landsat 8 satellite for a larger study area.
2. Similar studies, using a variety of approaches, are being conducted to identify the best technique for measuring the land surface temperature.

3. It needs to provide a computer that has a high memory in order to be able to store the large amount of data.

4.4 Future Works

1. More research to other parts of Iraq is required, and compare with Babylon governorate results in order to figure out if it is locally issues or globally issues.
2. Studying the heat islands in detail and comparing them with the heat islands of earlier years, such as 2012, to see how the climate factors had affect by the bad use by humans in the study area.

References

[1] Zhou, L., Dickinson, R.E., Tian, Y., Jin, M., Ogawa, K., Yu, H., Schmugge,

[2] T.," A sensitivity study of climate and energy balance simulations with use of satellite-derived emissivity data over Northern Africa and the Arabian Peninsula", Journal of Geophysical Research: Atmospheres, Vol. 108 , 4795p, (2003).

[3] Le Marshall, J., Jung, J., Derber, J., Chahine, M., Treadon, R., Lord, S.J., Goldberg, M., Wolf, W., Liu, H.C., Joiner, J., Woollen, J., Todling, R., van Delst, P., Tahara, Y.," Improving global analysis and forecasting with AIRS. Bulletin of the American Meteorological Society", Vol.87, pp.891-894, (2006).

[4] Valor, E., Caselles, V., " Mapping land surface emissivity from NDVI: Application to European, African, and South Americanareas. Remote Sensing of Environment", Vol. 57, pp.167-184, (1996).

[5] Rhee, J., Im, J., Carbone, G.J., " Monitoring agricultural drought for arid and humid regions using multi-sensor remote sensing data. Remote Sensing of Environment", Vol. 114, pp. 2875-2887, (2010).

[6] Li, Z.-L., Tang, B.-H., Wu, H., Ren, H., Yan, G., Wan, Z., Trigo, I.F., Sobrino, J.A., " Satellite-derived land surface temperature: Current status and perspectives. Remote Sensing of Environment", Vol.131, pp.14-37**,** (2013).

[7] D. W. Wong and M. Sun, "Handling Data Quality Information of Survey Data in GIS: A Case of Using the American Community Survey Data", (2013).

[8] P. K. Kingra, D. Majumder and S. P. Singh, "Application of Remote Sensing And GIS in Agriculture and Natural Resource Management Under Changing Climatic Conditions", Journal of Agric Res, Vol.53, No.3, pp.295-302, (2016).

[9] Raman, C. R. V., Y. P. Rao, and S. M. A. Alvi., "The role of interaction with

middle latitude circulation in the behaviour of the southwest monsoon of and 1979.", Journal of Current Science, pp. 123-129, (1980).

[10] Schmugge, T., S. J. Hook, and C. Coll., "Recovering surface temperature and emissivity from thermal infrared multispectral data.", Journal of Remote Sensing of Environment, Vol.65, No.2, pp.121-131 (1998).

[11] Streutker, David R., "Satellite-measured growth of the urban heat island of Houston, Texas.", Journal of Remote Sensing of Environment, Vol. 85, No.3, pp. 282-289 (2003).

[12] Chapin, F.; Sturm, M.; Serreze, M.; McFadden, J.; Key, J.; Lloyd, A.; McGuire, A.; Rupp, T.; Lynch, A.; Schimel, J., "Role of Land-Surface Changes in Arctic Summer Warming", Journal of Science, Vol. 310, pp. 657–660, (2005).

[13] Karnieli, A., Agam, N., Pinker, R. T., Anderson, M., Imhoff, M. L., Gutman, G. G., Goldberg, A., "Use of NDVI and land surface temperature for drought assessment: Merits and limitations", Journal of climate, Vol. 23, No.3, pp. 618-633, (2010).

[14] Agam, N., Kustas, W. P., Anderson, M. C., Li, F., and Colaizzi, P. D., "Utility of thermal image sharpening for monitoring field-scale evapotranspiration over rainfed and irrigated agricultural regions", Journal of Geophysical Research Letters, Vol.35, No. 2, (2008).

[15] Li, Z. L., Tang, B. H., Wu, H., Ren, H., Yan, G., Wan, Z., and Sobrino, J. A.,"Satellite-derived land surface temperature: Current status and perspectives", Journal of Remote sensing of environment, Vol. 131, pp.14-37, (2013).

[16] Duan, S. B., Li, Z. L., Wu, H., Leng, P., Gao, M., & Wang, C., "Radiance-based validation of land surface temperature products derived from

Collection 6 MODIS thermal infrared data", Journal of International journal of applied earth observation and geoinformation, Vol. 70, pp. 84-

[17] Chen, X. L., Zhao, H. M., Li, P. X., & Yin, Z. Y., "Remote sensing image based analysis of the relationship between urban heat island and land use/cover changes", Journal of Remote sensing of environment, Vol. 104, No.2, pp. 133-146, (2006).

[18] Njoku, E. A., "Analysis of spatial-temporal pattern of Land Surface Temperature (LST) due to NDVI and elevation in Ilorin, Nigeria", Master Thesis in Geographical Information Science, (2019).

[19] Guha, Subhanil, et al. "Analytical study on the relationship between land surface temperature and land use/land cover indices." Annals of GIS 26.2 (2020): 201-216 .

[20] M. Georgescu et al., "An alternative explanation of the semiarid urban area 'oasis effect', Journal of Geophys. 116 (D24), D24113 (2011). http://dx.doi.org/10.1029/2011JD016720 JGREA2 0148-0227 Google Scholar.

[21] Junxiang, L. I. Yujie, W. A. N. G., Xiaohong, S. H. E. N. and Yongchang, S., "Landscape pattern analysis along an urban-rural gradient in the Shanghai metropolitan region", Journal of Acta Ecologica Sinica, Vol. 24, No.9 ,(2004).

[22] Gill, S. E., Handley, J. F., Ennos, A. R., and Pauleit, S., "Adapting cities for climate change: the role of the green infrastructure", Journal of Built environment, Vol.33, No.1, pp. 115-133, (2007).

[23] Grover, H. S., Dadlani, H., Bhardwaj, A., Yadav, A., and Lal, S., " Evaluation of patient response and recurrence of pigmentation folloing gingival depigmentation using laser and scalpel technique: A

clinical study", Journal of Indian Society of Periodontology, Vol.18, No.5, pp.586, (2014).

[24] Bauer, M. E., Loffelholz, B. C., and Wilson, B., "Estimating and mapping impervious surface area by regression analysis of Landsat imagery", In Remote sensing of impervious surfaces, pp. 31-48. CRC Press, (2007).

[25] Bórnez, K., Verger, A., Filella, I., and Penuelas, J., "Land surface phenology from Copernicus Global Land time series". Journal of International Workshop on the Analysis of Multitemporal Remote Sensing Images (MultiTemp) (pp. 1-4), (2017).

[26] Q. Weng, "A remote sensing-GIS evaluation of urban expansion and its impact on surface temperature in Zhujiang Delta, China", Journal of. Remote Sens., Vol.22, No.10, (2001). http://dx.doi.org/10.1080/713860788 IJSEDK 0143-1161 .

[27] Qin, Z. H., Zhang, M. H., Karnieli, A., and Berliner, P., "Mono-window algorithm for retrieving land surface temperature from Landsat TM6 data", Journal of Acta Geographica Sinica, Vol.56, No.4, pp. 456-466, (2001).

[28] Jimenez-Munoz, J. C., Cristobal, J., Sobrino, J. A., Sòria, G., Ninyerola, M., and Pons, X., "Revision of the single-channel algorithm for land Of IEEE Transactions on geoscience and remote sensing, Vol.47,No.1,pp.339-349,(2008). http://dx.doi.org/10.1109/TGRS.2008.2007125 IGRSD2 0196-2892 .

[29] Gillespie, A., Rokugawa, S., Matsunaga, T., Cothern, J. S., Hook, S., and Kahle, A. B., "A temperature and emissivity separation algorithm for imag56es", Journal of IEEE transactions on geoscience and remote sensing, Vol.36, No.4, pp. 1113-1126, (1998). doi.org/10.1109/36.700995 IGRSD2 0196-2892

[30] Sobrino, J. A., Li, Z. L., Stoll, M. P., and Becker, F., "Multi-channel and

multi-angle algorithms for estimating sea and land surface temperature with ATSR data", Journal of International Journal of Remote Sensing, Vol.17, No.11, pp. 2089-2114, (1996).

[31] García, D. H., and Díaz, J. A., "Space–time analysis of the earth's surface temperature, surface urban heat island and urban hotspot: relationships with variation of the thermal field in Andalusia (Spain)", Journal of Urban Ecosystems, pp.1-22, (2023).

[32] García, D. H., and Díaz, J. A., "Space–time analysis of the earth's surface temperature, surface urban heat island and urban hotspot: relationships with variation of the thermal field in Andalusia (Spain)", Journal of Urban Ecosystems, pp.1-22, (2023).

[33] Kafy, A. A., Shuvo, R. M., Naim, M. N. H., Sikdar, M. S., Chowdhury, R. R., Islam, M. A., and Kona, M. A., "Remote sensing approach to simulate the land use/land cover and seasonal land surface temperature change using machine learning algorithms in a fastest-growing megacity of Bangladesh", Journal of Remote Sensing Applications: Society and Environment, Vol.21, (2021).

[34] Planck, Max. *The theory of heat radiation*. Blakiston, 1914.

[35] Kirchhoff, G., "On the relation between the radiating and absorbing powers of different bodies for light and heat", *The London, Edinburgh, and Dublin Philosophical Magazine and Journal of Science*, *Vol.20*, No.130, pp. 1-21. (1860).

[36] Yu, Z., Sergeant, N. P., Skauli, T., Zhang, G., Wang, H., and Fan, S., "Enhancing far-field thermal emission with thermal extraction", Journal of Nature communications, Vol.4, No.1, (2013).

[37] Bohren, C. F., and Huffman, D. R. "Absorption and scattering of light by small particles", John Wiley and Sons. (2008).

[38] S. E. Profile, "A Business Model Monitoring Using Autonomous Drones in Smart Agriculture", *A Bus. Model Monit. Using Auton. Drones Smart Agric.*, No. January, p. 7, (2021).

[39] Planck, M., "Entropie und temperatur strahlender wärme. Annalen der Physik", Vol.306, No. 4, pp. 719-737, (1900).

[40] Klein, Martin J. "Max Planck and the beginnings of the quantum theory." Archive for History of Exact Sciences 1 (1961): 459-479

[41] Planck, M., "The theory of heat radiation", Blakiston., (1914).

[42] Planck, M. (2006) Entropie und Temperatur strahlender Wa¨rme. Ann Phys, Vol. 306(4), pp.719–737.

[43] Frank, Till Daniel. Nonlinear Fokker-Planck equations: fundamentals and. applications. Springer Science & Business Media, 2005.

[44] Halliday, D., Resnick, R., and Walker, J., "Fundamentals of physics. John Wiley and Sons, (2013).

[45] Frank, T. D. "Classical Langevin equations for the free electron gas and blackbody radiation." Journal of Physics A: Mathematical and General 37.11 (2004): 3561 .

[46] Lillesand, T., Kiefer, R. W., and Chipman, J., "Remote sensing and image interpretation", John Wiley and Son (2015).

[47] Overland, J. E., Hanna, E., Hanssen-Bauer, I., Kim, S. J., Walsh, J. E., Wang, M. and Ballinger, T. J., "Surface air temperature". Arctic report card, Vol. 5., (2019).

[48] Reygadas, Y., Jensen, J. L., Moisen, G. G., Currit, N., & Chow, E. T., "Assessing the relationship between vegetation greenness and surface temperature through Granger causality and Impulse-Response

coefficients: A case study in Mexico", Journal of International Journal of Remote Sensing, Vol. 41, No.10, 3761-3783 (2020).

[49] Oyler, J. W., Mildrexler, D. J., Comiso, J. C. and Hulley, G. C., "Surface temperature interrelationships", In Taking the temperature of the earth, pp. 185-202, Elsevier, (2019). https://doi.org/10.1016/B978-0-12-814458-9.00006 -X .

[50] Landsberg, Peter T., and Alexis De Vos. "The Stefan-Boltzmann constant in n-dimensional space." Journal of Physics A: Mathematical and General 22.8 (1989): 1073.

[51] Elliott, W. P. and Gaffen, D. J., "On the utility of radiosonde humidity archives for climate studies", Journal of Bulletin of the American Meteorological Society, Vol. 72, No. 10, pp. 150 (1991) .doi.org/10.1175/1520-0477(1991)072<1507:OTUORH>2.0.CO;2.

[52] Elliott, W. P., Gaffen, D. J., Angell, J. K. and Kahl, J. D. W., "The effect of moisture on layer thicknesses used to monitor global temperatures ", Journal of climate, Vol. 7, No. 2, pp. 304-308, (1994).

[53] Singh, R. B., Grover, A., & Zhan, J.," Inter-seasonal variations of surface temperature in the urbanized environment of Delhi using Landsat thermal data", Journal of Energies, Vol. 7, No. 3, pp. 1811-1828, (2014). doi.org/10.3390/en7031811.

[54] Singh, S., and Prasad, S. M., "Growth, photosynthesis and oxidative responses of Solanum melongena L. seedlings to cadmium stress: mechanism of toxicity amelioration by kinetin", Journal of Scientia Horticulturae, Vol. 176, pp. 1-10, (2014). https://doi.org/10.1016/ scienta.2014.06.022.

[55] M. Sharma , "What is Active and Passive Remote Sensing", (2019).

[56] Maguire, D. J., "An overview and definition of GIS", Journal of Geographical information systems: Principles and applications, Vol. 1,No. 1, pp. 9-20, (1991).

[57] Kathryn Clifton, "Geographic Information Systems Master Plan. GIS Coordinator and Members of the GIS Users Group", (2001 – 2002)

[58] Goodchild, M., "Twenty years of progress: GIScience in 2010". Journal of spatial information science, No. 1, 3-20, (2010). doi:10.5311/JOSIS.2010.1.2.

[59] Goodchild MF , "Towards an enumeration and classification of GIS functions In : Aangeenbrug RT . Schiffman Y M (eds .) International Geographic Information Systems GIS) Symposium", Falls Church Virginia, pp. 67-77, (1988).

[60] Anselin, L., "What is special about spatial data? Alternative perspectives on spatial data analysis", University of California, pp. 89-4, (1989).

[61] H. S. Abbas and A. S. Mahdi, "Study of Desertification using Remote Sensing Imagery in South Iraq", Iraqi Journal of Science, No. 4, vol. 60, p. 904, (2019).

[62] M. A. Ridwan, N. A. M. Radzi, W. Siti, H. Munirah, W. Ahmad, and I.S. Mustafa "Applications of Landsat-8 Data : a Survey Applications of Landsat-8 Data : a Survey", (2018)

[63] United Nations Publications, Handbook on geographic information systems and digital mapping, No. 79, vol. 1, (2000).

[64] Koroleva, E. V., & Nikitin, Y. Y., "U-max-statistics and limit theorems for perimeters and areas of random polygons", Journal of Multivariate Analysis, Vol127,98-111,(2014).

https://doi.org/10.1016/j.jmva.2014.02.006.

[65] B. Gorain and S. Paul, "Hardware and Software Components of a Geographic Informaion System (GIS)", AGROBIOS Newsl., (2017).

[66] V. N. Sambrani, "Business graphics a new approach to decision making", (2007).

[67] B. Gorain and S. Paul, "Hardware and Software Components of a Geographic Informaion System (GIS)", Journal of AGROBIOS Newsl., V. N. Sambrani, "Business graphics a new approach to decision making", (2007).

[68] Muhsin, I. J., "Assessment of vegetal cover changes using Normalized Difference Vegetation Index (NDVI) and subtractive (NDVI) time-series, Karbala province, Iraq", Iraqi Journal of Physics, Vol. 15, No. 35, pp. 133-141, (2017).

[69] Kumar, K. S., Bhaskar, P. U., and Padmakumari, K., "Estimation of land surface temperature to study urban heat island effect using Landsat ETM+ image", Journal of International journal of Engineering Science and technology, Vol. 4, No. 2, pp. 771-778, (2012).

[70] Yue W, Xu J, Tan W, Xu L., "The relationship between land surface temperature and NDVI with remote sensing: application to Shanghai Landsat and ETM+ data", Journal of International Journal of Remote Sensing, Vol. 15, No. 2, ISSN : 3205-3226, 2007.

[71] Ali, F. R. A. K. M., Fouad, K. M. A., & Abdul-Rahman, B. A., " Evaluation of impact of vegetation decrease on precipitation rates in Baghdad City using remote sensing technique", Journal of BUNYANI AND BLEGUR 25, (2019). ISSN 0971–765X.

[72] B. Gorain and S. Paul, "Hardware and Software Components of a

Geographic Informaion System (GIS)", *AGROBIOS Newsl.*, (2017).

[73] I. J. Muhsin, "Assessment of vegetal cover changes using Normalized Difference Vegetation Assessment of vegetal cover changes using Normalized Difference Vegetation Index (NDVI) and subtractive (NDVI) time-series , Karbala province , Iraq", (2017).

[74] Chander, G., Markham, B. L., and Helder, D. L., "Summary of current radiometric calibration coefficients for Landsat MSS, TM, ETM+, and EO-1 ALI sensors", Journal of Remote sensing of environment, Vol., 113,No.5,pp.893-903,(2009). https://doi.org/10.1016/j.rse.2009.01.007.

[75] Roy, D. P., Wulder, M. A., Loveland, T. R., Woodcock, C. E., Allen, R. G., Anderson, M. C., and Zhu, Z., "Landsat-8: Science and product vision for terrestrial global change research", Journal of Remote sensing of Environment, Vol. 145, pp. 154-172, (2014). https://doi.org/10.1016/j.rse.2014.02.001.

[76] H. S. Abbas and A. S. Mahdi, "Study of Desertification using Remote Sensing Imagery in South Iraq", Iraqi Journal of Science, No. 4, vol. 60, p. 904, (2019).

[77] Wulder, M. A. and Masek, J. G., "Landsat legacy", Journal of Remote Sensing of Environment, Vol. 122, pp. 1-202. (2012).

[78] Goward, S. N., Masek, J. G., Williams, D. L., Irons, J. R. and Thompson, R. J., "The Landsat 7 mission: Terrestrial research and applications for the 21st century", Journal of Remote Sensing of Environment, Vol. 78, pp. 3-12, (2001).

[79] Barsi, J. A., Lee, K., Kvaran, G., Markham, B. L. and Pedelty, J. A., "The spectral response of the Landsat-8 operational land imager", Journal of Remotesensing, Vol.6,No.10,(2014). https://doi.org/10.3390/rs61010232.

[80] Parente, C. and Santamaria, R., "Synthetic sensor of Landsat 7 ETM+ imagery to compare and evaluate pan-sharpening methods", Journal of Sensors and Transducers, Vol. 177, Issue 8,, pp. 294, (2014).

[81] Tollefson, Jeff. "Landsat 8 to the rescue: NASA prepares to launch satellite that will continue historic record of global change." Nature 494.7435 (2013): 13-15.

[82] Sobrino, J. A., Jiménez-Muñoz, J. C.and, Paolini, L., "Land surface temperature retrieval from LANDSAT TM 5", Journal of Remote Sensing of environment, Vol.90,No.4,pp.434-440,(2004) https://doi.org/10.1016/j.rse.2004.02.003.

[83] Walawender, J. P., Hajto, M. J. and Iwaniuk, P., "A new ArcGIS toolset for automated mapping of land surface temperature with the use of LANDSAT satellite data", Journal of international geoscience and remote sensing symposium, pp. 4371-4374, (2012). doi. 10.1109/IGARSS.2012.6350405 .

[84] Stathopoulou, M. Cartalis, C., "Daytime urban heat islands from Landsat ETM+ and Corine land cover data: An application to major cities in Greece", Journal of Solar Energy, Vol.81, No.3, pp. 358- 368, (2007). https://doi.org/10.1016/j.solener.2006.06.014.

[85] Sobrino, J.A., Jiménez-Muñoz, J.C., Paolini, L., "Land surface temperature retrieval from LANDSAT TM 5", Journal of Remote Sensing of Environment, Vol. 90, pp. 434-440, (2004). https://doi.org/10.1016/j.rse.2004.02.003.

[85] Jiménez-Muñoz J.C., Sobrino J., Skokovic D., Mattar C., Cristóbal J., "\ Land Surface Temperature Retrieval Methods from Landsat-8 Thermal Infrared Sensor Data", Journal of Geoscience and remote sensing letters, Vol.11,No.10,pp. 1840-1843, (2014). dOI. 10.1109/LGRS.2014.2312032

[86] Pearsall, H., "Staying cool in the compact city: Vacant land and urban heating in Philadelphia, Pennsylvania", Journal of Applied geography, Vol. 79, pp. 84-92, (2017). https://doi.org/10.1016/j.apgeog.2016.12.010 .

[87] Hidalgo García, D. and Arco Díaz, J., "Space–time analysis of the earth's surface temperature, surface urban heat island and urban hotspot: relationships with variation of the thermal field in Andalusia (Spain)", (2023). doi.10.1007/s11252-022-01321-9.

[88] Kafy, A. A., Shuvo, R. M., Naim, M. N. H., Sikdar, M. S., Chowdhury, R. R., Islam, M. A. and Kona, M. A., "Remote sensing approach to simulate the land use/land cover and seasonal land surface temperature change using machine learning algorithms in a fastest-growing megacity of Bangladesh", Journal of Remote Sensing Applications: Society and Environment, Vol21,(2021). https://doi.org/10.1016/j.rsase.2020.100463.

[89] Bokaie, M., Zarkesh, M. K., Arasteh, P. D. and Hosseini, A., "Assessment of urban heat island based on the relationship between land surface temperature and land use/land cover in Tehran", Journal of Sustainable Cities and Society, Vol. 23, pp. 94-104, (2016). https://doi.org/10.1016/j.scs.2016.03.009.

[90] Duan, S. B., Li, Z. L., Wu, H. and Tang, B. H., "Temporal normalization of Terra-MODIS land surface temperature product", Journal of International Geoscience and Remote Sensing Symposium-IGARSS, pp. 461-464, (2013). **doi.**10.1109/IGARSS.2013.6721192 .

[91] Zhou, L., Dickinson, R. E., Tian, Y., Jin, M., Ogawa, K., Yu, H. and

Schmugge, T., "A sensitivity study of climate and energy balance simulations
with use of satellite-derived emissivity data over Northern Africa and the Arabian Peninsula", Journal of Geophysical Research: Atmospheres, Vol. 108, (2003).https://doi.org/10.1029/2003JD004083

[92] Al-Timimi, Y. K., Al-Salihi, A. M. and Al-lami, A. M., "Estimation of Land Surface Temperature for Different Regions in Iraq Using Remote Sensing Technique (ETM+)", Journal of Engineering and Technology Journal, Vol. 32, No.6, (2014).

[93] Orhan, O., Dadaser-Celik, F., and Ekercin, S., "Investigating land surface temperature changes using Landsat-5 data and real-time infrared thermometer measurements at Konya closed basin in Turkey", Journal of International Journal of Engineering and Geosciences, Vol. 4,No. 1,pp. 16-27, (2019). https://doi.org/10.26833/ijeg.417151.

[94] Feng, X. and Myint, S. W., "Exploring the effect of neighboring land cover pattern on land surface temperature of central building objects", Journal of Building and Environment, Vol.95, pp.346-354, (2016). https://doi.org/10.1016/j.buildenv.2015.09.019.

[95] Mushore, T. D., Mutanga, O., Odindi, J. and Dube, T., "Linking major shifts in land surface temperatures to long term land use and land cover changes: A case of Harare, Zimbabwe", Journal of Urban Climate Vol.20,pp.120-13(2017). https://doi.org/10.1016/j.uclim.2017.04.005

[96] Salih, M. M., Jasim, O. Z., Hassoon, K. I. and Abdalkadhum, A. J., "Land surface temperature retrieval from LANDSAT-8 thermal infrared sensor data and validation with infrared thermometer camera", Journal of International Journal of Engineering & Technology, Vol. 7, (2018).

[97] Beg, A., "Assessment of land surface temperature variation over Rusafa

side of Baghdad city, Iraq", In MATEC Web of Conferences (Vol. 162,(2018).https://doi.org/10.1051/matecconf/201816203032

[98] Njoku, E. A., "Analysis of spatial-temporal pattern of Land Surface Temperature (LST) due to NDVI and elevation in Ilorin, Nigeria", Master Thesis in Geographical Information Science, (2019).

[99] Halder, B., Bandyopadhyay, J., Khedher, K. M., Fai, C. M., Tangang, F. and Yaseen, Z. M., "Delineation of urban expansion influences urban heat islands and natural environment using remote sensing and GIS-based industrial area", Journal of Environmental Science and Pollution Resear Research, Vol. 29, No. 48,(2022

[100] Liang, S. (2005). Quantitative Remote Sensing of Land Surfaces. John Wiley & Sons. https://doi.org/10.1016/j.agsy.2005.11.003.

[101] https://power.larc.nasa.gov/data-access-viewer, accessed on July 13, 2020.

[102] https://meteonorm.com, accessed on Aug. 20, 2020.

[103] https://solargis.com, accessed on Aug. 20, 2020.

الخلاصة

تضمنت الرسالة دراسة درجة حرارة سطح الارض (LST) وارتباطها بعوامل المناخ مثل درجة حرارة الهواء والرطوبة النسبية الخاصة بمحافظة بابل لسنة2022 بعد قمنا بتقسيمها الى الفصول الاربعة (الشتاء، الربيع، الصيف، والخريف) من خلال اختيار الاشهر التالية (كانون الثاني، نيسان، اب، تشرين الثاني) لسنة 2022. تم ذلك باعتماد البيانات التي يوفرها القمر الصناعي لاندسات الاصدار 8 حيث له المقدرة على تصوير عالية النطاق ولها القدرة للدقة عالية وكذلك تحتوي اطياف مختلفة تكون الصور بدقة (30 -100) م. في البحث تم اعتماد الحزم التالية: الحمراء (الرابعة)، تحت الحمراء القريبة (الخامسة)، والاشعة تحت الحمراء الحرارية (العاشرة) من خلال متحسسين.

(Thermal Infrared and Operational Land Imager Sensor (TIRS)) ثم تحميل مقطعين لكل حزمه (لتغطية محافظة بابل التي تبلغ مساحتها 5119 م2 لكل شهر قيد الدراسة من موقع المسح الجغرافي الامريكي (USGS). في مثل هذه الحالة هنالك خطوه مهمه قبل القيام بالتصحيحات الهندسية والمكانية هي دمج المقطعين باستخدام برنامج الموزائيك ثم استقطعت منطقة البحث (محافظة بابل) عن طريق استخدام التقنية المعروفة باسم الاستشعارعن بعد (RS) وتقنية نظم المعلومات الجغرافية (Arc GIS).

قد تم الحصول هو اربع خرائط التي تخص منطقة دراستنا والمتمثلة ب(محافظة بابل) لتوضيح التباين في درجات حرارة سطح الارض التي تمثل الفصول الاربعة للسنة المدروسة. نلاحظ تباين كبير بين الفصلين الرئيسية بألسنه في العراق وهما الصيف والشتاء حيث تصل درجة الحرارة العظمى لسطح الارض خلال فصل الصيف الى تقريبا 70 درجة مئوية لكن في الشتاء تنخفض الى 24 درجة مئوية اي بفارق 46 درجة مئوية. بينما الاختلاف بدرجة حرارة سطح الارض الصغرى بين الفصلين تكون تقريبا (14م). اما الفصلين (الربيع والخريف) فالفارق كان بدرجة الحرارة العظمى(2 م) (1 م) درجة مئوية.

تم دراسة العلاقة بين عوامل المناخ مثل درجة حرارة الهواء والرطوبة النسبية مع درجة حرارة السطح وذلك باعتماد محطة الانواء الجوية في محافظة بابل وايضا تم تكوين10 محطات افتراضية ولاحظنا ان عند مقارنة درجة حرارة الهواء مع درجة حرارة سطح الارض نلاحظ ان الفرق بينهم من (2-3) درجات مئوية اما الرطوبة فانها تتناسب عكسي مع درجات حرارة سطح الارض.وتم قياس الجزر الحضرية (UHI) والجزرغير الحضرية (non-UHI) والمناطق الحضرية الساخنة (UHS) مؤشرالتباين في المجال

الحراري الحضري (UTFVI) وهي قياس مدى ارتفاع درجات الحرارة في المناطق الحضرية نتيجة السكن والتنمية الحضرية حيث نلاحظ من النتائج التي تم الحصول عليها ان هناك تباين كبير من موسم لاخر ومن منطقة لاخرى من مناطق محافظة بابل حيث كان التباين الكبير بين فصل الشتاء والربيع من حيث توزيعها في المناطق الشمالية ففي فصل الشتاء تكون خالية من الجزر الحضرية وفي فصل الربيع تحتوي على الجزر الحضرية اما في فصل الصيف والخريف فيكونان متشابهتان في التوزيع تكون المناطق الشمالية والغربية لا تحتوي جزر حرارية والمناطق الشرقية والجنوبية الغربية تحتوي على جزر الحرارية.

جمهورية العراق

وزارة التعليم العالي و البحث العلمي

جامعة بابل / كلية العلوم

قسم الفيزياء

دراسة درجة حرارة سطح الأرض (LST) لفصول مختلفة في محافظة بابل باستخدام تقنيات GIS

رسالة مقدمة الى قسم الفيزياء كلية العلوم جامعة بابل وهي جزء من متطلبات نيل شهادة الماجستير في علوم الفيزياء

من قبل

ميساء مزهر كاظم حسين

(بكالوريوس علوم فيزياء, 2018)

بأشراف

أ. د. أميرة أبو السود حمادي مهجج السعدوني

1445هـ **2023م**